Distortion Invariant Class-Associative Target Detection Using Joint Transform Correlation

by

Sharif Md Ataullah Bhuiyan

MASTER OF SCIENCE IN ELECTRICAL AND ELECTRONIC ENGINEERING

DEPARTMENT OF ELECTRICAL AND ELECTRONIC ENGINEERING
BANGLADESH UNIVERSITY OF ENGINEERING AND TECHNOLOGY

2003

The thesis titled "**Distortion Invariant Class-Associative Target Detection Using Joint Transform Correlation**", submitted by Sharif Md Ataullah Bhuiyan, Roll No.: 100106249P, Session: October 2001, has been accepted as satisfactory in partial fulfillment of the requirement for the degree of MASTER OF SCIENCE IN ELECTRICAL AND ELECTRONIC ENGINEERING on 01 July 2003.

BOARD OF EXAMINERS

1. July 01, 2003

Dr. M. Nazrul Islam
Associate Professor
Department of Electrical and Electronic Engineering
BUET, Dhaka-1000, Bangladesh

Chairman
(Supervisor)

2. 01/07/03

Dr. Satya Prasad Majumder
Professor
Department of Electrical and Electronic Engineering
BUET, Dhaka-1000, Bangladesh

Member

3. 1.7.2003

Dr. Md. Kamrul Hasan
Associate Professor
Department of Electrical and Electronic Engineering
BUET, Dhaka-1000, Bangladesh

Member

4. 1.7.2003

Dr. Mohammad Ali Choudhury
Professor and Head
Department of Electrical and Electronic Engineering
BUET, Dhaka-1000, Bangladesh

Member
(Ex-officio)

5. 1.7.2003

Dr. Farruk Ahmed
Professor
Department of Applied Physics and Electronics
University of Dhaka, Dhaka-1000, Bangladesh

Member
(External)

DECLARATION

It is hereby declared that this thesis or any part of it has not been submitted elsewhere for the award of any degree or diploma.

Signature of the Candidate

SABhuiyan
01.7.2003

Sharif Md Ataullah Bhuiyan

DEDICATION

To my parents

CONTENTS

LIST OF TABLES

LIST OF FIGURES

LIST OF ABBREVIATIONS

ACMF	Amplitude modulated complex matched filter
AMPOF	Amplitude modulated phase-only filter
CCD	Charge coupled device
CFAF	Class-associative fringe-adjusted filter
CGFAF	Class-associative generalized fringe-adjusted filter
CH	Circular harmonic method
CMF	Complex matched filter
FAF	Fringe-adjusted filter
FJTC	Fringe-adjusted joint transform correlator
FPFJTC	Fractional power fringe-adjusted joint transform correlator
GFAF	Generalized fringe-adjusted filter
GFJTC	Generalized fringe-adjusted joint transform correlator
IF	Inverse filter
JPS	Joint power spectrum
JTC	Joint transform correlator
MACE	Minimum average correlation energy filter
MTDA	Multi-target detection algorithm
MVSDF	Minimum variance synthetic discriminant filter
POF	Phase-only filter
SDF	Synthetic discriminant function
SLM	Spatial light modulator
VLC	VanderLugt Correlator

LIST OF SYMBOLS

α	Power spectra parameter of reference 1 in class detection
β	Power spectra parameter of reference 2 in class detection
γ	Power spectra parameter of reference 3 in class detection
λ	Wavelength of collimated light in JTC scheme
ξ	Normalized acceptable error limit in SDF generation
$\Im$	Fourier transform operation
$\Im^{1}$	Inverse Fourier transform operation
$\otimes$	Correlation operation
$*$	Complex conjugate
f	Focal length of Fourier lenses
x, y, x', y'	Space domain variables
u, v	Frequency domain variables
rf	Relaxation factor in SDF generation
m, C, D	GFAF or CGFAF filter parameters
H_{cmf}	CMF filter function in VLC
H_{if}	IF filter function in VLC
H_{pof}	Phase-only filter function in VLC
H_{acmf}	Amplitude modulated CMF filter function in VLC
H_{ampof}	Amplitude modulated POF filter function in VLC
H_{faf}	Fringe-adjusted filter function in JTC
H_{gfaf}	Generalized fringe-adjusted filter function in JTC
H_{gfaf}^{c}	Classical filter function of GFAF in JTC
H_{gfaf}^{f}	Fringe-adjusted filter function of GFAF in JTC
H_{gfaf}^{p}	Phase-only filter of GFAF in JTC
H_{cgfaf}	Class-associative GFAF filter function in JTC
H_{gfaf}^{SDF}	GFAF filter function with SDF as reference in JTC
r_{SDF}	SDF reference image

r_{SDF}^{c} SDF reference image generated by classical JTC

r_{SDF}^{f} SDF reference image generated by fringe-adjusted JTC

r_{SDF}^{p} SDF reference image generated by phase-only JTC

ACKNOWLEDGEMENTS

The author expresses his profound gratitude to his supervisor Dr. M. Nazrul Islam, Associate Professor, Department of Electrical and Electronic Engineering, Bangladesh University of Engineering and Technology (BUET), Dhaka, for his guidance, suggestions and supervision throughout the work. The whole-hearted co-operation of Dr. Nazrul made this work completed timely and successfully.

The author is very much grateful to Dr. Mohammad S. Alam, Professor, Department of Electrical and Computer Engineering, University of South Alabama, USA for providing books, journals and research materials along with a very good support for the work. The author is also thankful to Bangladesh University of Engineering and Technology, Dhaka, for providing various resources required for this work. The author would like to thank his friends, colleagues and well-wishers who extended their hands directly or indirectly to complete this work.

The author expresses profound gratitude to his family members and relatives for their support, help, inspiration and patience, which made this work come to a fruitful end.

ABSTRACT

This thesis is concerned with the application of synthetic discriminant function (SDF) to the class-associative target detection technique to get distortion invariant detection for the objects of the class by using optical correlator. A class of objects may be defined as a group of objects with similarity or dissimilarity among them. On the other hand synthetic discriminant function is a synthesized reference image used for joint transform correlation (JTC) operation. It is actually a weighted sum of the training set containing the original image and the possible distorted versions of the original image. As the target members of the class are known, the SDF based reference images can be generated by computer before applying to the real time optical detection scheme. Class-associative target detection employs a multi-target detection algorithm (MTDA) facilitating multiple reference images for which more than one dissimilar objects or images of a class can be detected. In MTDA several combinations of input spectra are produced using each reference and input scene separately. For distortion invariant class-associative target recognition, all the references are replaced by SDF based references. The class-associative generalized fringe-adjusted filter is also modified by using the Fourier transform of SDF references in place of the Fourier transform of the actual references. Thus employing SDF to the class-associative detection scheme provides distortion invariant class-associative target detection. A simplified method for generating SDF is devised which is found to be successful in the implementation. The conditions for generating SDF and employing into class-associative generalized fringe-adjusted filter have also been suggested. The simulation shows satisfactory performance of the proposed scheme in getting distortion invariant detection of the members of the class mainly with scale variation and rotation giving almost equal correlation peaks for all the distorted and undistorted images while no or negligible correlation peaks for the non-targets. This scheme works almost successfully for both binary and gray level images.

Chapter 1

INTRODUCTION

1.1 Introduction

Pattern recognition techniques are an important component of intelligent systems and are used for both data preprocessing and decision making. Broadly speaking, pattern recognition is the science that concerns the description or classification (recognition) of measurements. It deals with the detection and identification of a desired pattern or target in an unknown input scene, which may or may not contain the target, and with the determination of the spatial location of any target present. It is a rapidly developing technology with cross-disciplinary interest and participation. Some major applications of pattern recognition techniques are image preprocessing, computer vision, seismic analysis, face recognition, fingerprint identification, character recognition, medical diagnosis, crop assessment, still and moving object detection etc.

In pattern recognition or classification the input is an image while the output is a decision signal based on some characteristic features of the input. The number of features is virtually always chosen to be fewer than the total necessary to describe the complete target of interest, and this leads to a loss of information. It defers from classical statistical hypothesis testing, wherein the sensed data are used to decide whether or not to reject a null hypothesis in favor of some alternative hypothesis depending on some threshold. It also differs from image processing, where, the input is an image and the output is also an image. Pattern classification is also contrasted with the acts of associative memory. In acts of associative memory, the system takes in a pattern and emits another pattern, which is representative of a general group. It thus reduces the information somewhat, but rarely to the extent that pattern classification does. Because of the crucial role of a decision in pattern recognition, it is fundamentally an information reduction process, whereby, it is not possible to reconstruct the pattern but it is possible to give a precise decision [1-2].

1.2 Pattern Recognition Approaches

Generally an underlying and quantifiable statistical basis or underlying structure of a pattern provides the fundamental information about that particular pattern. Sometimes a pattern may be described by both the above features. Based on this fact historically there are two major approaches to pattern recognition, namely, statistical (or decision theoretic) pattern recognition and syntactic (or structural) pattern recognition. Recently a third approach has been emerged named neural pattern recognition though it is still undecided whether it is a novel approach or an alternative technique of implementing the statistical or syntactical approach [1-2].

1.2.1 Statistical Pattern Recognition

This approach assumes a statistical basis for classification algorithm. A set of characteristic measurements, denoted features, is extracted from the input data and is used to assign each feature vector to one of the classes. Features are assumed to be generated by a state of nature, and therefore the underlying model is of a state of nature or class-conditioned set of probabilities and/or probability density functions.

Various methods for finding decision functions in decision theoretic approach are: matching, optimum statistical classifier and neural networks. And there are two ways of matching- one is minimum distance classifier and the other is matching by correlation [3].

1.2.2 Syntactic Pattern Recognition

Very often the significant information in a pattern is not merely the presence or absence of a set of features. Rather, the interrelationship or interconnections of features yield important structural information, which facilitates structural description or classification. This is the basis of syntactic pattern recognition. In this case however we must be able to quantify and extract structural information and to assess structural similarity of patterns.

1.3 Implementation Techniques of Pattern Recognition

Digital computers, as well as, optical systems can be utilized for the implementation of pattern recognition. Signal processing through computer for traditional digital pattern recognition has the temporal advantage, whereas optical system has an additional manipulation advantage. Most of the digital pattern recognition operations suffer from huge amount of computation burden, the implementation difficulty, slow speed and cost. If the pattern recognition is implemented optically, it is possible to alleviate these problems considerably. Optical techniques inherently provide parallelism, ultrahigh processing speed, noninterfering communication, massive interconnection capability and offer a significantly better alternative to the conventional digital pattern recognition approach.

1.4 Optical Pattern Recognition

Optical techniques use correlation approach for pattern recognition. Correlation pattern recognition offers several unique advantages in machine vision applications. Correlation is a sensor independent approach that generally does not require data specific operations (such as segmentation, feature extraction, on-line model synthesis, or other processes). Since the throughput of a correlator generally depends on the dimensions of the image, the algorithm complexity depends on the scene size and not on the number of objects to be detected. Not only does this provide a precise estimate for throughput, but it also avoids the computational bottlenecks faced by some approaches due to scene complexity, clutter and the number of objects present. Correlation pattern recognition is a unique blend of concepts from the fields of signals and systems, Fourier optics and statistical pattern recognition.

Correlation between two functions in spatial domain is equivalent to conjugate multiplication in frequency domain. Thus optical correlators for pattern recognition use Fourier transform properties of a lens. If the input transparency is placed in the front focal plane of the lens and illuminated with coherent collimated light, the optical field at the back focal plane of the lens will be the Fourier transform of the input transparency [4-5]. An optical correlator usually contains two lenses, thus it performs two Fourier transform successively. The first lens transforms the input function from the space domain to the frequency domain and the second lens transforms the frequency function back to the space function. The input function and output function (both in the space domain) are related by a linear system. This linear system can perform correlation or convolution. Other then lens, the optical devices that are used are spatial light modulators (SLMs), charged coupled device (CCD) array, mirror, beam splitter etc.

When an optical correlator processes a scene using the inherent Fourier transform properties of lenses, it optically compares all pixels in the input scene to all pixels in the reference image simultaneously. This parallel processing capability of optical correlators provides a significant processing speed advantage over their digital counterparts, where the input scene must be processed sequentially.

There are two widely used optical correlators: namely, VanderLugt correlator and joint transform correlator (JTC).

1.4.1 VanderLugt Correlator

The VanderLugt type correlator (VLC) also known as the matched filter based correlator was first introduced in 1964 and since then it has spurred myriad of applications [6-11]. It requires *a priori* fabrication of a complex matched filter used in the Fourier plane. In other words, the performance of the VLC depends on the construction of a spatial frequency filter. This filter must be accurately aligned along the optical axis in the Fourier plane and requires close positioning between the filter and the Fourier transform of the input. Thus real time operation of the VanderLugt correlator is quite complicated and any type of misalignment results in output intensity degradation for correlation operation. VLC filter is, however, input signal independent, that is, its physical properties are not altered by the input scene [12-14].

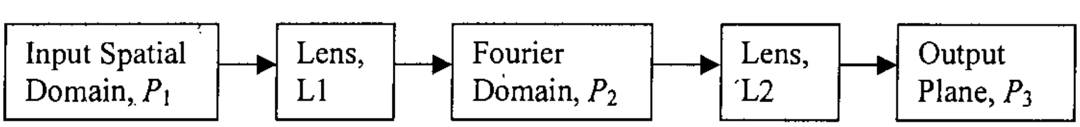

Fig. 1.1 VanderLugt correlator

A matched filter based optical signal processor is shown in Fig. 1.1 where P_1, P_2 and P_3 represent the input, the Fourier plane and the output plane respectively. The input plane P_1 contains the input signal $f(x,y)$ and is illuminated by a monochromatic point source located at the front focal length of a collimating lens. The complex light field distribution at plane P_2 is given by

$$F(u,v)=\mathfrak{I}[f(x,y)] \tag{1.1}$$

Where, $\mathfrak{I}$ represents Fourier transform operation and $u=(2\pi/\lambda f)x$ and $v=(2\pi/\lambda f)y$ respectively, λ=wavelength of collimating light and f=focal length of Fourier transforming lens.

The phase fronts of the wave emanating from plane P_1 and incident on plane P_2 are both curved and distorted. The phase transmittance of the matched filter $H(u,v)$ at plane P_2 must be the conjugate match to the phase of the Fourier transform of $f(x,y)$ [i.e $H(u,v)=F^*(u,v)$]. Accordingly, the phase variations in the wave front incident on plane P_2 are canceled by the filter and the resulting distribution beyond the plane P_2 becomes a parallel beam. Lens L2 performs a Fourier transform on this wave and produces the output at plane P_3. If the input is different from $f(x,y)$, the phase-front will not be exactly canceled by the filter, and the light distribution in plane P_3 will produce a spot of poor intensity or no spot at all. The complex light distribution at plane P_3 is given by

$$g(x,y)= \mathfrak{I}^1[F(u,v)H(u,v)] \tag{1.2}$$

where, $\mathfrak{I}^1$ represents an inverse Fourier transform operation.

If the input object is moved laterally in the input plane, the Fourier transform remains fixed in space but is multiplied by a phase factor that depends on the lateral movement. Therefore, the coordinates of the bright correlation output in plane P_3 is proportional to the coordinates of the signal $f(x,y)$ located at the input plane. The intensity of the bright correlation spot is proportional to the degree to which the input and the filter functions are matched. Since the system is linear, superposition theorem holds. The aforementioned arguments are also valid for multiple objects present at different locations of the input plane. This correlation system provides a great deal of sensitivity since it is both phase matched and amplitude matched.

For the complex matched filter (CMF), the frequency plane filter function is expressed by

$$H_{cmf}=R^{*}(u,v)=|R(u,v)|\exp[-j\phi(u,v)] \tag{1.3}$$

Where, $|R(u,v)|$ is the amplitude and $\phi(u,v)$ is the phase factor of the Fourier spectrum of the reference function $r(x,y)$. When the input is similar to $r(x,y)$, the phase variation is canceled at the Fourier plane thus producing a plane wave of light. The correlation peak corresponding to CMF is not very sharp due to the squaring of the magnitude of $r(x,y)$. Consequently, the resulting diffraction efficiency of a CMF is very poor.

To overcome the drawbacks of CMF, the inverse filter (IF) may be used. The frequency plane expression for the IF is given by

$$H_{if}(u,v)=R(u,v)^{-1}=|R(u,v)|^{-1}\exp[-j\phi(u,v)] \tag{1.4}$$

For this filter, the correlation peak is enhanced since the Fourier amplitude becomes unity after filtering. However, with one or more poles, the function $|R(u,v)|^{-1}$ becomes indeterminate thereby creating a serious design problem in realizing this filter.

The optimum case with respect to light efficiency for a matched filter is realized by a phase only filter (POF) structure [15]. This filter is obtained by omitting the amplitude information

$$H_{pof}(u,v)=\frac{R^{*}(u,v)}{|R(u,v)|}=\exp[-j\phi(u,v)] \tag{1.5}$$

Besides the improvement in light efficiency, the correlation peak intensity is also enhanced. However, although the autocorrelation peak intensity is higher than that of a CMF, it is not as sharp as might be produced by an IF, since the product $H_{pof}(u,v)R(u,v)$ is not necessarily a constant.

To enhance the correlation peak even more, a modified version of the IF called amplitude modulated complex matched filter (ACMF) has been developed [16]. The corresponding filter expression is given by

$$H_{acmf}(u,v) = \frac{C}{R(u,v)} = \frac{C}{|R(u,v)|}\exp[-j\phi(u,v)] \tag{1.6}$$

The main feature of this filter is that one can avoid having optical gain greater than unity by properly selecting C. Although the ACMF still has the pole problem, it yields much higher correlation discrimination than POF.

To solve both the pole and the optical gain problem of IF, another modified version of IF was proposed. The resulting filter, called amplitude modulated phase only filter (AMPOF), is given by

$$H_{ampof}(u,v) = \frac{D}{A+|R(u,v)|}\exp[-j\phi(u,v)] \tag{1.7}$$

where, D and A are either constants or functions of u and v. this information guarantees that transmittance of the filter is less than unity. With the inclusion of A, the pole problem is solved and at the same time it is possible to choose very high autocorrelation peak.

1.4.2 Joint Transform Correlator

Joint transform correlator (JTC) is a device consisting of two optical systems in which two signals are simultaneously transformed to produce their spectra, and these spectra are multiplied and inversely transformed to produce the output correlation signal. Fig. 1.2 shows a block diagram of a joint transform correlation scheme.

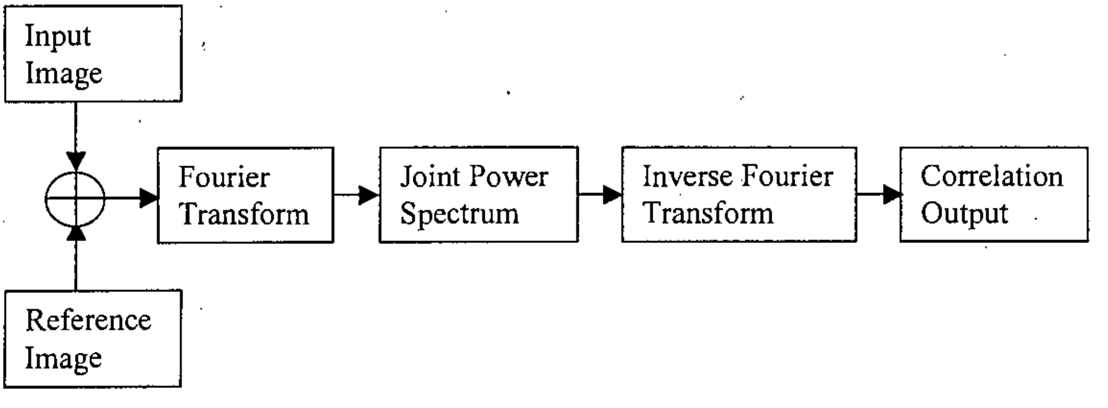

Fig. 1.2 Joint transform correlator

Optical Pattern recognition by JTC was first introduced in 1966 [17]. However, first real-time programmable JTC was introduced in 1984 with the development of real-time electronically addressable spatial light modulator (SLM) [18]. JTC does not require any complex Fourier domain filter fabrication; rather it uses a spatial (impulse response) domain filter. In other words, performance of JTC depends on spatial domain filter synthesis. In contrast to VLC, joint transform power spectrum in JTC is dependent on input signal. JTC has shown remarkable promise for real-time pattern recognition and tracking applications [18-19]. Other advantages of JTC are that it allows real-time update of the reference image, permits parallel Fourier transform of the reference image and the unknown input scene, and avoids the precise positioning otherwise required in matched filter based correlators. Although the classical JTC provides many attractive advantages over matched filter based correlators, it is found to suffer from large correlation sidelobes, large correlation width, strong zero order peak (or dc term) and low optical efficiency.

To improve the quality of the classical JTC, a binary JTC was introduced, where the joint power spectrum (JPS) is binarized based on a hard-clipping nonlinearity at the Fourier plane to only two values before applying the inverse Fourier transform operation [20-22]. It gives high correlation peak intensity, high correlation discrimination ratio and narrow correlation width. A binary JTC however involves computation intensive Fourier plane joint power spectrum (JPS) binarization, which limits the system processing speed [23]. For multi-object input scenes, in particular, the JPS binarization process introduces harmonic correlation peaks, which may cause spurious correlation peaks and, thus, result in misses and thereby complicating the target detection process [24-25]. In addition, a binary JTC does not completely overcome the problem of producing a strong zero-order term at the output plane.

More recently, Tang *et al.* proposed a chirp-encoded JTC, which requires multiple spatial light modulators for the input planes (to display the reference and the input scene) as well as multiple detectors for the output planes [26]. Thus, a large space-bandwidth product may be required for the chirp-encoded JTC especially for multiple target detection.

To improve the performance of the JTC some dc or zero order term elimination techniques have been proposed in the literature [27-30]. Phase shifting schemes have been used to eliminate the zero order and to improve the poor detection efficiency [31]. A new class of JTCs, which employ Fourier plane JPS apodization based on the reference image, has been found to yield better correlation output than both classical and binary JTCs. For instance, Feng *et al.* proposed the amplitude-modulated JTC, which yields better correlation output than the classical and binary JTCs but suffers from practical implementation difficulties especially if the power spectrum of the reference image contains zeros or very small values [32].

However, the above-mentioned JTCs still produce relatively broad correlation profiles, which hinder their application to multi-target detection. JTCs also suffer from high sensitivity to distortions in the input image. To yield sharper correlation peaks, one of the recent apodization based approaches is the use of a fringe-adjusted JTC based on Newton-Raphson algorithm [33]. It avoids many problems otherwise associated with the alternate JTC techniques. The fringe-adjusted JTC employs a real-valued filter called fringe-adjusted filter (FAF) at the Fourier plane and is found to yield significantly better correlation performance when compared to the existing JTCs. In the fringe-adjusted JTC the JPS is multiplied by FAF before applying the inverse Fourier transform to yield the correlation output. The fringe-adjusted JTC yields better correlation performance than alternate JTCs for the case of noise-free single target and multi-target binary input scenes under normal as well as poor illumination conditions [34]. However, for noise corrupted input scenes, whenever the reference power spectrum contains very low values ($|R(u,v)|^2 \cong 0$), a fringe-adjusted JTC has been found to yield low correlation peak intensity.

To overcome this limitation, a fractional power fringe-adjusted JTC has been developed for single target detection, which employs a family of real-valued filters, called generalized fringe-adjusted filters (GFAF) [35]. By adjusting a parameter (m), one can obtain classical JTC ($m = 0$), fringe-adjusted JTC ($m = 2$) or phase-only JTC ($m = 1$) for various practical applications without actually fabricating these complex-valued filters. The phase-only JTC has been found to be more tolerant with respect to the input scene noise. It may be mentioned that if matched filter based correlators are used to achieve classical matched filtering, inverse filtering and/or phase-only filtering, a complex filter must be fabricated beforehand and the filter must be replaced by another filter to detect a new target.

A number of various other non-linear joint transform correlation have been proposed for optical pattern recognition among which all-optical photo refractive crystal based JTC have been found to be particularly attractive [36-39]. For efficient multiple target detection several phase encoding techniques have been proposed [40-43]. Phase encoding operation gives excellent correlation output, especially for input scenes involving multiple identical targets and non-targets. As it uses separate input and reference planes and yields one peak per target instead of a pair of peaks produced by alternate JTCs, it ensures better utilization of space-bandwidth.

1.5 Distortion Invariant Pattern Recognition

A desired target in an input scene may be distorted or corrupted in many different ways. It may be in-plane or out-of-plane rotation, scale variation or shifting of position of an object. Clutter, noise, obscuration and low illumination are some of the other contributing factors of distortion. Many methods for invariant recognition have been proposed by using transform coefficient features, algebraic features, visual features, moment-based methods and synthetic discriminant function based methods.

Moment invariant methods are found to be effective in obtaining full geometrical invariance, such as rotation and translation [44-45]. Moment invariant method is often utilized for invariant character recognition [46-47]. The disadvantage of moment invariant method is the relatively time consuming computation and its inaminability of optical implementation. It also falls short of expectation in case of noise degradation. Circular harmonic (CH) method has been well utilized to deal with the issue of rotation invariant recognition [48-49]. The technique equivalent to CH is the Mellin radial harmonics, which was employed for scale invariant recognition [50]. Fourier Mellin descriptors and Fang's self-transform employ the pattern itself in the Kernel of a transform that is invariant to objects scale, rotation and translation variations [51-52]. Log-polar mapping is another popular method by which object scale and orientation can be transformed into translation [53].

Basic synthetic discriminant function (SDF) based technique uses a training set of distorted images, which are assumed to be representative of possible distortion [54]. The minimum variance synthetic discriminant filter (MVSDF) and minimum average correlation energy filter (MACE) are examples of two such composite filter fabrications [55-56]. Several researchers have used synthetic discriminant function for distortion invariant pattern recognition [57-58]. Javidi successfully applied the SDF formulation in a bipolar nonlinear JTC whereby SDF was used as the reference [59]. More recently a rotation-invariant fringe-adjusted joint transform correlation system and a distortion-invariant fractional power fringe-adjusted joint transform correlation system have been proposed [60-61]. A modification of the SDF algorithm has been proposed recently named projection slice SDF to create a matched filter pattern recognition system capable of discerning in-plane and out of plane 3D distortions [62]. Wavelet transformation and neural networks have also been investigated recently with promising results for distortion invariant pattern recognition [63-66].

1.6 Class-associative Pattern Recognition

Sometimes a class of similar or dissimilar objects needs to be detected from a group of different objects. For classification of objects from a given class, recently proposed filter-based techniques utilized phase information from the Fourier transform of each of the objects in that class. In this case consequent addition of objects requires a change in the phase of the filter. Casasent and Telfer proposed a pattern recognition technique that can perform hetero association based pattern recognition [67]. Later Khoury *et al.* proposed a new class-associative filter using cross-correlation enhancement. This algorithm has the advantage of adding additional objects by changing only the amplitude of the filter, i.e., it is phase restricted. In this technique the phase may result from an object of one class or even from an object that may be completely different from the classification set of objects [68]. The hetero-correlation techniques are used to classify hetero-associative or class-associative sets of objects. More recently a class-associative target detection technique has been proposed by using a new multi-target detection algorithm [69]. Here an enhanced version of the fringe-adjusted filter called class-associative fringe-adjusted filter (CFAF) has been developed to perform the class-associative multiple target detection. Implementation of the new multi-target detection algorithm optimizes the correlation performance by yielding only one correlation peak per target instead of pair of peaks produced by alternate JTCs.

1.7 Objective of the Thesis

Though distortion invariant recognition has been made for single or multiple target of same object, still no work has been reported on distortion invariant optical target recognition for a class of objects. Moreover no clear evidence is found for the class recognition of gray level images and detection of the class in noisy scene.

The main objective of this work is to develop a method for getting distortion-invariant class associative target recognition for both binary and gray level images. For this a simplified but efficient method of formulating SDF is presented using the JTC technique to get mainly rotation and scale invariant recognition. By combining the above-mentioned SDF and the multi-target detection algorithm a class detection technique will be adopted which will be able to detect the objects of a class of similar or dissimilar objects. It will also give equal correlation peak for all the targets in the class whether the targets are distorted or undistorted and whether there is noise in the input scene or not.

1.8 Thesis Outline

This thesis consists of six chapters. In this chapter some introduction on optical pattern recognition has been given, especially on joint transform correlation. Also brief introductions on the theories and problems related to this work along with the indication of the aim of this work have been given. Chapter 2 deals with joint transform correlation in details. Classical JTC, fringe-adjusted JTC and fractional power fringe-adjusted JTC are analyzed there with theory and simulation. Chapter 3 deals with the theory and simulation of multi-target detection algorithm, which is the basis for class-associative target detection technique used in this work. Application of this theory to class detection has also been shown. Chapter 4 deals with the formulation and simulation of a simplified SDF generation technique for the distortion invariant target detection. Chapter 5 is mainly based on simulation. Here the application of SDF has been shown to get distortion-invariant class-associative target detection. Chapter 6 is the final chapter giving a conclusive remark on this work along with a suggestion of future work in this area.

Chapter 2

JOINT TRANSFORM CORRELATOR

2.1 Introduction

Joint transform correlator (JTC) is one of the two major techniques of optical pattern recognition. In a JTC, the unknown input scene and the known reference image is displayed side-by-side in the input plane, illuminated by a coherent, collimated laser beam. The input joint image plane is located at a distance of one focal length from a lens, which Fourier transforms the input joint image at the Fourier plane. The Fourier transformed patterns constructively interfere with each other to create an interference pattern called joint power spectrum (JPS). This interference pattern is recorded in real time using a square law device such as a CCD camera. The joint power spectrum is inverse Fourier transformed by another Fourier transform lens to yield the correlation output. For a match, two correlation peaks or bright spots are produced and for a mismatch, negligible or no correlation peaks are produced. Several modification and/or improvement have been made on the JTC techniques. In this chapter the classical JTC and fringe-adjusted JTC are discussed along with the effect of Fourier plane image subtraction.

2.2 Classical Joint Transform Correlator

A classical JTC architecture is shown in Fig. 2.1, where the reference and the input scene are introduced in the input plane using a spatial light modulator (SLM) such as a liquid crystal television illuminated by a laser light source. The combined light distribution passes through the first Fourier lens L1. The complex light distribution is read by a square-law device at the back-focal plane of L1 and then introduced at lens L2 that gives the inverse Fourier transform. Thus the correlation output is obtained at the back focal plane of the lens L2. In this section theory and simulation of classical JTC will be discussed first for single target detection and then for multiple target detection.

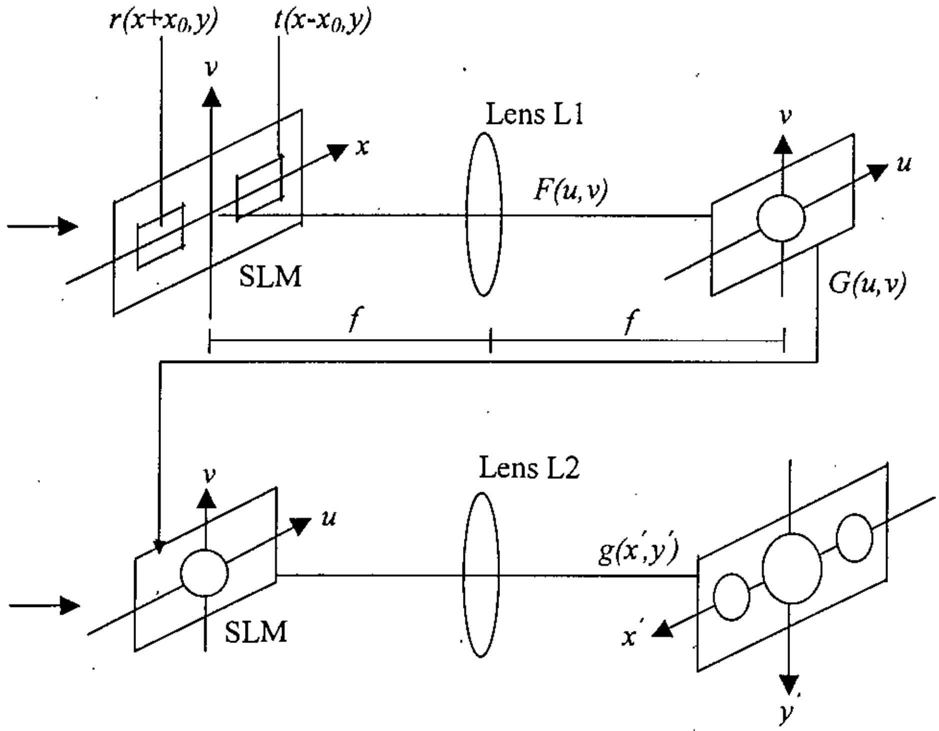

Fig. 2.1 A classical JTC scheme

2.2.1 Single Target Detection

2.2.1.1 Theoretical Analysis

Let us assume that $r(x+x_0, y)$ represents the reference image and $t(x-x_0, y)$ represents the input image which are separated by a distance $2x_0$ along the x-axis. Then the input joint image may be expressed as

$$f(x,y) = r(x+x_0, y) + t(x-x_0, y) \tag{2.1}$$

The Fourier transform of the input joint image, produced by lens L1 is given by

$$F(u,v) = R(u,v)\exp(jux_0) + T(u,v)\exp(-jux_0) \tag{2.2}$$

where $R(u,v)$ and $T(u,v)$ are the Fourier transforms of $r(x,y)$ and $t(x,y)$ respectively, u and v are mutually independent frequency-domain variables scaled by a factor $2\pi/\lambda f$, where, λ is the wavelength of the collimating light and f is the focal length of the Fourier transforming lenses L1 and L2. The intensity of the complex light distribution produced in the back focal plane of L1, i.e., the JPS, is then detected by a square-law detector such as the charge coupled device (CCD) array and is given by

$$G(u,v) = |F(u,v)|^2 = F(u,v)F^*(u,v)$$
$$= |R(u,v)|^2 + |T(u,v)|^2 + R(u,v)T^*(u,v)\exp(j2ux_0) \qquad (2.3)$$
$$+ R^*(u,v)T(u,v)\exp(-j2ux_0)$$

In a classical JTC, this JPS is introduced into a second SLM, which is illuminated by the same laser using a beam splitter and mirror combination. Lens L2 performs the inverse Fourier transform of the JPS to yield the correlation output. The final complex light distribution at the final output plane becomes

$$\begin{aligned} g(x',y') &= r(x',y') \otimes r^*(x',y') + t(x',y') \otimes t^*(x',y') \\ &\quad + r(-x'-2x_0,-y') \otimes t^*(-x',-y') + r^*(x'-2x_0,y') \otimes t(x',y') \end{aligned} \qquad (2.4)$$

Where ⊗ denotes correlation operation. At the output plane we have correlation terms in three different positions. It is evident that the first two terms on the right hand side in Eq. (2.4) are dc terms or the zero-order diffractions at the origin of the output plane. The last two terms, representing the two cross-correlation terms between the reference image and the input image object, produce the desired cross-correlation, around (0, $-2x_0$) and (0, $2x_0$), respectively.

2.2.1.2 Simulation

To analyze the performance of the classical JTC for single target in the input scene, a binary input image such as English alphabet 'E' of size 32x32 pixels has been taken as the target, which is placed in a 256x256 pixel zero-padded input scene. The reference image, 'E' is placed in the middle of the same 256x256 pixel zero-padded matrix to ensure the desired location of the correlation output. Thus the peaks in the output plane are organized in such a way that they can accurately represent the position of the objects in the input scene $t(x,y)$. The computer simulation has been made by 2-D fast Fourier transform algorithm using MATLAB software with its image processing toolbox.

In Fig. 2.2(a) the center of the 32x32 pixel reference image is placed at the position (x=129, y=129) of the 256x256 pixel image matrix and that of the input image is placed at the position (x=49, y=129) of the same image matrix.

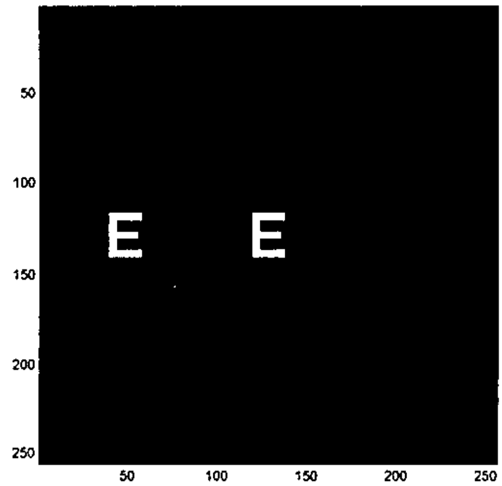

(a)

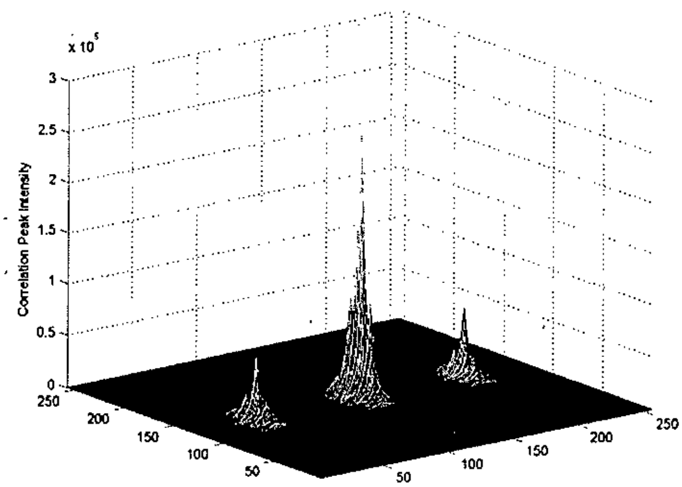

(b)

Fig. 2.2 (a) Input joint image with desired target (target at the left and reference at the center), (b) Correlation output.

From the correlation output of Fig. 2.2(b) for the joint input image in Fig 2.2(a) it is observed that there is a strong zero order peak at the center (129, 129) and a pair of cross-correlation peak indicating the presence of the target. The position of the two cross-correlation peaks are at positions (129, 49) and (129, 209), where the first one is at the exact location of the target and the another one is at mirror position of the target. Locations of the correlation peaks actually depend on the relative placement of the input and reference image in the joint image. As in this example the reference is placed at the center (x_0=0), the cross-correlation peaks are obtained at the exact location of the target with respect to reference.

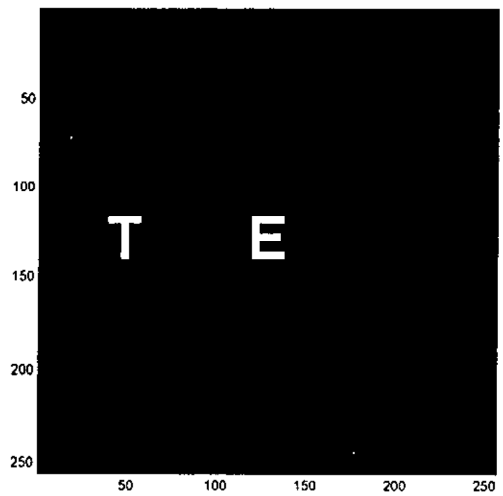

(a)

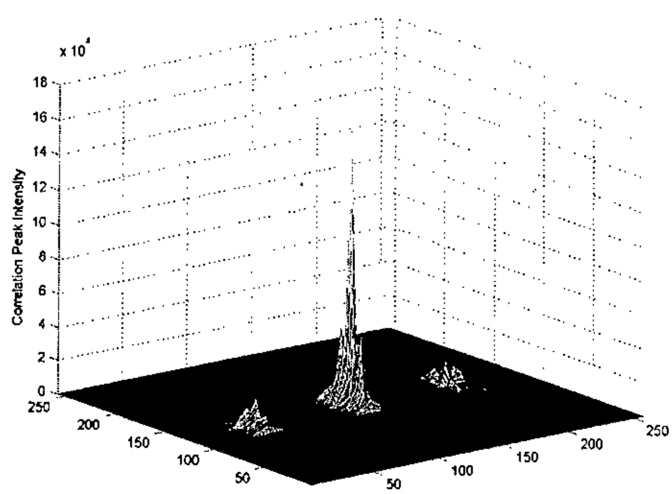

(b)

Fig. 2.3 (a) Input joint image with non-target (non-target at the left and reference at the center), (b) Correlation output.

The same analysis has been made with a non-target image 'T' with the same reference image 'E' as shown in Fig. 2.3. In this case a pair of correlation peaks is obtained for the non-target, but with negligible peak intensity.

From both Fig. 2.2 and Fig. 2.3 it is evident that a dc term or zero-order diffraction is obtained at the center of the output plane with very high correlation peak intensity compared to the target peaks which deteriorates the detection performance and lowers the optical efficiency. For both cases a pair of cross-correlation peak is presented at the same location in the correlation output plane though the height of those peaks differ much between two cases. The existence of any cross-correlation peak provides the information about the presence of any object in the input scene while the height of the cross-correlation peak indicates the degree of similarity between the reference image and the objects present in the input scene.

2.2.2 Multiple Target Detection

2.2.2.1 Theoretical Analysis

If $r(x,y+y_0)$ represents the reference image and $t(x-x_i,y-y_i-y_0)$ represents the input scene containing n objects $t_1(x - x_1, y - y_1 - y_0)$, $t_2(x - x_2, y - y_2 - y_0)$, ..., $t_n(x - x_n, y - y_n - y_0)$ respectively, and if the input scene is also assumed to be corrupted by noise $n(x,y-y_0)$, the input joint image becomes

$$f(x,y) = r(x,y+y_0) + \sum_{i=1}^{n} t_i(x-x_i, y-y_i-y_0) + n(x,y-y_0) \tag{2.5}$$

Referring to Fig. 2.1, lens L1 performs Fourier transform of the input joint image given by Eq. (2.5). The intensity of the complex light distribution produced in the back focal plane of L1, called the JPS, is then detected by a square-law detector and is given by Eq. (2.6), where, $|R(u,v)|$, $|T_i(u,v)|$ and $|N(u,v)|$ are the amplitudes, and $\phi_r(u,v)$, $\phi_{ti}(u,v)$ and $\phi_n(u,v)$ are the phases of the Fourier transforms of $r(x,y)$, $t_i(x,y)$, and $n(x,y)$ respectively, u and v are mutually independent frequency-domain variables scaled by a factor $2\pi/\lambda f$, λ is the wavelength of the collimating light and f is the focal length of the Fourier transforming lenses L1 and L2.

$$\begin{aligned}|F(u,v)|^2 &= |R(u,v)|^2 + \sum_{i=1}^{n}|T_i(u,v)|^2 + |N(u,v)|^2 \\ &+2\sum_{i=1}^{n}|T_i(u,v)||R(u,v)|\cos[\phi_{ti}(u,v)-\phi_r(u,v)-ux_i-vy_i-2vy_0] \\ &+2|R(u,v)||N(u,v)|\cos[\phi_r(u,v)-\phi_n(u,v)+2vy_0)] \\ &+2\sum_{i=1}^{n}|T_i(u,v)||N(u,v)|\cos[\phi_{ti}(u,v)-\phi_n(u,v)-ux_i-vy_i] \\ &+2\sum_{i=1}^{n-1}\sum_{k=i+1}^{n}|T_i(u,v)||T_k(u,v)|\cos[\phi_{ti}(u,v)-\phi_{tk}(u,v)-ux_i+ux_k-vy_i+vy_k]\end{aligned} \tag{2.6}$$

The first three terms of Eq. (2.6) result to the zero-order peak, the fourth term result to the desired cross-correlation between the reference image and the input scene objects, the fifth and sixth terms to the cross-correlation between the reference image and the noise term and the input scene objects and noise term respectively and the last term to the cross-correlations between the different input scene objects. If multiple identical targets are present in the input scene, then in addition to the desired autocorrelation peaks between the reference and the targets, other correlation peaks will be produced due to the autocorrelation between the targets themselves [corresponding to the last term of Eq. (2.6)], which yield false correlation peaks (called false alarms) in the output plane. Such false alarms may be avoided by eliminating the cross-correlation terms among the different input scene objects.

$$\begin{aligned}g(x',y') &= r(x',y')\otimes r^*(x',y') + \sum_{i=1}^{n} t_i(x',y')\otimes t_i^*(x',y') \\ &+ n(x',y')\otimes n^*(x',y') + \sum_{i=1}^{n} r(-x'-x_i,-y'-y_i-2y_0)\otimes t_i^*(-x',-y') \\ &+ \sum_{i=1}^{n} r^*(x'-x_i,y'-y_i-2y_0)\otimes t_i(x',y') \\ &+ r(-x',-y'+2y_0)\otimes n^*(-x',-y') + r^*(x',y'+2y_0)\otimes n(x',y') \\ &+ \sum_{i=1}^{n} n(-x'-x_i,-y'-y_i)\otimes t_i^*(-x',-y') \\ &+ \sum_{i=1}^{n} n^*(x'-x_i,y'-y_i)\otimes t_i(x',y') \\ &+ \sum_{i=1}^{n-1}\sum_{k=i+1}^{n} t_i(-x'-x_i+x_k,-y'-y_i+y_k)\otimes t_k^*(-x',-y') \\ &+ \sum_{i=1}^{n-1}\sum_{k=i+1}^{n} t_i^*(x'-x_i+x_k,y'-y_i+y_k)\otimes t_k(x',y')\end{aligned} \tag{2.7}$$

In a classical JTC, the JPS expressed by Eq. (2.6) is directly introduced into a second SLM, which is illuminated by the same light source using beam splitter and mirror.

Lens L2 performs the inverse Fourier transform of the JPS to yield the correlation output. The final complex light distribution at the final output plane becomes as that of Eq. (2.7), where ⊗ denotes correlation operation. First three terms of Eq. (2.7) denote the correlation terms at the center of output plane. These are the dc terms or zero-order diffractions due to auto-correlation for the reference image, input scene objects and noise term. Fourth and fifth terms give the desired cross-correlation between the reference image and the input scene objects, which also give the locations of the objects in the input scene. Sixth and seventh terms give the undesired cross-correlation between the reference and the noise term. The rest terms are the autocorrelation among the different desired and undesired objects in the input scene.

2.2.2.2 Simulation

To simulate the performance of classical joint transform correlator in case of multiple objects (target and non-targets) present simultaneously in the input scene the same 256x256 zero-padded image matrix is taken for the input scene. Here as usual the alphabet 'E' is placed as the reference image at the center of the input plane as shown in Figs. 2.4(a), 2.5(a) and 2.6(a). Three cases have been shown for three combinations of input objects.

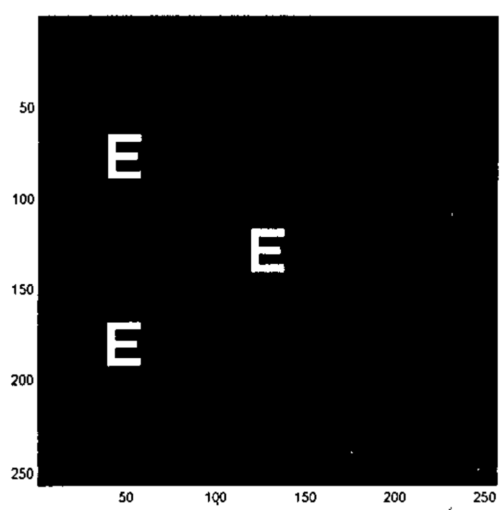

(a)

Fig. 2.4 (a) Input joint image with identical targets (targets at the left and reference at the center).

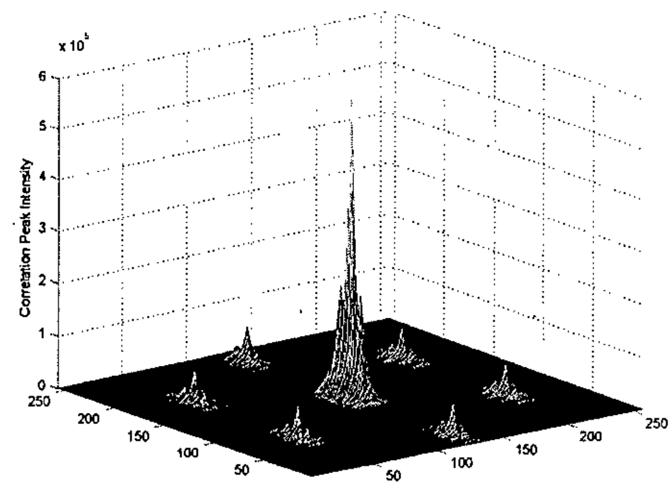

(b)

Fig. 2.4 (contd.) (b) Correlation output.

Case 1: Two target images 'E' are the input objects placed at the left column of the input plane as shown in Fig. 2.4(a). The joint image of Fig 2.4(a) has been processed to find the correlation output of Fig. 2.4(b). The correlation output shows a strong zero-order peak at the center. Two pairs of cross-correlation peaks indicate two target images. But another pair of autocorrelation peaks between the targets produces a false alarm and thus obscures the detection.

Case 2: One target image 'E' and one non-target image 'O' are the input objects placed at the left column of the input plane as shown in Fig. 2.5(a). The joint image of Fig 2.5(a) has been processed to find the correlation output of Fig. 2.5(b). The correlation output gives strong zero-order diffraction at the center, a pair of cross-correlation peaks for the target, a pair of cross-correlation peaks for the non-target (which is smaller than the peaks for the target) and a pair of autocorrelation peaks between the target and non-target.

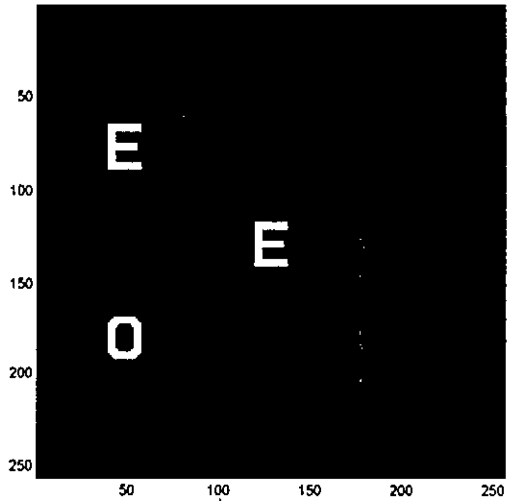

(a)

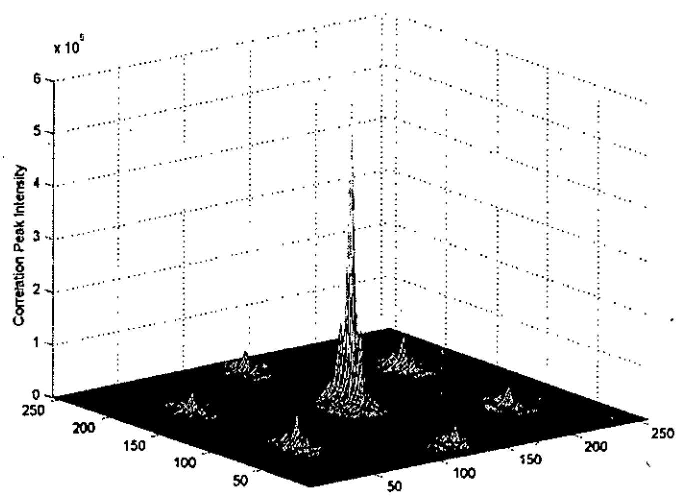

(b)

Fig. 2.5 (a) Input joint image with one target and one non-target (target and non-target at the left and reference at the center), (b) Correlation output.

Case 3: Multiple target images and multiple non-target images are the input objects placed at the left column of the input plane as shown in Fig. 2.6(a). The joint image of Fig 2.6(a) has been processed to find the correlation output of Fig. 2.6(b). The correlation output shows strong zero-order diffraction at the center, several cross-correlation peaks for the targets and non-targets and several false alarms due to auto-correlation among the targets and non-targets. Here it is quite difficult to find the location of the actual target images in the input scene due to presence of considerable peak intensity of the false alarms relative to the desired cross-correlation peaks.

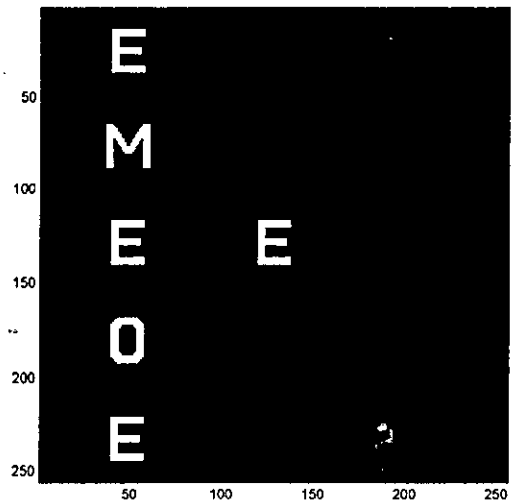

(a)

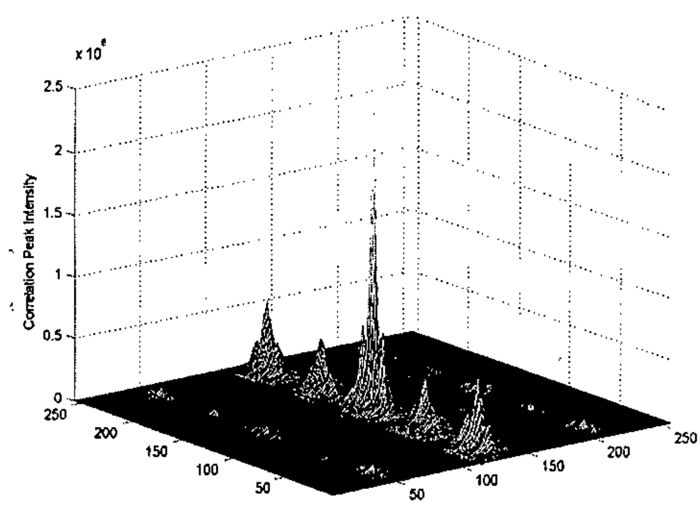

(b)

Fig. 2.6 (a) Input joint image with multiple identical targets and multiple non-targets (targets and non-targets at the left and reference at the center), (b) Correlation output.

From case 1 to case 3 it is clear that as the number of simultaneous targets and/or non-targets increases in the input scene, the zero-order diffraction and the false alarms make the detection impossible in a classical JTC.

2.3 Classical Joint Transform Correlator with Fourier-plane Image Subtraction

2.3.1 Theoretical Analysis

If the zero-order terms are removed from the joint power spectrum in Eq. (2.3) for the single object input scene, the on-axis correlation distribution can be avoided. Since the zero-order correlation are derived from the power spectra of $t(x,y)$ and $r(x,y)$, respectively, these terms can be eliminated from the recorded JPS. For example, the power spectral distributions of $|T(u,v)|^2$ and $|R(u,v)|^2$ can be recorded before the joint transform operation, then these two zero-order power spectra can be removed by the computer before being sent to the correlation cycle. After subtracting these two terms from Eq. (2.3), the JPS for single object input scene becomes

$$\begin{aligned} P_s(u,v) &= |F(u,v)|^2 - |R(u,v)|^2 - |T(u,v)|^2 \\ &= R(u,v)T^*(u,v)\exp(j2ux_0) + R^*(u,v)T(u,v)\exp(-j2ux_0) \end{aligned} \tag{2.8}$$

Now inverse Fourier transform of Eq. (2.8) gives the final correlation output light distribution as

$$g_s(x',y') = r(-x'-2x_0,-y') \otimes t^*(-x',-y') + r^*(x'-2x_0,y') \otimes t(x',y') \tag{2.9}$$

In Eq. (2.9) there are only the cross correlation terms between the reference and the target image of the input scene.

In the same way for multi-object input the zero-order correlations are derived from the power spectra of $r(x,y+y_0)$, $t_1(x - x_1, y - y_1-y_0)$, $t_2(x - x_2, y - y_2-y_0)$, ..., $t_n(x - x_n, y - y_n-y_0)$ and $n(x,y-y_0)$ respectively. By subtracting the reference image only power spectra and input scene only power spectra from the JPS of Eq. (2.6) we get the modified JPS for multi-object input scene as

$$\begin{aligned} P_m(u,v) &= |F(u,v)|^2 - |R(u,v)|^2 - \sum_{i=1}^{n}|T_i(u,v)|^2 \\ &= 2\sum_{i=1}^{n}|T_i(u,v)||R(u,v)|\cos[\phi_{ti}(u,v) - \phi_r(u,v) - ux_i - vy_i - 2vy_0] \\ &\quad + 2|R(u,v)||N(u,v)|\cos[\phi_r(u,v) - \phi_n(u,v) + 2vy_0)] \end{aligned} \tag{2.10}$$

Inverse Fourier transform of Eq. (2.10) gives the correlation output for the multi-object input scene as expressed below

$$\begin{aligned} g_m(x',y') &= \sum_{i=1}^{n} r(-x'-x_i,-y'-y_i-2y_0)\otimes t_i^*(-x',-y') \\ &+\sum_{i=1}^{n} r^*(x'-x_i,y'-y_i-2y_0)\otimes t_i(x',y') \\ &+r(-x',-y'+2y_0)\otimes n^*(-x',-y')+r^*(x',y'+2y_0)\otimes n(x',y') \end{aligned} \tag{2.11}$$

In Eq. (2.11) also there are only the cross-correlation terms between the reference and the input scene objects.

The above process of subtracting the reference power spectra and input power spectra from the joint power spectra at the Fourier plane is known as Fourier-plane image subtraction technique. The subtraction operation eliminates the zero-order terms as well as the false alarms generated by similar input targets and the cross-correlation terms among the other objects that may be present in the input scene.

2.3.2 Simulation

Fourier plane image subtraction technique to remove the zero order correlation peak and the unwanted false alarms has been examined for the same joint image with multiple targets and non-targets that has been used previously and is shown here again in Fig. 2.7(a) for convenience. The correlation output is shown in Fig. 2.7(b). From the correlation output of Fig. 2.7(b) it is seen that the zero order diffraction and the unwanted false alarms are completely eliminated. So there are only the pairs of conjugate cross-correlation peaks for the input scene objects. The desired target peaks are of higher intensity and the non-target peaks are of lower intensity as seen in the figure.

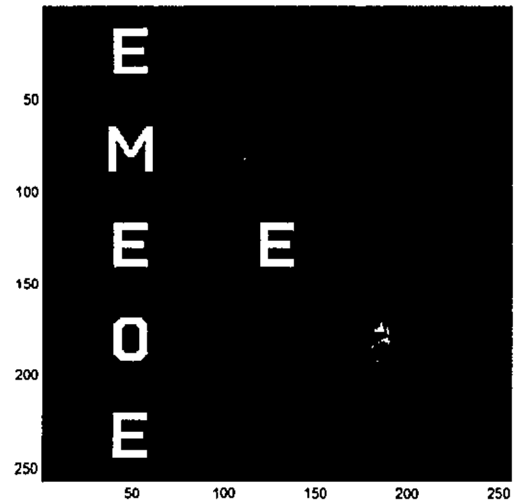

(a)

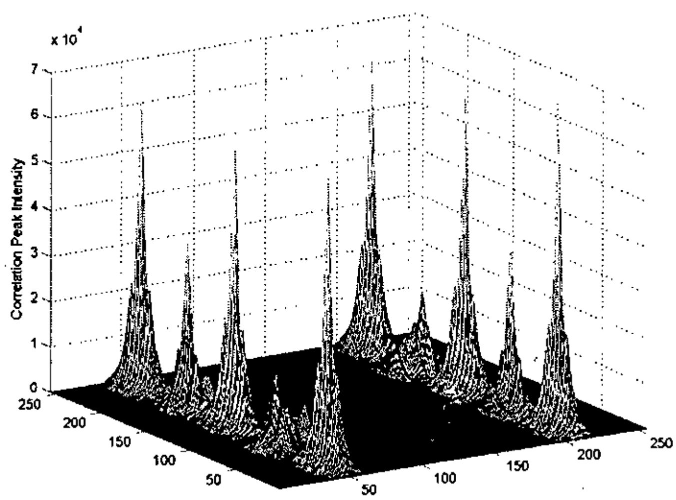

(b)

Fig. 2.7 (a) Input joint image with multiple identical targets and multiple non-targets (targets and non-targets at the left and reference at the center), (b) Correlation output after Fourier plane image subtraction.

The Fourier plane image subtraction thus eliminates the unwanted peaks and permits more clear identification of the objects in the input scene. Besides, it helps efficient utilization of the input pixels. In other words, the reference object and the input scene can be located as closely as we wish. But still large correlation width and large correlation side-lobes lowers the optical efficiency of the detection scheme.

2.4 Fringe-adjusted Joint Transform Correlator with Fourier Plane Image Subtraction

2.4.1 Theoretical Analysis

The fringe-adjusted JTC (FJTC) has been found to yield better correlation performance compared to the alternate JTCs for single/multiple target detection under various illumination conditions of the input scene [33]. In FJTC the joint power spectrum (JPS) is multiplied by a filter called fringe-adjusted filter (FAF) before applying the inverse Fourier transform. The FAF used in a fringe-adjusted JTC is defined as

$$H_{faf}(u,v) = \frac{C(u,v)}{D(u,v) + |R(u,v)|^2} \tag{2.12}$$

where $C(u,v)$ and $D(u,v)$ are either constants or functions of u and v. When $C(u,v)$ is properly selected, one can avoid having an optical gain greater than unity. With very small values of $D(u,v)$, the pole problem otherwise associated with an inverse filter is overcome, and it is still possible to obtain a large auto-correlation peak. When $D(u,v) << |R(u,v)|^2$, $C(u,v)=1$, Eq. (2.12) may be approximated as $H_{faf}(u,v) \approx |R(u,v)|^{-2}$. The function $C(u,v)$ can also be used to suppress noise or band limit the signal or both. Thus, in the fringe-adjusted JTC, amplitude matching can be implemented more effectively to yield sharper and larger correlation peak intensity. When $C(u,v) = 1$ and $D(u,v) << |R(u,v)|^2$, the FAF becomes a perfect real-valued inverse filter function unlike the VanderLugt filter, which consists of both magnitude and phase terms. Therefore, the FAF is more suitable for practical implementation. The computation associated with the FAF can be completed before the input scene is actually introduced into the input plane. So, the use of this additional filter may not have any detrimental effect on the system processing speed.

For the single-object input scene the fringe-adjusted JPS is obtained by multiplying the JPS of Eq. (2.3), by $H_{faf}(u,v)$ and is thus given by

$$G_f(u,v) = H_{faf}(u,v) \times |F(u,v)|^2 \approx |R(u,v)|^{-2} \times |F(u,v)|^2 \tag{2.13}$$

Assuming that the reference is the same as the input image, Eq. (2.13) may be rewritten as

$$\begin{aligned} G_f(u,v) &\approx |R(u,v)|^{-2} \times |R(u,v)|^2[2+\exp(j2ux_0)+\exp(-j2ux_0)] \\ &= 2[1+\cos(2ux_0)] \end{aligned} \tag{2.14}$$

An inverse Fourier transform of Eq. (2.14) yields the correlation output. The first term of Eq. (2.14) generates a delta-function-like zero-order term on the optical axis, flanked by the desired pair of delta-function-like auto-correlation outputs that are separated on the optical axis by a distance $2x_0$.

To include the Fourier plane image subtraction in case of single target input scene, modified fringe-adjusted JPS is obtained by multiplying the JPS of Eq. (2.8) by $H_{faf}(u,v)$ and is thus given by

$$G_{sn}(u,v) = H_{faf}(u,v) \times P_s(u,v) \approx |R(u,v)|^{-2} \times P_s(u,v) \tag{2.13}$$

For the multiple-object input scene the fringe-adjusted JPS is obtained by multiplying the JPS of Eq. (2.6), by $H_{faf}(u,v)$ and is thus given by

$$G_f(u,v) = H_{faf}(u,v) \times |F(u,v)|^2 \approx |R(u,v)|^{-2} \times |F(u,v)|^2 \tag{2.14}$$

To include the Fourier plane image subtraction in case of multiple target input scene, modified fringe-adjusted JPS is obtained by multiplying the JPS of Eq. (2.10) by $H_{faf}(u,v)$ and is thus given by

$$G_{mn}(u,v) = H_{faf}(u,v) \times P_m(u,v) \approx |R(u,v)|^{-2} \times P_m(u,v) \tag{2.15}$$

By applying inverse Fourier transform to the modified JPS ($G_{sn}(u,v)$ for single target case) given in Eq. 2.13 and ($G_{mn}(u,v)$ for multiple targets) given in Eq. 2.15, desired correlation can be obtained for single target and multi targets respectively.

2.4.2 Simulation

The simulation for the fringe-adjusted joint transform correlator has been performed with Fourier plane image subtraction so as to avoid the zero-order terms and unwanted false alarms. As a test frame the previously considered input scene with multiple identical targets and multiple non-targets has been taken where the reference image is placed at the center as shown in Fig. 2.8(a). The simulation has been done for various values of parameter $D(u,v)$ of the H_{faf}. Corresponding correlation output is shown in Fig. 2.8(b) to Fig. 2.8(e).

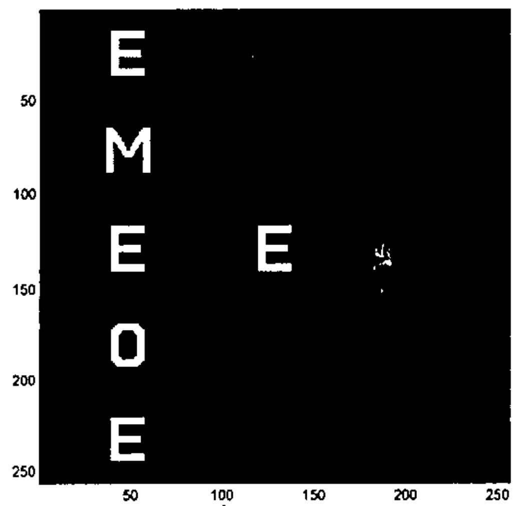

(a)

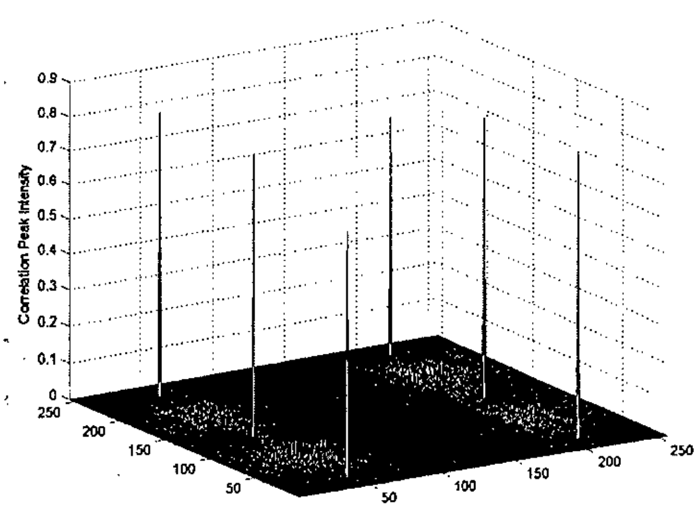

(b)

Fig. 2.8 (a) Input joint image with multiple identical targets and multiple non-targets (targets and non-targets at the left and reference at the center), (b) Correlation output using FAF filter ($C(u,v)=1$, $D(u,v)=10^{-1}$) with Fourier plane image subtraction.

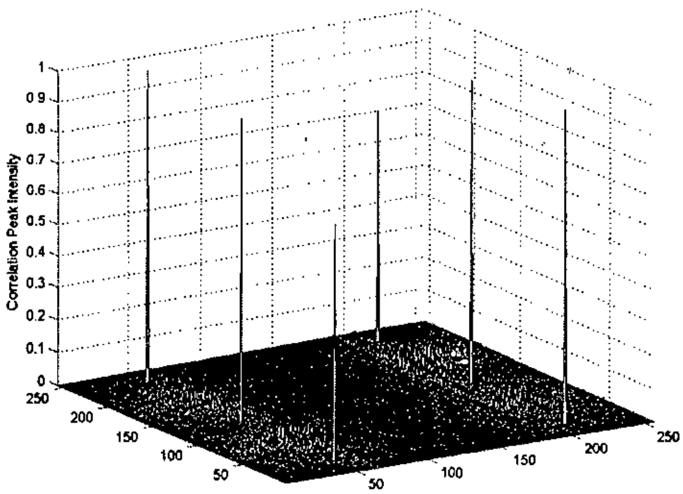

(c)

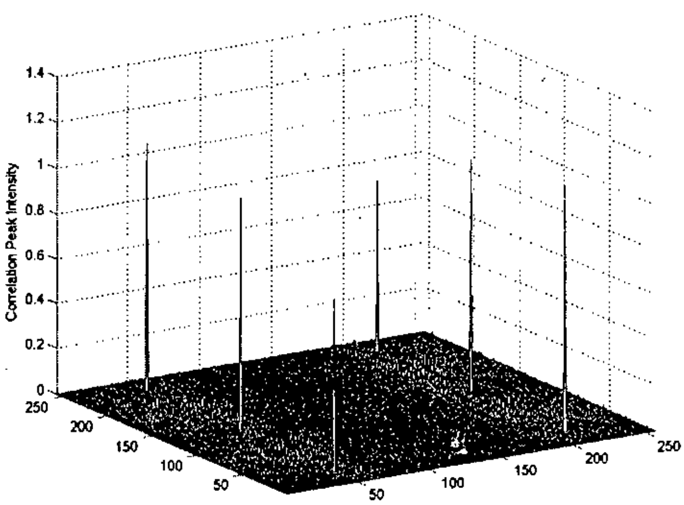

(d)

Fig. 2.8 (contd.) (c) Correlation output using FAF filter ($C(u,v)$ =1, $D(u,v)$ =10^{-2}) with Fourier plane image subtraction, (d) Correlation output using FAF filter ($C(u,v)$ =1, $D(u,v)$ =10^{-3}) with Fourier plane image subtraction.

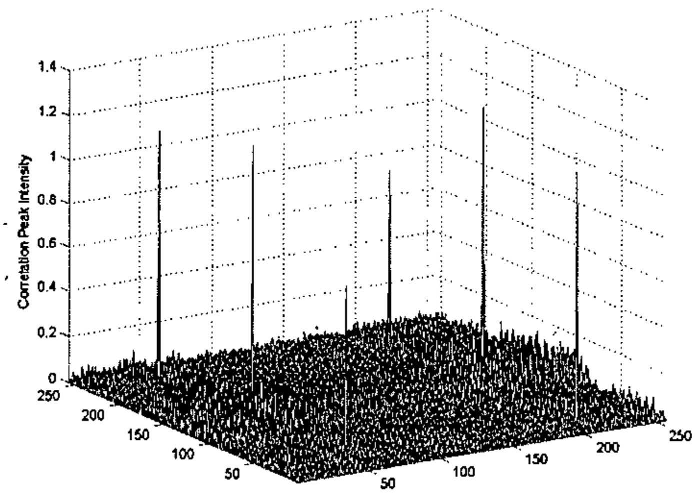

(e)

Fig. 2.8 (contd.) (e) Correlation output using FAF filter ($C(u,v)$ =1, $D(u,v)$ =10^{-6}) with Fourier plane image subtraction.

From the correlation output as shown in Fig. 2.8(b) to Fig. 2.8(e) it is observed that by using FAF filter sharp delta-function-like correlation peaks are obtained for the objects in the input scene. It also totally eliminates the correlation peaks for all the non-target objects in the scene and thus improves the detection efficiency significantly along with increasing the optical efficiency. The target peaks are almost of same intensity or height. For noise free input scene, as in this case, the FAF filter parameter $D(u,v)$ however plays an important role in the correlation output. As the value of $D(u,v)$ is reduced, the correlation performance deteriorates as can be understood by observing Fig. 2.8(b) through Fig. 2.8(e).

2.5 Fractional Power Fringe-adjusted Joint Transform Correlator

2.5.1 Theoretical Analysis

For noise-free input scenes, the fringe-adjusted JTC has been found to yield significantly better correlation output when compared to the alternate JTCs. However, for noisy input scenes, whenever the reference power spectrum contains very low values ($|R(u,v)|^2 \approx 0$), it may accentuate the noise component of the input scene, which may degrade the system performance. To overcome the aforementioned problems, and at the same time, to utilize the fringe-adjusted filter as a versatile tool for various practical applications, a fractional power fringe-adjusted JTC (FPFJTC) has been proposed also termed as generalized fringe-adjusted JTC (GFJTC) [35]. In this GFJTC a generalized fringe-adjusted filter (GFAF) is defined as

$$H_{gfaf}(u,v) = C(u,v)\left[D(u,v) + |R(u,v)|^{m}\right]^{-1} \tag{2.16}$$

where m is a constant, and $C(u,v)$ and $D(u,v)$ are either constants or functions of u and v. When $C(u,v)$ is properly selected, one can avoid having an optical gain greater than unity. With very small values of $D(u,v)$, the pole problem otherwise associated with an inverse filter is overcome. The JPS is multiplied by the GFAF before applying the inverse Fourier transform to obtain the correlation output. By adjusting the parameter m, a family of different types of real-valued filters can be achieved.

In Sec. 1.4.1, three major types of matched filters for optical correlation; namely, complex matched filter, inverse filter and phase-only filter have been discussed. The fabrication of all of those filters requires the phase information of the reference image, thus a complex filter must be fabricated beforehand to detect a target. But by using GFAF those filters can be achieved for various practical applications without actually fabrication those complex valued filters.

When $m = 0$, $D(u,v) = 0$ and $C(u,v) = 1$, the GFAF-based JTC corresponds to the classical JTC; when $m = 2$, $D(u,v) << |R(u,v)|^2$ and $C(u,v) = 1$, the GFAF-based JTC corresponds to the fringe-adjusted JTC or inverse filter based JTC; and when $m = 1$, $D(u,v) << |R(u,v)|$ and $C(u,v) = 1$, the GFAF-based JTC corresponds to the phase-only JTC. Corresponding filter functions may be expressed as

$$H^{c}_{gfaf} = 1 \tag{2.17}$$

$$H^{f}_{gfaf} = \frac{C(u,v)}{D(u,v) + |R(u,v)|^{2}} \tag{2.18}$$

$$H^{p}_{gfaf} = \frac{C(u,v)}{D(u,v) + |R(u,v)|} \tag{2.19}$$

where Eq. (2.17) is for classical JTC, Eq. (2.18) is for fringe-adjusted JTC and Eq. (2.19) is for phase-only JTC.

The aforementioned three cases correspond to the complex matched filtering ($m = 0$), inverse filtering ($m = 2$) and phase-only filtering ($m = 1$). Thus, all important types of matched filter based correlators can be implemented in real time using the fractional power fringe-adjusted JTC while avoiding the limitations of matched filter based correlators. For noise-free input scenes, the fringe-adjusted JTC yields the highest correlation output. However, for noise corrupted input scenes, the phase-only JTC yields better correlation output than the fringe-adjusted JTC.

2.6 Conclusion

Joint transform correlator is a versatile tool for optical pattern recognition. However classical JTC gives poor performance in the sense that it gives large correlation width, large sidelobes, strong zero order term and false alarms in case of multiple object input scene. So it is not suitable for multi-object case. On the other hand fringe-adjusted JTC gives sharper and larger correlation peaks for the targets, eliminates the non-target and provides the facility to adjust the gain. Fourier plane image subtraction eliminates the zero-order terms and the false alarms and thus facilitates the detection of objects from a multi-object input scene. Fractional power fringe-adjusted JTC provides three types of JTC, namely, classical JTC, fringe-adjusted JTC and phase-only JTC by changing the parameters of a generalized fringe adjusted filter (GFAF). According to the condition of the input scene or reference image, the required JTC can be chosen. In this thesis the concept of this Fractional power fringe-adjusted JTC has been used extensively.

Chapter 3

MULTI TARGET DETECTION ALGORITHM

3.1 Introduction

If the input scene consists of multiple identical objects, then in addition to the desired autocorrelation peaks between the reference and the targets, additional correlation peaks will be produced due to autocorrelation between identical input scene objects themselves, which will in turn yield false alarms. The exclusion of cross-correlation terms among the similar or dissimilar objects may overcome the possibility of false alarms. The undesired zero-order terms and the effects of input scene noise and clutter may also increase the chance of triggering false alarms. Fourier-plane image subtraction is one technique suitable to remove zero-order diffraction and the undesired false alarms. The aforementioned false alarms and the undesired zero-order terms can also be alleviated by using a new algorithm known as multi-target detection algorithm (MTDA) [69]. This algorithm ensures the detection and tracking of multiple similar or dissimilar targets. This technique is better than the image subtraction technique used in alternate JTCs in the sense that it yields only one peak per target instead of a pair of peaks. It ensures better utilization of the space-bandwidth product by using separate input and reference planes and by giving one peak per target. The main achievement of this algorithm is that it facilitates class-associative target detection [69].

3.2 Multi-target Detection

3.2.1 Theoretical Analysis

Consider a reference image, denoted by $r(x\,,\, y + y_0)$, and an input scene, denoted by $s(x,\, y - y_0)$, which contains n objects, $p_1(x - x_1,\, y - y_1 - y_0)$, $p_2(x - x_2,\, y - y_2 - y_0)$, …, and $p_n(x - x_n,\, y - y_n - y_0)$, embedded in noise $n(x,\, y - y_0)$. In the multi-target detection algorithm, the following combinations of the input joint image involving the reference image $r(x,y+y_o)$ and the unknown input scene $s(x,y-y_o)$ as shown in the following equations are taken.

$$\begin{aligned} f_1(x,y) &= r(x,y+y_o)+s(x,y-y_o) \\ &= r(x,y+y_o)+\sum_{i=1}^{n} p_i(x-x_i,y-y_i-y_o)+n(x,y-y_o) \end{aligned} \tag{3.1.a}$$

$$\begin{aligned} f_2(x,y) &= r(x,y+y_o)-js(x,y-y_o) \\ &= r(x,y+y_o)-j\sum_{i=1}^{n} p_i(x-x_i,y-y_i-y_o)-jn(x,y-y_o) \end{aligned} \tag{3.1.b}$$

$$\begin{aligned} f_3(x,y) &= r(x,y+y_o)-s(x,y-y_o) \\ &= r(x,y+y_o)-\sum_{i=1}^{n} p_i(x-x_i,y-y_i-y_o)-n(x,y-y_o) \end{aligned} \tag{3.1.c}$$

$$\begin{aligned} f_4(x,y) &= r(x,y+y_o)+js(x,y-y_o) \\ &= r(x,y+y_o)+j\sum_{i=1}^{n} p_i(x-x_i,y-y_i-y_o)+jn(x,y-y_o) \end{aligned} \tag{3.1.d}$$

Applying Fourier transform to Eq. (3.1), we get

$$\begin{aligned} F_1(u,v) &= |R(u,v)|\exp[j\phi_r(u,v)+jvy_o] \\ &+\sum_{i=1}^{n}|P_i(u,v)|\exp[(j\phi_{pi}(u,v)-jux_i-jvy_i-jvy_o] \\ &+|N(u,v)|\exp[(j\phi_n(u,v)-jvy_o] \end{aligned} \tag{3.2.a}$$

$$\begin{aligned} F_2(u,v) &= |R(u,v)|\exp\{j\phi_r(u,v)+jvy_o\} \\ &+\sum_{i=1}^{n}|P_i(u,v)|\exp\left\{j\phi_{pi}(u,v)-jux_i-jvy_i-jvy_o-j\frac{\pi}{2}\right\} \\ &+|N(u,v)|\exp\left\{j\phi_n(u,v)-jvy_o-j\frac{\pi}{2}\right\} \end{aligned} \tag{3.2.b}$$

$$\begin{aligned} F_3(u,v) &= |R(u,v)|\exp\{j\phi_r(u,v)+jvy_o\} \\ &-\sum_{i=1}^{n}|P_i(u,v)|\exp\{j\phi_{pi}(u,v)-jux_i-jvy_i-jvy_o\} \\ &-|N(u,v)|\exp\{j\phi_n(u,v)-jvy_o\} \end{aligned} \tag{3.2.c}$$

$$F_4(u,v) = |R(u,v)|\exp\{j\phi_r(u,v) + jvy_o\}$$
$$+\sum_{i=1}^{n}|P_i(u,v)|\exp\left\{j\phi_{pi}(u,v) - jux_i - jvy_i - jvy_o + j\frac{\pi}{2}\right\} \quad (3.2.d)$$
$$+|N(u,v)|\exp\left\{j\phi_n(u,v) - jvy_o + j\frac{\pi}{2}\right\}$$

where F_1, F_2, F_3 and F_4 are the Fourier transforms of f_1, f_2, f_3 and f_4 respectively. The corresponding joint power spectra can be expressed as

$$T_1(u,v) = |F_1(u,v)|^2 = |R(u,v)|^2 + \sum_{i=1}^{n}|P_i(u,v)|^2 + |N(u,v)|^2$$
$$+2\sum_{i=1}^{n-1}\sum_{k=i+1}^{n}|P_i(u,v)||P_k(u,v)|\cos[\phi_{pi}(u,v) - \phi_{pk}(u,v) - ux_i + ux_k - vy_i + vy_k]$$
$$+2\sum_{i=1}^{n}|P_i(u,v)||R(u,v)|\cos[\phi_{pi}(u,v) - \phi_r(u,v) - ux_i - vy_i - 2vy_o] \quad (3.3.a)$$
$$+2|R(u,v)||N(u,v)|\cos[\phi_r(u,v) - \phi_n(u,v) + 2vy_o]$$
$$+2\sum_{i=1}^{n}|P_i(u,v)||N(u,v)|\cos[\phi_{pi}(u,v) - \phi_n(u,v) - ux_i - vy_i]$$

$$T_2(u,v) = |F_4(u,v)|^2 = |R(u,v)|^2 + \sum_{i=1}^{n}|P_i(u,v)|^2 + |N(u,v)|^2$$
$$-2|R(u,v)|\,|N(u,v)|\,\sin[\phi_r(u,v) - \phi_n(u,v) + 2vy_o]$$
$$+2\sum_{i=1}^{n-1}\sum_{k=i+1}^{n}|P_i(u,v)||P_k(u,v)|\cos[\phi_{pi}(u,v) - \phi_{pk}(u,v) - ux_i + ux_k - vy_i + vy_k] \quad (3.3.b)$$
$$+2\sum_{i=1}^{n}|P_i(u,v)||R(u,v)|\sin[\phi_{pi}(u,v) - \phi_r(u,v) - ux_i - vy_i - 2vy_o]$$
$$+2\sum_{i=1}^{n}|P_i(u,v)||N(u,v)|\cos[\phi_{pi}(u,v) - \phi_n(u,v) - ux_i - vy_i]$$

$$T_3(u,v) = |F_3(u,v)|^2 = |R(u,v)|^2 + \sum_{i=1}^{n}|P_i(u,v)|^2 + |N(u,v)|^2$$
$$-2|R(u,v)|\,|N(u,v)|\,\cos[\phi_r(u,v) - \phi_n(u,v) + 2vy_o]$$
$$+2\sum_{i=1}^{n-1}\sum_{k=i+1}^{n}|P_i(u,v)||P_k(u,v)|\cos[\phi_{pi}(u,v) - \phi_{pk}(u,v) - ux_i + ux_k - vy_i + vy_k] \quad (3.3.c)$$
$$-2\sum_{i=1}^{n}|P_i(u,v)||R(u,v)|\cos[\phi_{pi}(u,v) - \phi_r(u,v) - ux_i - vy_i - 2vy_o]$$
$$+2\sum_{i=1}^{n}|P_i(u,v)||N(u,v)|\cos[\phi_{pi}(u,v) - \phi_n(u,v) - ux_i - vy_i]$$

$$
\begin{aligned}
T_4(u,v) = |F_2(u,v)|^2 = |R(u,v)|^2 + \sum_{i=1}^{n} |P_i(u,v)|^2 + |N(u,v)|^2 \\
+ 2|R(u,v)|\,|N(u,v)| \sin[\phi_r(u,v) - \phi_n(u,v) + 2vy_o] \\
+ 2\sum_{i=1}^{n-1}\sum_{k=i+1}^{n} |P_i(u,v)||P_k(u,v)| \cos[\phi_{pi}(u,v) - \phi_{pk}(u,v) - ux_i + ux_k - vy_i + vy_k] \\
- 2\sum_{i=1}^{n} |P_i(u,v)||R(u,v)| \sin[\phi_{pi}(u,v) - \phi_r(u,v) - ux_i - vy_i - 2vy_o] \\
+ 2\sum_{i=1}^{n} |P_i(u,v)||N(u,v)| \cos[\phi_{pi}(u,v) - \phi_n(u,v) - ux_i - vy_i]
\end{aligned}
\tag{3.3.d}
$$

Using the four expressions of Eq. (3.3), the modified JPS may be expressed as

$$
\begin{aligned}
T(u,v) &= T_1(u,v) + jT_2(u,v) - T_3 - jT_4 \\
&= 4\sum_{i=1}^{n} |P_i(u,v)||R(u,v)| \exp[j\phi_{pi}(u,v) - j\phi_r(u,v) - jux_i - jvy_i - 2jvy_o] \\
&\quad + 4|R(u,v)|\,|N(u,v)| \exp[-j\phi_r(u,v) + j\phi_n(u,v) - 2jvy_o]
\end{aligned}
\tag{3.4}
$$

The first term of Eq. (3.4) produces a delta-function-like correlation output corresponding to the desired input scene targets, whereas the remaining terms yield a negligible cross-correlation output between the reference and the non-target objects. The final correlation output can be obtained by applying inverse Fourier transform to the modified JPS of Eq. (3.4), given by

$$
\begin{aligned}
t(x',y') = 4\sum_{i=1}^{n} p_i(x'-x_i, y'-y_i-2y_o) \otimes r^*(x', y'+2y_o) \\
+ 4r(x', y'+2y_o) \otimes n^*(x', y'-2y_o).
\end{aligned}
\tag{3.5}
$$

From Eq. (3.5), it is evident that this technique effectively detects multiple targets and yields one correlation peak per target while alleviating the problems associated with alternate techniques.

The correlation output produced by the aforementioned algorithm can be further enhanced by utilizing the concept of fractional power fringe-adjusted JTC as described in section 2.5. The filter function GFAF used in a fractional power fringe-adjusted JTC is defined as

$$
H_{gfaf}(u,v) = \frac{C(u,v)}{D(u,v) + |R(u,v)|^m}
\tag{3.6}
$$

where $C(u,v)$ and $D(u,v)$ can be constants or functions of u and v, and $R(u,v)$ is the Fourier transform of the reference image. Depending upon the choice of $C(u,v)$, $D(u,v)$ and m, different types of filter namely classical JTC, fringe-adjusted JTC and phase-only JTC are achieved. The generalized fringe-adjusted JPS in multi-target detection algorithm is obtained by multiplying the filter H_{gfaf} with the JPS, expressed as

$$G_{mtda}(u,v) = H_{gfaf}(u,v) \times T(u,v) \tag{3.7}$$

where $T(u,v)$ corresponds to the modified JPS of Eq. (3.4). An inverse Fourier transform of the JPS of Eq. (3.7) yields single delta-function-like correlation output for each target in the input scene while yielding negligible or no correlation peaks for non-target objects.

3.2.2 Simulation

The above mentioned multi-target detection algorithm has been used to detect the targets of a multi-object input scene containing several target and non-target objects simultaneously in the input scene. Reference image (target) is shown in Fig. 3.1(a) and the input scene containing the objects are shown in Fig. 3.1(b).

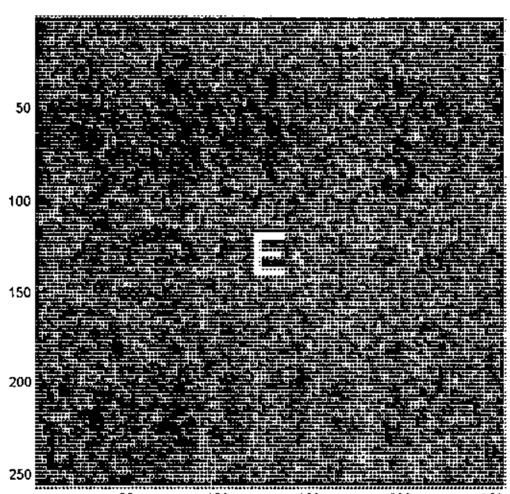

(a)

Fig. 3.1 (a) Reference image (target).

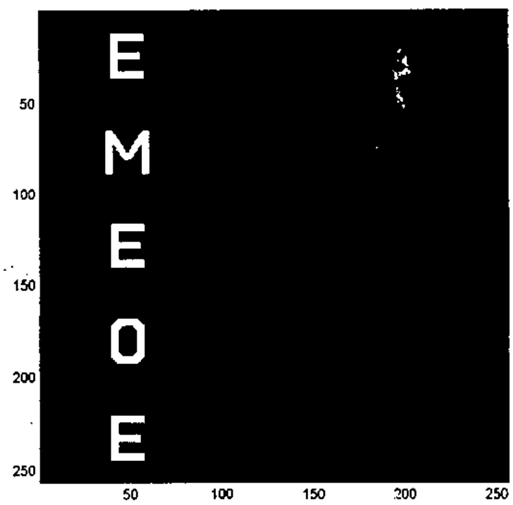

(b)

Fig. 3.1 (contd.) (b) Input scene with multiple targets and non-targets.

The simulation has been done with all three types of filter possible with GFAF. The corresponding correlation outputs are shown in Fig. 3.2(a) to Fig. 3.2(e).

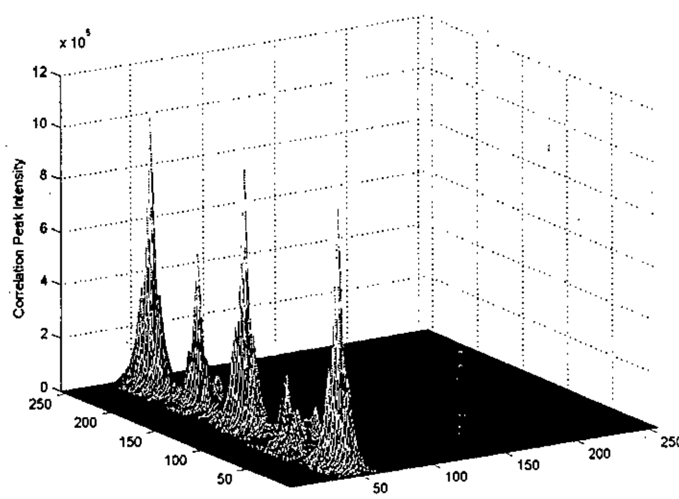

(a)

Fig. 3.2 (a) Correlation output with classical JTC (C=1, D=0, m=0).

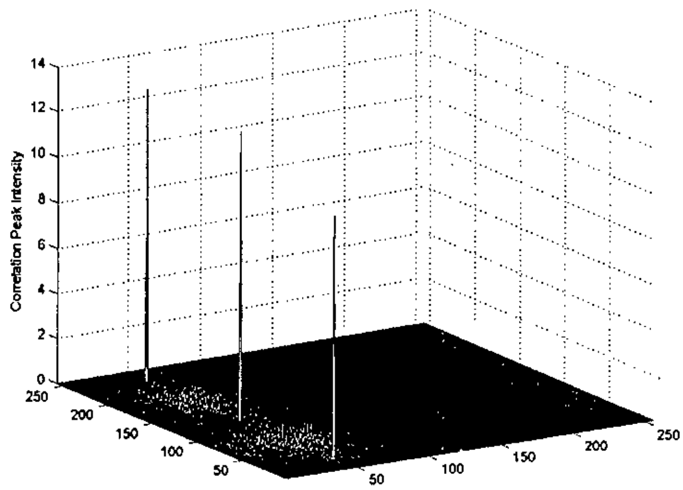

(b)

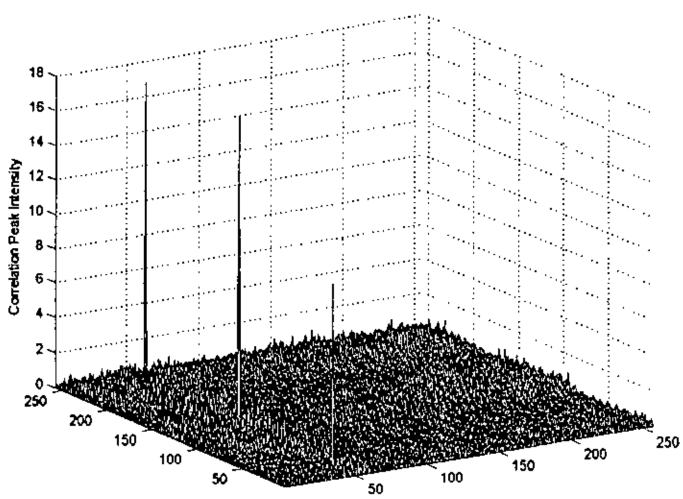

(c)

Fig. 3.2 (contd.) (b) Correlation output with fringe-adjusted filter (C=1, D=10^{-1}, m=2), (c) Correlation output with fringe-adjusted filter (C=1, D=10^{-6}, m=2)

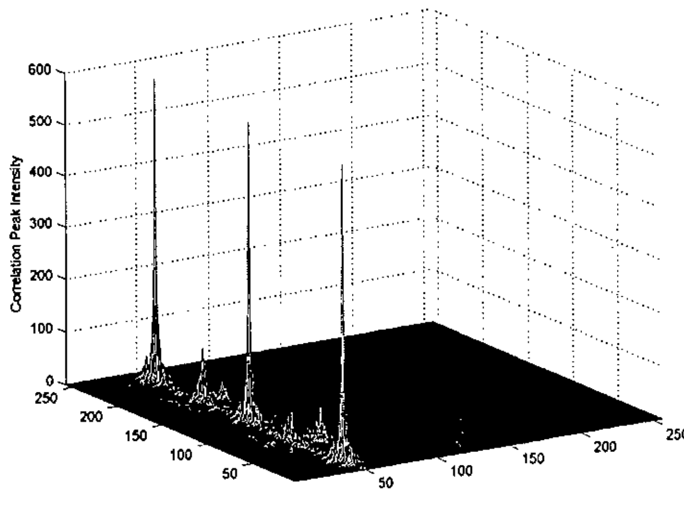

(d)

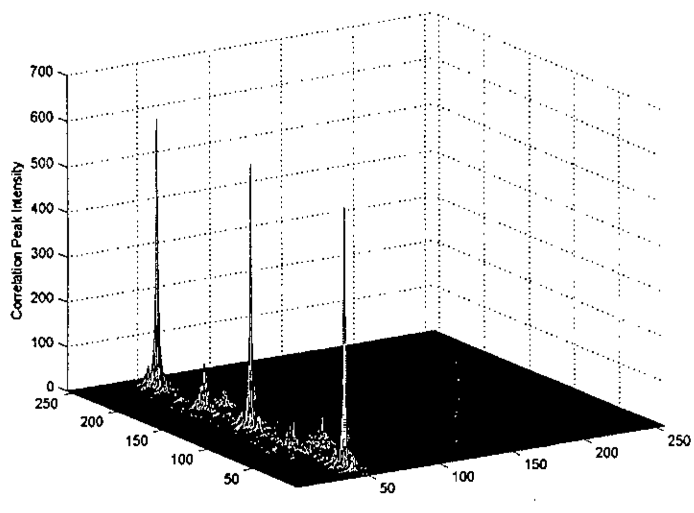

(e)

Fig. 3.2 (contd.) (d) Correlation output with phase-only filter (C=1, D=10^{-1}, m=1), (e) Correlation output with phase-only filter (C=1, D=10^{-6}, m=1).

From the correlation output of Fig. 3.2(a) to 3.2(e) it is evident that multi-target detection algorithm gives single correlation peak per target and indicates the exact location of the target when the reference image is placed at the center of the reference plane. As usual the classical JTC gives larger correlation width and sidelobes as shown in Fig. 3.2(a). Fringe-adjusted JTC gives the best performance with delta-function like correlation peaks when the value of $D(u,v)$ is comparatively higher as shown in Fig. 3.2(b). But the FJTC performance becomes poor if the value of $D(u,v)$ is lower as shown in Fig. 3.2(c). With phase-only JTC we get also sharper correlation peaks though there are some sidelobes too and small peaks for non-target objects as shown in Fig. 3.2(d) and Fig. 3.2(e). Phase only JTC however is quite insensitive to the choice of $D(u,v)$ in case of this multi-target detection algorithm.

3.3 Class-associative Target Detection

3.3.1 Theoretical Analysis

Class-associative target detection means detecting a group of objects, which may be similar, slightly similar or totally dissimilar. The class-associative target detection technique is formulated by combining the algorithm discussed in the previous section and an enhanced version of the generalized fringe-adjusted filter.

3.3.1.1 Two Objects in a Class

Consider two dissimilar objects $r_1(x,y)$ and $r_2(x,y)$ which are used as the reference images, and $s(x,y)$ is the input scene that contains various unknown objects containing targets and non-targets. Following the algorithm described in section 3.2, two sets of power spectra are generated in the spatial domain by utilizing the reference images $r_1(x,y)$ and $r_2(x,y)$. Accordingly using $r_1(x,y)$ and $s(x,y)$ four input spectra are obtained as given in Eq. (3.8).

$$\begin{aligned} f_{11}(x,y) &= r_1(x,y+y_o)+s(x,y-y_o) \\ &= r_1(x,y+y_o)+\sum_{i=1}^{n} p_i(x-x_i,y-y_i-y_o)+n(x,y-y_o) \end{aligned} \tag{3.8.a}$$

$$\begin{aligned} f_{21}(x,y) &= r_1(x,y+y_o)-js(x,y-y_o) \\ &= r_1(x,y+y_o)-j\sum_{i=1}^{n} p_i(x-x_i,y-y_i-y_o)-jn(x,y-y_o) \end{aligned} \tag{3.8.b}$$

$$\begin{aligned} f_{31}(x,y) &= r_1(x,y+y_o)-s(x,y-y_o) \\ &= r_1(x,y+y_o)-\sum_{i=1}^{n} p_i(x-x_i,y-y_i-y_o)-n(x,y-y_o) \end{aligned} \tag{3.8.c}$$

$$f_{41}(x,y)=r_1(x,y+y_o)+js(x,y-y_o)$$
$$=r_1(x,y+y_o)+j\sum_{i=1}^{n}p_i(x-x_i,y-y_i-y_o)+jn(x,y-y_o) \tag{3.8.d}$$

Similarly by using $r_2(x,y)$ another four input spectra are generated as given in Eq. (3.9).

$$f_{12}(x,y)=r_2(x,y+y_o)+s(x,y-y_o)$$
$$=r_2(x,y+y_o)+\sum_{i=1}^{n}p_i(x-x_i,y-y_i-y_o)+n(x,y-y_o) \tag{3.9.a}$$

$$f_{22}(x,y)=r_2(x,y+y_o)-js(x,y-y_o)$$
$$=r_2(x,y+y_o)-j\sum_{i=1}^{n}p_i(x-x_i,y-y_i-y_o)-jn(x,y-y_o) \tag{3.9.b}$$

$$f_{32}(x,y)=r_2(x,y+y_o)-s(x,y-y_o)$$
$$=r_2(x,y+y_o)-\sum_{i=1}^{n}p_i(x-x_i,y-y_i-y_o)-n(x,y-y_o) \tag{3.9.c}$$

$$f_{42}(x,y)=r_2(x,y+y_o)+js(x,y-y_o)$$
$$=r_2(x,y+y_o)+j\sum_{i=1}^{n}p_i(x-x_i,y-y_i-y_o)+jn(x,y-y_o) \tag{3.9.d}$$

The joint power spectra corresponding to Eq. (3.8) and Eq. (3.9), may be expressed as Eq. (3.10) and Eq. (3.11) respectively.

$$\begin{aligned}
T_{11}(u,v) &= |F_{11}(u,v)|^2 = |R_1(u,v)|^2 + \sum_{i=1}^{n}|P_i(u,v)|^2 + |N(u,v)|^2 \\
&+ 2\sum_{i=1}^{n}\sum_{k=i+1}^{n}|P_i(u,v)||P_k(u,v)|\cos[\phi_{pi}(u,v)-\phi_{pk}(u,v)-ux_i+ux_k-vy_i+vy_k] \\
&+ 2\sum_{i=1}^{n}|P_i(u,v)||R_1(u,v)|\cos[\phi_{pi}(u,v)-\phi_{r1}(u,v)-ux_i-vy_i-2vy_o] \\
&+ 2|R_1(u,v)||N(u,v)|\cos[\phi_{r1}(u,v)-\phi_n(u,v)+2vy_o] \\
&+ 2\sum_{i=1}^{n}|P_i(u,v)||N(u,v)|\cos[\phi_{pi}(u,v)-\phi_n(u,v)-ux_i-vy_i]
\end{aligned} \tag{3.10.a}$$

$$
\begin{aligned}
T_{21}(u,v) = |F_{41}(u,v)|^2 &= |R_1(u,v)|^2 + \left|\sum_{i=1}^{n} |P_i(u,v)|\right|^2 + |N(u,v)|^2 \\
&- 2|R_1(u,v)|\,|N(u,v)|\,\sin[\phi_{r1}(u,v) - \phi_n(u,v) + 2vy_o] \\
&+ 2\sum_{i=1}^{n}\sum_{k=i+1}^{n} |P_i(u,v)||P_k(u,v)|\cos[\phi_{pi}(u,v) - \phi_{pk}(u,v) - ux_i + ux_k - vy_i + vy_k] \\
&+ 2\sum_{i=1}^{n} |P_i(u,v)||R_1(u,v)|\sin[\phi_{pi}(u,v) - \phi_{r1}(u,v) - ux_i - vy_i - 2vy_o] \\
&+ 2\sum_{i=1}^{n} |P_i(u,v)||N(u,v)|\cos[\phi_{pi}(u,v) - \phi_n(u,v) - ux_i - vy_i]
\end{aligned}
\tag{3.10.b}
$$

$$
\begin{aligned}
T_{31}(u,v) = |F_{31}(u,v)|^2 &= |R_1(u,v)|^2 + \left|\sum_{i=1}^{n} |P_i(u,v)|\right|^2 + |N(u,v)|^2 \\
&- 2|R_1(u,v)|\,|N(u,v)|\,\cos[\phi_{r1}(u,v) - \phi_n(u,v) + 2vy_o] \\
&+ 2\sum_{i=1}^{n}\sum_{k=i+1}^{n} |P_i(u,v)||P_k(u,v)|\cos[\phi_{pi}(u,v) - \phi_{pk}(u,v) - ux_i + ux_k - vy_i + vy_k] \\
&- 2\sum_{i=1}^{n} |P_i(u,v)||R_1(u,v)|\cos[\phi_{pi}(u,v) - \phi_{r1}(u,v) - ux_i - vy_i - 2vy_o] \\
&+ 2\sum_{i=1}^{n} |P_i(u,v)||N(u,v)|\cos[\phi_{pi}(u,v) - \phi_n(u,v) - ux_i - vy_i]
\end{aligned}
\tag{3.10.c}
$$

$$
\begin{aligned}
T_{41}(u,v) = |F_{21}(u,v)|^2 &= |R_1(u,v)|^2 + \left|\sum_{i=1}^{n} |P_i(u,v)|\right|^2 + |N(u,v)|^2 \\
&+ 2|R_1(u,v)|\,|N(u,v)|\,\sin[\phi_{r1}(u,v) - \phi_n(u,v) + 2vy_o] \\
&+ 2\sum_{i=1}^{n}\sum_{k=i+1}^{n} |P_i(u,v)||P_k(u,v)|\cos[\phi_{pi}(u,v) - \phi_{pk}(u,v) - ux_i + ux_k - vy_i + vy_k] \\
&- 2\sum_{i=1}^{n} |P_i(u,v)||R_1(u,v)|\sin[\phi_{pi}(u,v) - \phi_{r1}(u,v) - ux_i - vy_i - 2vy_o] \\
&+ 2\sum_{i=1}^{n} |P_i(u,v)||N(u,v)|\cos[\phi_{pi}(u,v) - \phi_n(u,v) - ux_i - vy_i]
\end{aligned}
\tag{3.10.d}
$$

$$
\begin{aligned}
T_{12}(u,v) = |F_{12}(u,v)|^2 &= |R_2(u,v)|^2 + \sum_{i=1}^{n} |P_i(u,v)|^2 + |N(u,v)|^2 \\
&+ 2\sum_{i=1}^{n}\sum_{k=i+1}^{n} |P_i(u,v)||P_k(u,v)|\cos[\phi_{pi}(u,v) - \phi_{pk}(u,v) - ux_i + ux_k - vy_i + vy_k] \\
&+ 2\sum_{i=1}^{n} |P_i(u,v)||R_2(u,v)|\cos[\phi_{pi}(u,v) - \phi_{r2}(u,v) - ux_i - vy_i - 2vy_o] \\
&+ 2|R_2(u,v)||N(u,v)|\cos[\phi_{r2}(u,v) - \phi_n(u,v) + 2vy_o] \\
&+ 2\sum_{i=1}^{n} |P_i(u,v)||N(u,v)|\cos[\phi_{pi}(u,v) - \phi_n(u,v) - ux_i - vy_i]
\end{aligned}
\tag{3.11.a}
$$

$$T_{22}(u,v)=\left|F_{42}(u,v)\right|^2=\left|R_2(u,v)\right|^2+\sum_{i=1}^{n}\left|P_i(u,v)\right|^2+\left|N(u,v)\right|^2$$
$$-2\left|R_2(u,v)\right|\left|N(u,v)\right|\sin\left[\phi_{r2}(u,v)-\phi_n(u,v)+2vy_o\right]$$
$$+2\sum_{i=1}^{n}\sum_{k=i+1}^{n}\left|P_i(u,v)\right|\left|P_k(u,v)\right|\cos[\phi_{pi}(u,v)-\phi_{pk}(u,v)-ux_i+ux_k-vy_i+vy_k] \quad (3.11.b)$$
$$+2\sum_{i=1}^{n}\left|P_i(u,v)\right|\left|R_2(u,v)\right|\sin[\phi_{pi}(u,v)-\phi_{r2}(u,v)-ux_i-vy_i-2vy_o]$$
$$+2\sum_{i=1}^{n}\left|P_i(u,v)\right|\left|N(u,v)\right|\cos[\phi_{pi}(u,v)-\phi_n(u,v)-ux_i-vy_i]$$

$$T_{32}(u,v)=\left|F_{32}(u,v)\right|^2=\left|R_2(u,v)\right|^2+\sum_{i=1}^{n}\left|P_i(u,v)\right|^2+\left|N(u,v)\right|^2$$
$$-2\left|R_2(u,v)\right|\left|N(u,v)\right|\cos\left[\phi_{r2}(u,v)-\phi_n(u,v)+2vy_o\right]$$
$$+2\sum_{i=1}^{n}\sum_{k=i+1}^{n}\left|P_i(u,v)\right|\left|P_k(u,v)\right|\cos[\phi_{pi}(u,v)-\phi_{pk}(u,v)-ux_i+ux_k-vy_i+vy_k] \quad (3.11.c)$$
$$-2\sum_{i=1}^{n}\left|P_i(u,v)\right|\left|R_2(u,v)\right|\cos[\phi_{pi}(u,v)-\phi_{r2}(u,v)-ux_i-vy_i-2vy_o]$$
$$+2\sum_{i=1}^{n}\left|P_i(u,v)\right|\left|N(u,v)\right|\cos[\phi_{pi}(u,v)-\phi_n(u,v)-ux_i-vy_i]$$

$$T_{42}(u,v)=\left|F_{22}(u,v)\right|^2=\left|R_2(u,v)\right|^2+\sum_{i=1}^{n}\left|P_i(u,v)\right|^2+\left|N(u,v)\right|^2$$
$$+2\left|R_2(u,v)\right|\left|N(u,v)\right|\sin\left[\phi_{r2}(u,v)-\phi_n(u,v)+2vy_o\right]$$
$$+2\sum_{i=1}^{n}\sum_{k=i+1}^{n}\left|P_i(u,v)\right|\left|P_k(u,v)\right|\cos[\phi_{pi}(u,v)-\phi_{pk}(u,v)-ux_i+ux_k-vy_i+vy_k] \quad (3.11.d)$$
$$-2\sum_{i=1}^{n}\left|P_i(u,v)\right|\left|R_2(u,v)\right|\sin[\phi_{pi}(u,v)-\phi_{r2}(u,v)-ux_i-vy_i-2vy_o]$$
$$+2\sum_{i=1}^{n}\left|P_i(u,v)\right|\left|N(u,v)\right|\cos[\phi_{pi}(u,v)-\phi_n(u,v)-ux_i-vy_i]$$

Here F_{11}, F_{21}, F_{31}, F_{41}, F_{12}, F_{22}, F_{32} and F_{42} are the Fourier transforms of $f_{11}, f_{21}, f_{31}, f_{41}, f_{12}, f_{22}, f_{32}$ and f_{42}, respectively. Using Eqs. (3.10) and (3.11), the modified joint power spectra may be expressed as

$$T_o(u,v)=T_{11}(u,v)+jT_{21}(u,v)-T_{31}-jT_{41}$$
$$=4\sum_{i=1}^{n}\left|P_i(u,v)\right|\left|R_1(u,v)\right|\exp[j\phi_{pi}(u,v)-j\phi_{r1}(u,v)-jux_i-jvy_i-2jvy_o] \quad (3.12)$$
$$+4\left|R_1(u,v)\right|\left|N(u,v)\right|\exp\left[-j\phi_{r1}(u,v)+j\phi_n(u,v)-2jvy_o\right]$$

$$T_b(u,v) = T_{12}(u,v) + jT_{22}(u,v) - T_{32} - jT_{42}$$
$$= 4\sum_{i=1}^{n}|P_i(u,v)||R_2(u,v)|\exp[j\phi_{pi}(u,v) - j\phi_{r2}(u,v) - jux_i - jvy_i - 2jvy_o] \tag{3.13}$$
$$+ 4|R_2(u,v)|\,|N(u,v)|\exp[-j\phi_{r2}(u,v) + j\phi_n(u,v) - 2jvy_o]$$

Using Eqs. (3.12) and (3.13), the final JPS can be generated as follows

$$T(u,v) = \alpha T_a(u,v) + \beta T_b(u,v)$$
$$= \alpha\begin{bmatrix} 4\sum_{i=1}^{n}|P_i(u,v)||R_1(u,v)|\exp[j\phi_{pi}(u,v) - j\phi_{r1}(u,v) - jux_i - jvy_i - 2jvy_o] \\ + 4|R_1(u,v)|\,|N(u,v)|\exp[-j\phi_{r1}(u,v) + j\phi_n(u,v) - 2jvy_o] \end{bmatrix} \tag{3.14}$$
$$+ \beta\begin{bmatrix} 4\sum_{i=1}^{n}|P_i(u,v)||R_2(u,v)|\exp[j\phi_{pi}(u,v) - j\phi_{r2}(u,v) - jux_i - jvy_i - 2jvy_o] \\ + 4|R_2(u,v)|\,|N(u,v)|\exp[-j\phi_{r2}(u,v) + j\phi_n(u,v) - 2jvy_o] \end{bmatrix}$$

where $\alpha + \beta = 1$. The ratio of α and β may be varied depending upon the energy content of the joint power spectra T_a and T_b in order to achieve equal correlation peak for both targets. Since there are two targets to be detected, the H_{gfaf} filter shown in Eq. (3.6) may be reformulated for class detection, which may be termed as class-associative generalized fringe-adjusted filter (CGFAF). The filter function is expressed as

$$H_{cgfaf}(u,v) \approx \frac{1}{D(u,v) + |R_1(u,v)|^m + |R_2(u,v)|^m} \tag{3.15}$$

where $R_1(u,v)$ and $R_2(u,v)$ are the Fourier transforms of $r_1(x,y)$ and $r_2(x,y)$, respectively and $C(u,v)$=1 in Eq. (3.6). As in the case of generalized fringe-adjusted filter (GFAF), for CGFAF also three types of filtering may be achieved by selecting the values of m and $D(u,v)$.

Using Eqs. (3.14) and (3.15), the modified joint power spectrum becomes

$$G_{cgfaf}(u,v) = H_{cgfaf} \times T(u,v) = \frac{\alpha T_a(u,v) + \beta T_b(u,v)}{D(u,v) + |R_1(u,v)|^m + |R_2(u,v)|^m} \tag{3.16}$$

The correlation output corresponding to $G_{cgfaf}(u,v)$ can be obtained by applying inverse Fourier transform to Eq. (3.16).

3.3.1.2 Three Objects in a Class

If there are three objects in the class, then there will be three references. Accordingly there will be three sets of input spectra made by various combinations of the input scene with the three references separately. So for three objects, in addition to Eq. (3.8) and Eq. (3.9) another set of input spectra will be generated as given by Eq. (3.17).

$$\begin{aligned} f_{13}(x,y) &= r_3(x,y+y_o)+s(x,y-y_o) \\ &= r_3(x,y+y_o)+\sum_{i=1}^{n} p_i(x-x_i,y-y_i-y_o)+n(x,y-y_o) \end{aligned} \tag{3.17.a}$$

$$\begin{aligned} f_{23}(x,y) &= r_3(x,y+y_o)-js(x,y-y_o) \\ &= r_3(x,y+y_o)-j\sum_{i=1}^{n} p_i(x-x_i,y-y_i-y_o)-jn(x,y-y_o) \end{aligned} \tag{3.17.b}$$

$$\begin{aligned} f_{33}(x,y) &= r_3(x,y+y_o)-s(x,y-y_o) \\ &= r_3(x,y+y_o)-\sum_{i=1}^{n} p_i(x-x_i,y-y_i-y_o)-n(x,y-y_o) \end{aligned} \tag{3.17.c}$$

$$\begin{aligned} f_{43}(x,y) &= r_3(x,y+y_{o)}+js(x,y-y_o) \\ &= r_3(x,y+y_o)+j\sum_{i=1}^{n} p_i(x-x_i,y-y_i-y_o)+jn(x,y-y_o) \end{aligned} \tag{3.17.d}$$

Accordingly in addition to the joint power spectra of Eq. (3.10) and Eq. (3.11) there will be a set due to Eq. (3.17) giving T_{13}, T_{23}, T_{33} and T_{43}. Using these values we will get another set of modified joint power spectra given by

$$T_c(u,v) = T_{13}(u,v) + jT_{23}(u,v) - T_{33} - jT_{43} \tag{3.18}$$

The final JPS is obtained by using Eq. (3.12), Eq. (3.13) and Eq. (3.18) given by

$$T(u,v) = \alpha T_a(u,v) + \beta T_b(u,v) + \gamma T_c(u,v) \tag{3.19}$$

where $\alpha+\beta+\gamma=1$. Since there are three targets to be detected, the H_{cgfaf} filter shown in Eq. (3.15) may be reformulated as

$$H_{cgfaf}(u,v) \approx \frac{1}{D(u,v)+|R_1(u,v)|^m+|R_2(u,v)|^m+|R_3(u,v)|^m} \tag{3.20}$$

where $R_1(u,v)$, $R_2(u,v)$ and $R_3(u,v)$ are the Fourier transforms of $r_1(x,y)$, $r_2(x,y)$ and $r_3(x,y)$ respectively. Using Eqs. (3.19) and (3.20), the modified joint power spectrum becomes

$$G_{cgfaf}(u,v) = H_{cgfaf} \times T(u,v) = \frac{\alpha T_a(u,v) + \beta T_b(u,v) + \gamma T_c}{D(u,v) + |R_1(u,v)|^m + |R_2(u,v)|^m + |R_3(u,v)|^m} \tag{3.21}$$

The correlation output corresponding to $G_{cgfaf}(u,v)$ can be obtained by applying inverse Fourier transform to Eq. (3.21).

3.3.1.3 Multiple Objects in a Class

By applying the procedure described in sections 3.3.1.1 and 3.3.1.2 we can formulate the detection algorithm for detection of a class of dissimilar objects when there are more than three objects in the class too. However as the member of the class increases, the detection technique becomes more and more complex.

3.3.2 Simulation

3.3.2.1 Two Objects in a Class

Let us consider that alphabet 'E' and alphabet 'H' are two objects forming a group or class to be detected in a binary input scene. Then these are the two reference objects of the analysis that are shown in Fig. 3.3(a) and Fig. 3.3(b) respectively. First let us assume that the input scene contains only these two objects as shown in Fig. 3.3(c). Now if the class-associative target detection theory is applied as described in section 3.3.1, the correlation output of Fig. 3.3(d) is obtained when the filter parameters are such that the CGFAF filter for class detection is a fringe adjusted filter (m=2) and the value of power spectra parameters are α=0.5 and β=0.5. Fringe-adjusted filter is chosen as it performed better with multi-target detection technique shown in section 3.2.2.

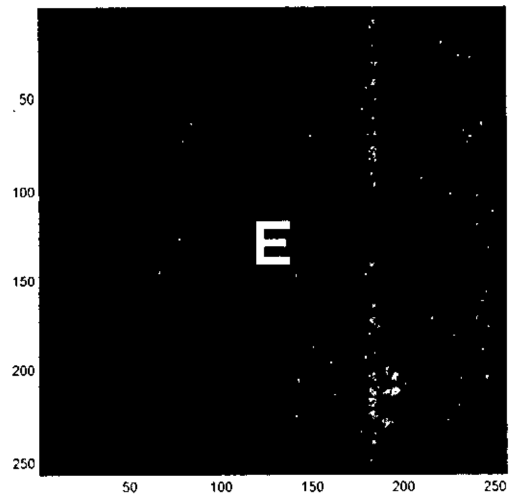

(a)

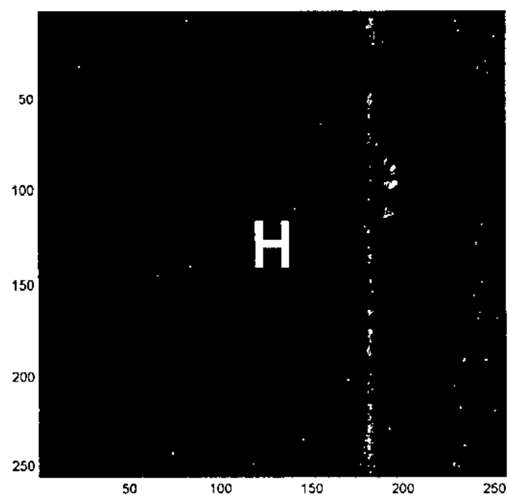

(b)

Fig. 3.3 (a) Reference image 1, (b) Reference image 2.

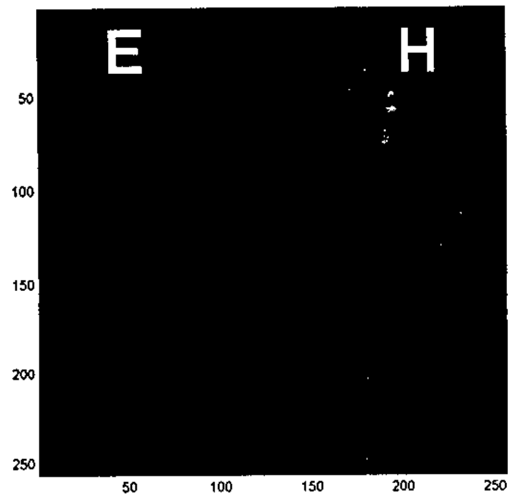

(c)

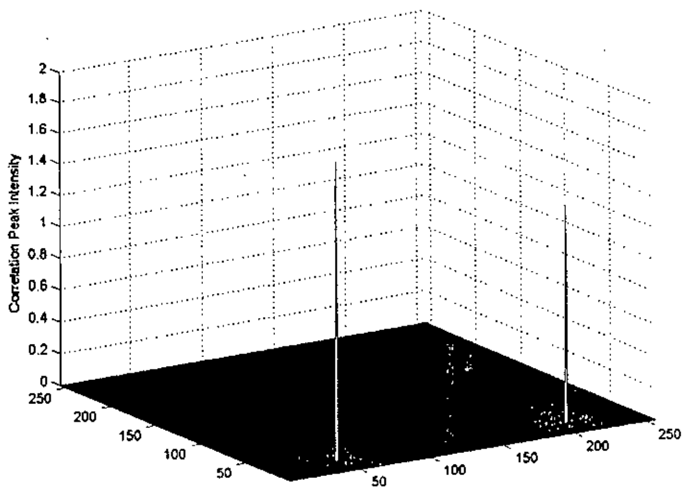

(d)

Fig. 3.3 (contd.) (c) Input scene, (d) Correlation output with C=1, D=10^{-1}, m=2 and α=0. 5, β=0.5.

From the correlation output of Fig. 3.3(d) it is observed that single correlation peak is obtained for each of the targets, which is obvious as class-associative target detection employed multi-target detection algorithm. However unequal correlation peaks are seen for the two objects of the class or group. From the simulation correlation peak intensities of 1.8908 for ‘E’ and 1.3594 for ‘H’ are found. This difference is due to the difference in energy contents of the two objects. So, by adjusting the power spectra parameters as α=0.4125 and β=0.5875 the correlation output for both the targets 'E' and 'H' of the class can be made equal as shown in Fig. 3.4. In this case the peak intensity for 'E' is 1.5671 and for 'H' it is 1.5678.

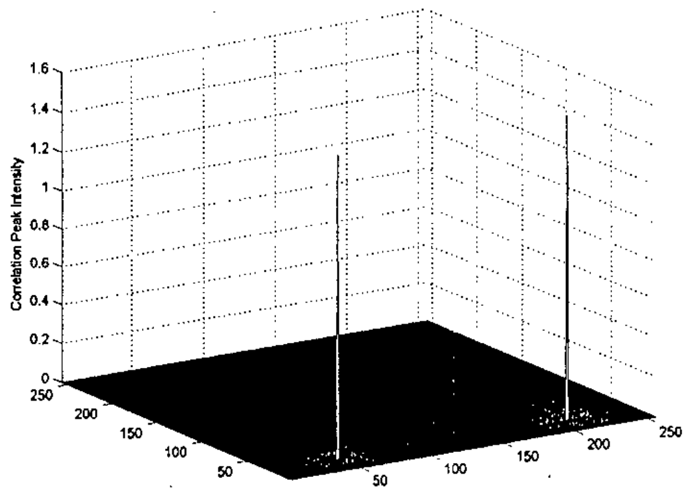

Fig. 3.4 Correlation output for the references and input scene of Fig. 3.3(a) to Fig. 3.3(c) with m=2, C=1, D=10^{-1} and α=0.4125, β=0.5875.

As a second example let us take multiple targets of the class and multiple non-targets in the input scene as shown in Fig. 3.5(a). The correlation output with fringe-adjusted filter and power spectra parameters adjusted is given in Fig. 3.5(b).

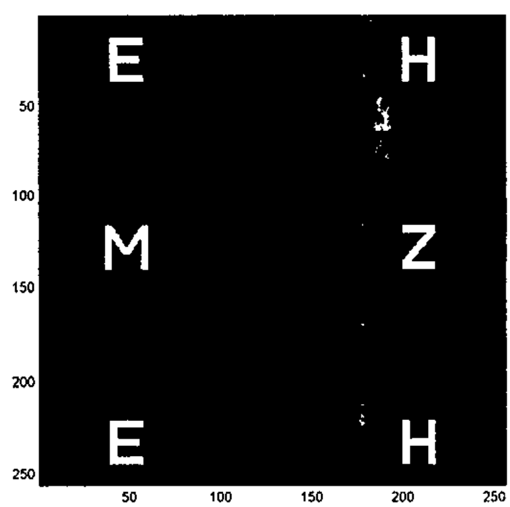

(a)

Fig. 3.5 (a) Input scene with multiple targets of the class and multiple non-targets.

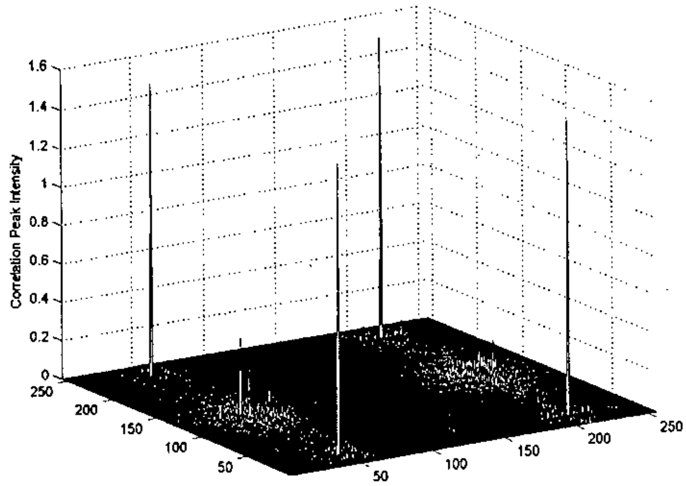

(b)

Fig. 3.5 (contd.) Input scene with multiple targets of the class and multiple non-targets, (b) Correlation output with m=2, C=1, D=10^{-1} and α=0.4125, β=0.5875.

In this case the values for power spectra parameters (α and β) are chosen as has been taken in the case of input scene of Fig. 3.3(c) with output of Fig. 3.4. The correlation peak intensities for the target and non-target objects in this case are given in Table 3.1.

Table 3.1 Correlation peak intensities for different objects for the input scene of Fig. 3.5(a) and output of Fig. 3.5(b).

	Peak Intensity		Peak Intensity
Upper 'E'	1.5018	Upper 'H'	1.5254
'M'	0.3963	'Z'	0.1901
Lower 'E'	1.5108	Lower 'H'	1.5355

Here it is observed that the peak intensities for all the four targets are almost equal and non-target peaks are negligible compared to the target peaks. Attempt could be made by adjusting the values of α and β to make the peak intensities for the targets much nearer. But it is insignificant and not necessary as with the present values of α and β the ratio of maximum target peak to minimum target peak is only 1.02.

So, once the targets of a class are defined or chosen, the required values of power spectra parameters can be selected by making test runs with only the desired objects of the class in the input scene. For these however several trail and error attempts are required. The determined values can then be used for a real input scene with multiple targets and non-targets with no or negligible degradation of performance. The above process of adjusting the power spectra parameters may seem uncomfortable sometime. In that case a technique may be adopted to determine the values of power spectra parameters automatically by the system. For this the target peaks of the objects of the class are first need to be known with equal values of the parameters. Then by an iterative process the peaks can be made nearly equal by gradually adjusting the values of the power spectra parameters depending on relative difference among the peaks obtained with equal values of parameters. Still this method does not guarantee fully equal correlation peaks for the dissimilar objects of the class. Moreover this technique becomes much more complex if the number of dissimilar objects in a class increases. As this is a computation intensive process, it cannot be implemented optically too.

3.3.2.2 Three Objects in a Class

Now let us take three different objects as the member of the target class. So there will be three reference objects as shown in Fig. 3.6(a) to Fig. 3.6(c). The input scene containing multiple targets of the class and several non-targets is shown in Fig. 3.6(d). The corresponding correlation output using fringe-adjusted filter is shown in Fig. 3.6(e). Table 3.2 summarizes the correlation peak intensities for all the objects of the input scene.

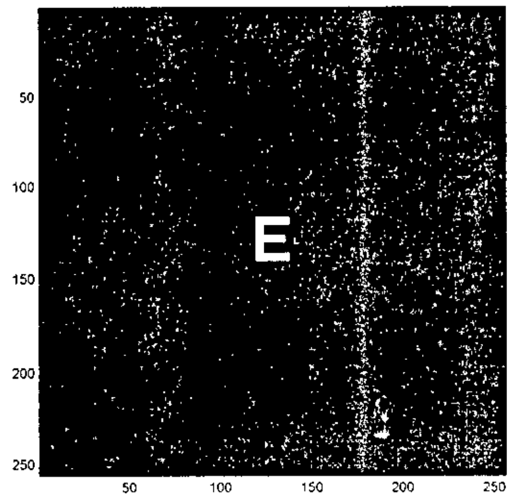

(a)

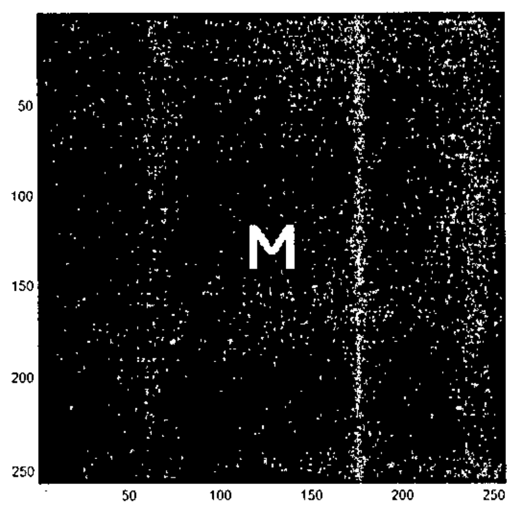

(b)

Fig. 3.6 (a) Reference image 1, (b) Reference image 2.

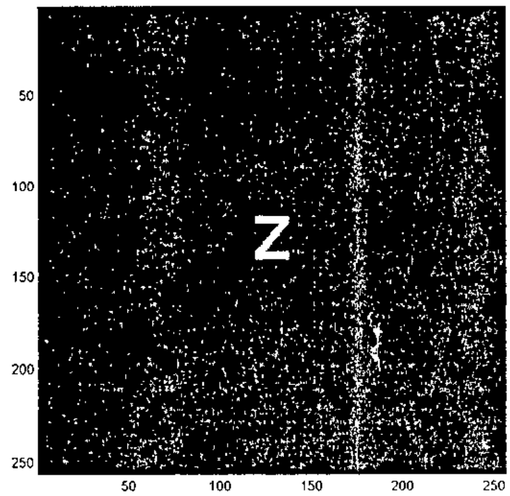

(c)

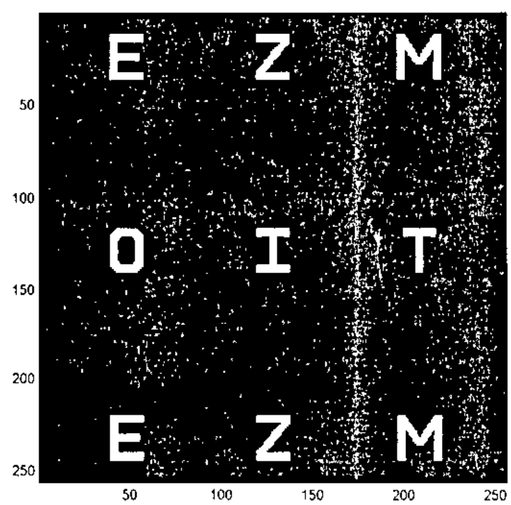

(d)

Fig. 3.6 (contd.) (c) Reference image 3, (d) Input scene with multiple targets of the class and multiple non-targets.

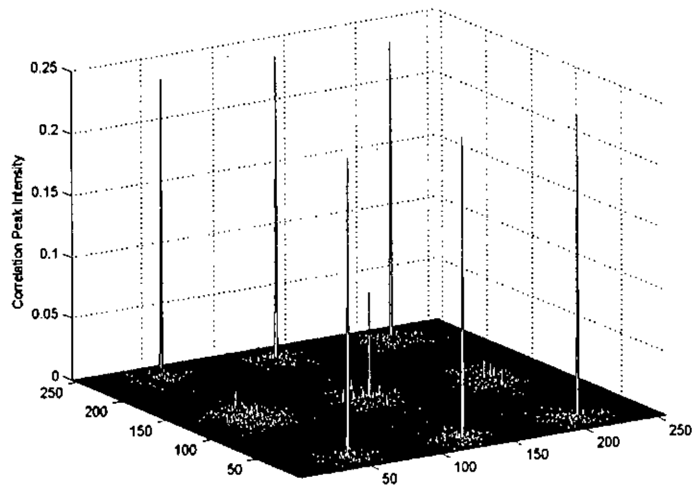

(e)

Fig. 3.6 (contd.) (e) Correlation output with m=2, C=1, D=10^{-1} and α=0.441, β=0.279 and γ=0.280.

Table 3.2 Correlation peak intensities for different objects for the input scene of Fig. 3.6(d) and correlation output of Fig. 3.6(e).

	Peak Intensity		Peak Intensity		Peak Intensity
Upper 'E'	0.2404	Upper 'Z'	0.2418	Upper 'M'	0.2437
'O'	0.0205	'I'	0.0843	'T'	0.0197
Lower 'E'	0.2414	Lower 'Z'	0.2434	Lower 'M'	0.2396

So from Fig. 3.6(e) and Table 3.2 it is evident that for all three target images of the class almost equal correlation peaks are obtained. Besides, the non-targets produce almost no or negligible peaks.

3.3.2.3 Multiple Objects in a Class

In the previous section the class-associative target detection technique has been tested for more than three dissimilar objects in the class. It is found that this technique is successful for even up to six objects as one particular class members. However, the technique becomes computation intensive and difficult for optical implementation as the number of dissimilar objects in a class increases. The main problem is to adjust the power spectra parameters.

Now let us verify the six-object case by taking alphabets 'E', 'M', 'Z', 'T', 'O' and 'H' as the object images of a class. So these are the reference images. The adjusted values for the power spectra parameters are 0.085, 0.130, 0.080, 0.3025, 0.180 and 0.2225 respectively. The input scene and corresponding correlation output are shown in Fig. 3.7.

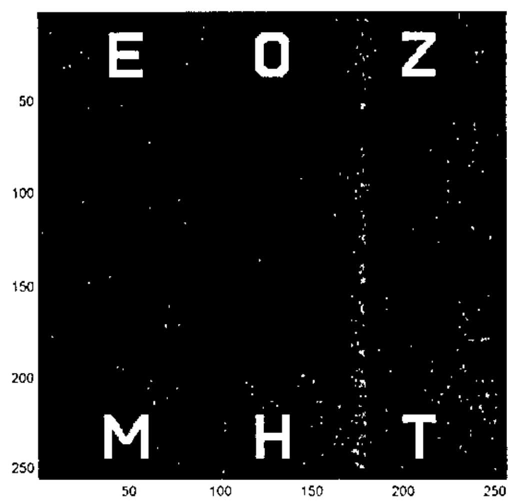

(a)

Fig. 3.7 (a) Input scene with six objects of a class

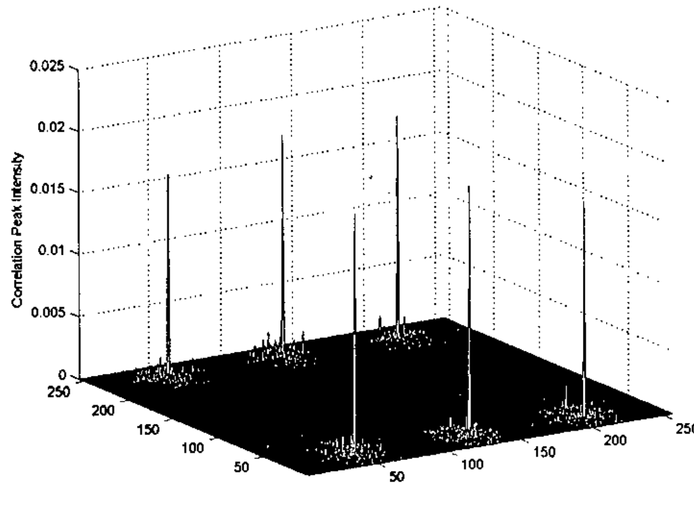

(b)

Fig. 3.7 (contd.) (b) Correlation output.

3.4 Conclusion

Multi-target detection algorithm (MTDA) can be considered as an extension of the fringe-adjusted JTC or generalized fringe-adjusted JTC, as, here the final joint power spectrum is multiplied by the generalized fringe-adjusted filter before the inverse Fourier transform operation. This MTDA also successfully detects the objects in a multi-object input scene giving sharp correlation peaks. By using multiple references in MTDA, a successful class-associative target detection can be achieved to detect multiple dissimilar objects simultaneously present in the input scene. In this work a simple modification has been adopted in the MTDA by adjusting the phase information of the input power spectra, which is directly introduced in Eqs. (3.1), (3.8), (3.9) and (3.17) in the preceding analyses. Due to this modification, the correlation peaks are obtained at the exact location of the targets besides getting single correlation peak per target in both multi-target detection and in class-associative detection. Single correlation peak is a great contribution of the MTDA, because, it provides an exact and unique correlation signal for the target. Thus detection accuracy is increased along with the optical efficiency.

Chapter 4

SYNTHETIC DISCRIMINANT FUNCTION

4.1 Introduction

Though successful in preserving the shift invariant pattern recognition property, all JTC techniques suffer from high sensitivity to distortions in the input scene, such as scale variations and rotations. To accommodate distortion invariance in JTC, synthetic discriminant function (SDF) concept is adopted. SDF can be synthesized by the linear combination of the images from a training set composed of the target image and its many distorted images. This SDF is used as the reference image in the JTC. When the input target is true, there will be a correlation peak in the correlation plane, which is constant with target's distorted versions. Theoretically, this method is distortion invariant to transposition, scale and rotation distortion.

4.2 SDF in Fractional Power FJTC

For the distortion invariant fractional power fringe-adjusted JTC or generalized FJTC, the reference image $r(x,y)$ is synthesized from a set of training images. Let us assume that the N centered training images, r_1, r_2, ..., r_n, containing the desired distortion invariant features, are used to construct the spatial SDF $r_{SDF}(x,y)$. Typically, $r_{SDF}(x,y)$ is a linear combination of the training images, given by

$$r_{SDF}(x,y) = \sum_{k=1}^{n} a_k r_k(x,y) \tag{4.1}$$

where a_k represents the weights or coefficients used. This composite image is used as the reference in all types of JTC for distortion invariant recognition. The generalized fringe-adjusted filter (GFAF) is now modified as

$$H_{gfaf}^{SDF} = \frac{C(u,v)}{D(u,v) + |R_{SDF}(u,v)|^m} \tag{4.2}$$

where $R_{SDF}(u,v)$ is the Fourier transform of the spatial SDF $r_{SDF}(x,y)$. The SDF-based JPS is obtained by multiplying the JPS with the filter function of Eq. (4.2). This modified JPS is inverse Fourier transformed to obtain the correlation output as usual.

4.3 Obtaining SDF

4.3.1 Theoretical Analysis

Determination of the spatial SDF $r_{SDF}(x,y)$ requires finding the values of coefficients in Eq. (4.1). To evaluate the coefficients a_k, k=1,2,.......,N, for the training images r_k, k=1,2,........,N, respectively, some iterative process is employed. Here a simplified process has been adopted for this purpose. First all the coefficients are taken as real and unity. Then a simple addition of the training set images gives a composite image. This composite image is now used as the reference image to find correlation with each of the images of the training set. To find the correlation, fractional power fringe-adjusted JTC or generalized fringe-adjusted JTC technique is chosen whereby we can employ classical JTC, fringe-adjusted JTC or phase-only JTC according to the requirement. In the first iteration of finding correlation with the training set, unequal correlation peak intensities are obtained due to dissimilarity in the images of the training set. Our aim is to make the correlation peak height equal for all the images of the training set. So the coefficients of the images of the training set are changed from first iteration to second iteration following an empirical iterative formula

$$a_k^{i+1} = a_k^i + (p_{\max}^i - p_k^i) \times rf \tag{4.3}$$

where a_k is the coefficient for kth image of the training set, i is the iteration number, p_{max} is the maximum correlation peak obtained from the correlation peaks of all the training set images in a particular iteration and p_k is the correlation peak for the kth image of the set. rf is the relaxation factor which has direct effect in changing the values of the coefficients from one iteration to next iteration. With the new values of the coefficients the composite reference is calculated again as the weighted sum as given in Eq. (4.1). This reference is again used for the next iteration to update the correlation outputs and the weights for the all the images in the training set. It may be mentioned that the filter function used in the generation of the SDF itself is also updated by using the SDF obtained in the iteration. This iterative process is continued until the correlation peaks for all the images of the training set become equal or when the difference between the maximum peak and minimum peak reaches within a predetermined range. This limiting value of the error or difference may be expressed as

$$\xi^i = (p^i_{\max} - p^i_{\min}) / p^i_{\max} \tag{4.4}$$

where ξ^i is the error calculated in ith iteration, $p_{max}{}^i$ is the maximum correlation peak obtained in ith iteration and $p_{min}{}^i$ is the minimum correlation peak obtained in ith iteration. The composite image thus obtained after final iteration is the desired spatial SDF, $r_{SDF}(x,y)$.

4.3.2 Simulation

To show the generation of SDF, nine images are taken as the training set which are alphabet 'E' and its rotated and/or distorted forms as shown in Fig. 4.1(a). Fig. 4.1(b) shows the SDF generated by the simple addition of the training set images assuming all the coefficients to be equal to unity. Fig. 4.1(c) shows the input joint image containing the training set images and the initial SDF as the reference for first iteration. This input joint image is used to find the final values of the coefficients and hence the final SDF by using the generalized fringe-adjusted joint transform correlation (GFJTC). The SDF generation program is simulated in a Pentium II 300 MHz computer using MATLAB software (Appendix I) by applying the generalized fringe-adjusted filter (GFAF) in joint transform correlator, which gives classical JTC, fringe-adjusted JTC and phase-only JTC. Simulation results obtained by all these three types of JTCs are shown. The performance of the SDFs obtained by these three types of JTCs are then evaluated by employing them separately for the detection of distorted images from the training set by using both fringe-adjusted JTC and phase-only JTC. For the SDF generation program an error limit ξ=0.01 and maximum iteration number i=500 have been taken. As in usual JTC techniques such as generalized FJTC, a pair of correlation peaks is obtained for each image, one peak for each image is zero padded for the correlation output in the SDF generation programs for clarity as will be seen in the figures of correlation outputs.

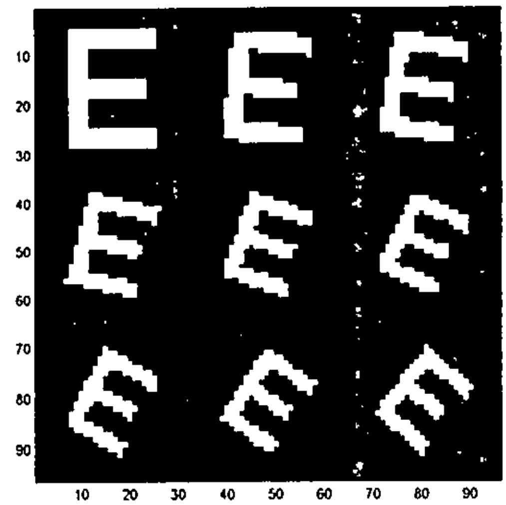

(a)

98227

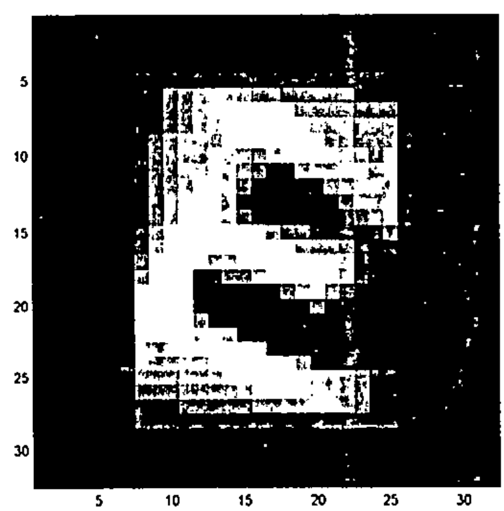

(b)

Fig. 4.1 (a) Training set containing 9 images, (b) Spatial SDF with the unity coefficients.

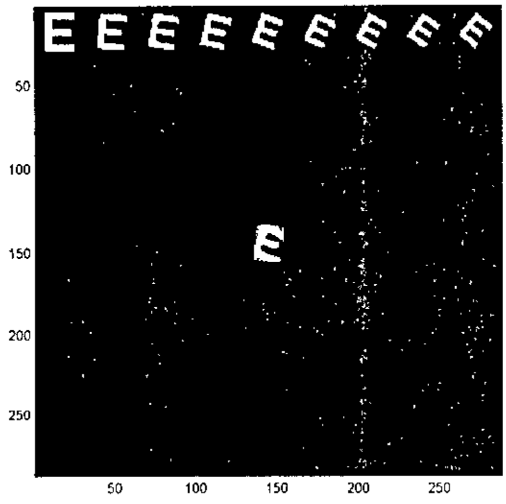

(c)

Fig. 4.1 (contd.) (c) Joint input image with initial SDF as reference and the training set images as the targets.

4.3.2.1 SDF Generated using Classical JTC

Classical JTC is obtained by taking C=1, D=0 and m=0 in the GFAF filter of Eq. (2.16). This filter is applied to the JPS derived from the input joint image of Fig. 4.1(c) to get the classical JTC for obtaining the correlation with the initial SDF and the training set images individually. A relaxation factor rf=0.5 has been selected in this case. Fig 4.2(a) shows the correlation output after first iteration and Fig. 4.2(b) clarifies the correlation peaks for all training set images. It is observed that initially the peaks are much different from each other. An iterative process is continued as stated in section 4.3.2. But here all the 500 iterations complete taking around 8 minutes, but the correlation peaks do not reach within the desired error limit or difference limit as is seen in Fig. 4.2(c) and Fig 4.2(d). The correlation peak intensity for each image is given in Table 4.1 after 500 iterations. Fig. 4.2(e) is the final SDF, termed as r_{SDF}^{c} which may be used as the reference for distortion invariant JTC. However as here the final correlation peaks for the images are not same, this r_{SDF}^{c} should not perform successfully in target detection.

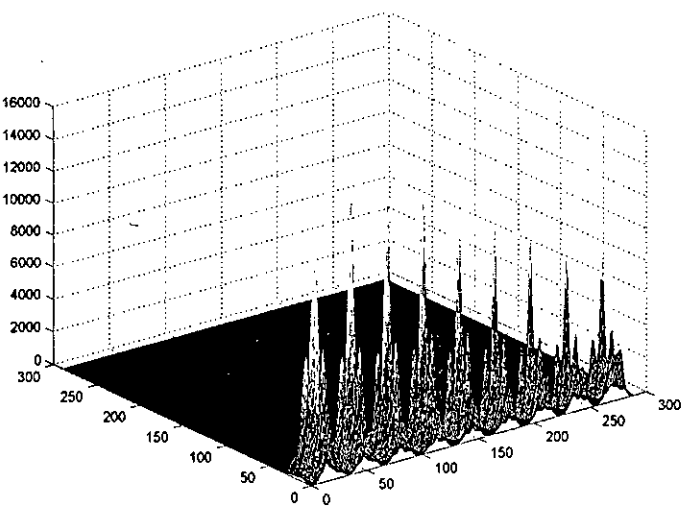

(a)

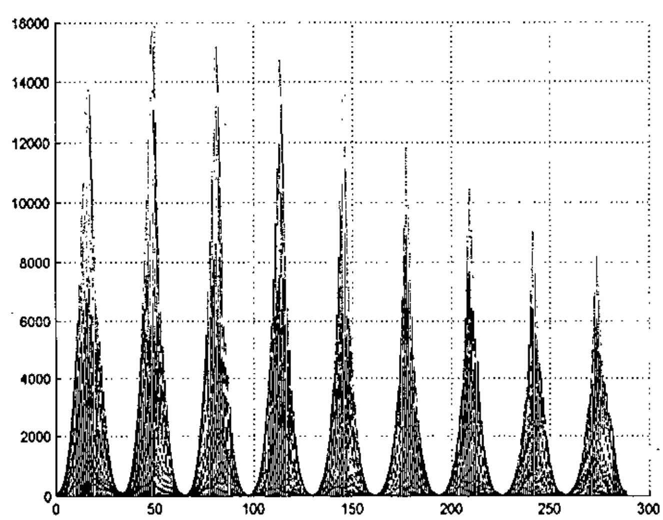

(b)

Fig. 4.2 Using classical JTC for SDF generation (a) Correlation output after one iteration, (b) Two dimensional view of the correlation output of (a).

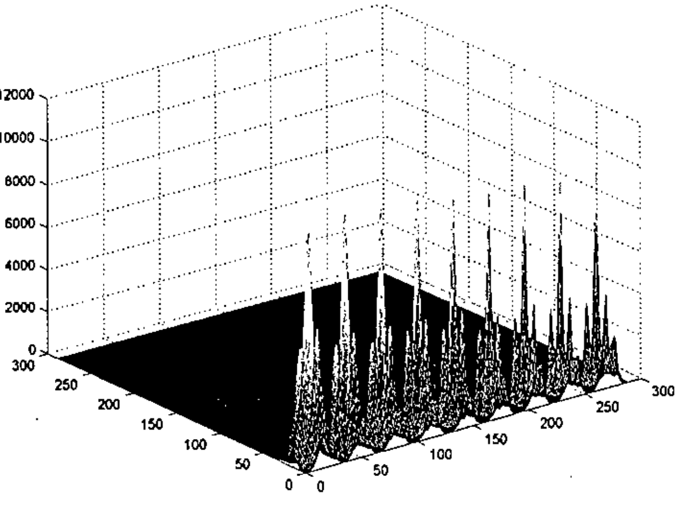

(c)

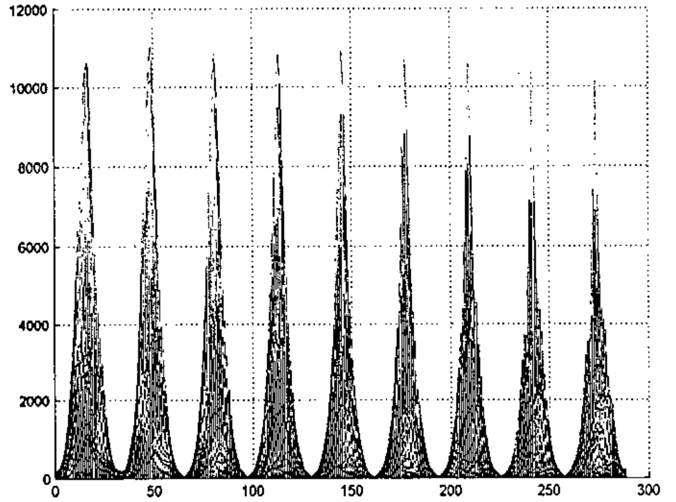

(d)

Fig. 4.2 (contd.) (c) Correlation output after 500 iterations, (d) Two dimensional view of the correlation output of (c).

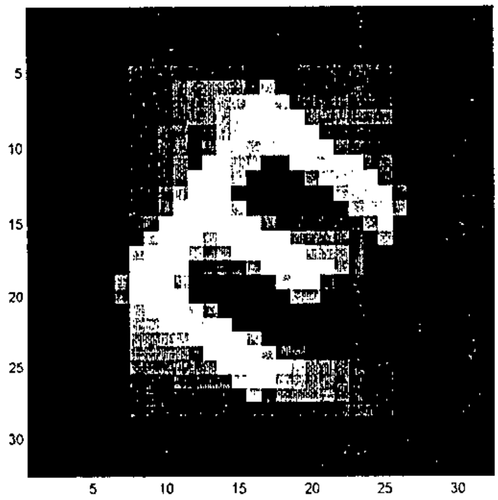

(e)

Fig 4.2 (contd.) (e) Spatial SDF r_{SDF}^{C} after 500 iterations.

Table 4.1 Correlation peak intensities for the training images of Fig. 4.1(a) after all iterations using classical JTC

	Image 1	Image 2	Image 3	Image 4	Image 5
Correlation peak intensity	10640	11005	10799	10872	10912
	Image 6	Image 7	Image 8	Image 9	
Correlation peak intensity	10863	10808	10497	10270	

4.3.2.2 SDF Generated using Fringe-adjusted JTC

For the same training set images, initial SDF and joint image of Fig. 4.1 the SDF is now generated by using fringe-adjusted JTC with C=1, D=10^{-1} and m=2 in the GFAF filter. The relaxation factor rf is now set to 0.1. Here also after first iteration the correlation peaks are much different for different images as shown in Fig 4.3(a) and Fig 4.3(b). After 500 iterations taking around 8 minutes, the difference in correlation peak intensities reduces, but still does not reach within the desired error limit as is seen from Fig 4.3(c) and Fig 4.3(d). Table 4.2 clarifies this situation by displaying the correlation peak intensities for different images. On the other hand after 500 hundred iterations a large number of correlation side lobes with considerable intensities are created in the correlation output for the images.

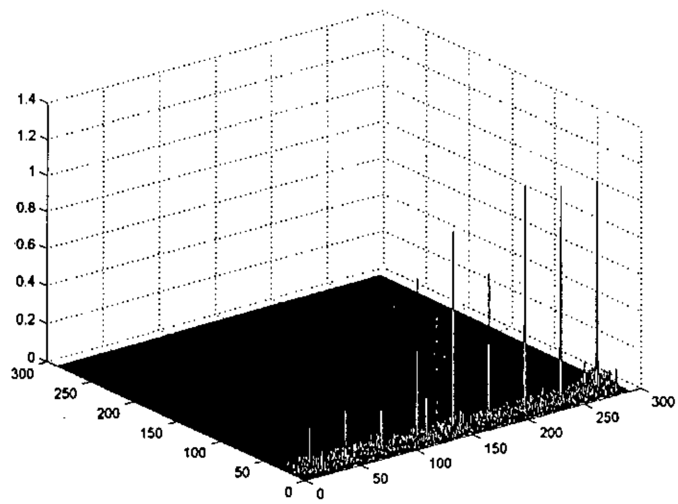

(a)

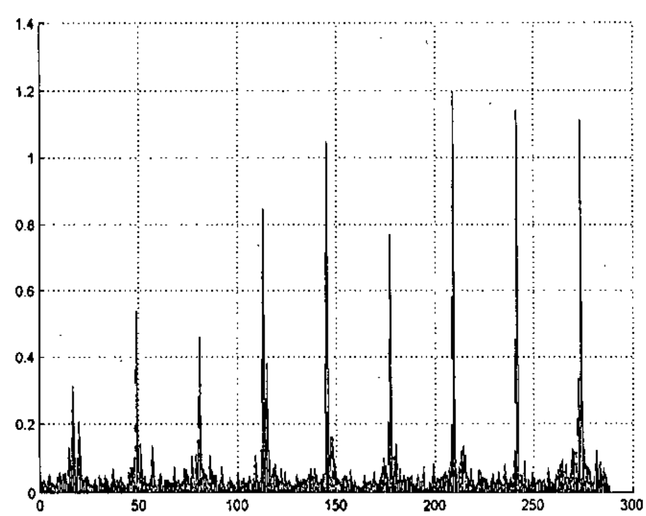

(b)

Fig. 4.3 Using fringe-adjusted JTC for SDF generation (a) Correlation output after one iteration, (b) Two dimensional view of the correlation output of (a).

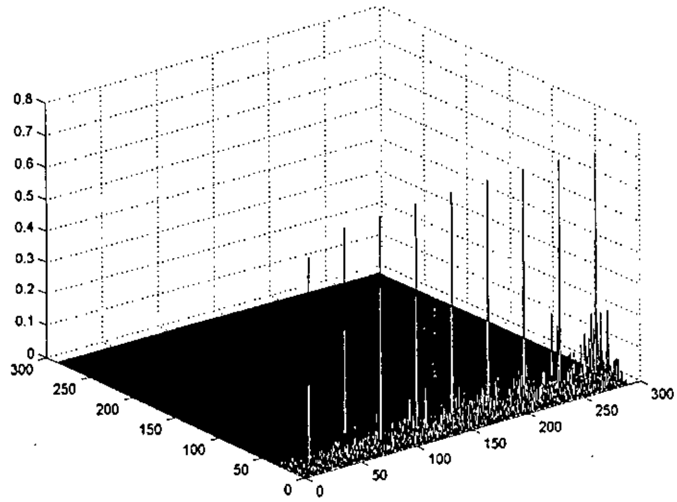

(c)

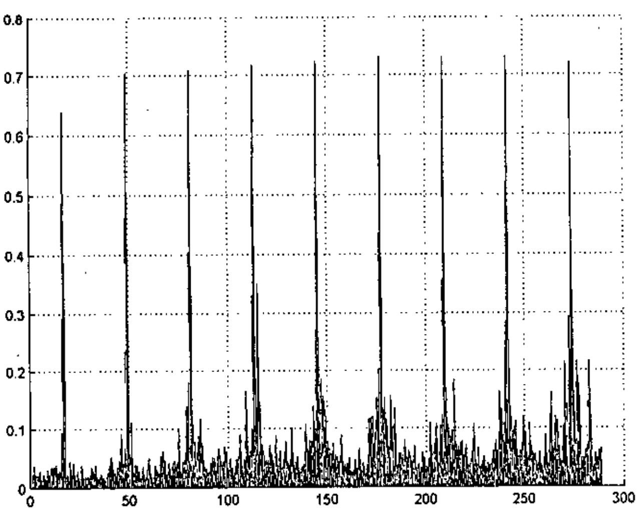

(d)

Fig. 4.3 (contd.) (c) Correlation output after 500 iterations, (d) Two dimensional view of the correlation output of (c).

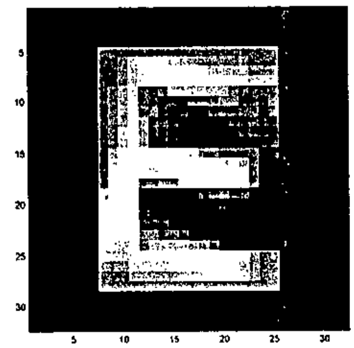

(e)

Fig. 4.3 (contd.) (e) Spatial SDF r_{SDF}^{f} after 500 iterations.

Table 4.2 Correlation peak intensities for the training images of Fig. 4.1(a) after all iterations using fringe-adjusted JTC

	Image I	Image 2	Image 3	Image 4	Image 5
Correlation peak intensity	0.6380	0.7036	0.7078	0.7171	0.7224
	Image 6	Image 7	Image 8	Image 9	
Correlation peak intensity	0.7305	0.7307	0.7307	0.7205	

So even if by increasing the number of iterations the peaks can be made equal, it will produce considerable sidelobe effect and thus deteriorating the performance of the generated SDF. Accordingly the final SDF in this case, termed as r_{SDF}^{f} obtained as in Fig. 4.3(e) should not also give satisfactory performance in distortion invariant detection.

4.3.2.3 SDF Generated using Phase-only JTC

For the same training image, initial SDF and joint image of Fig. 4.1 the SDF is generated by using phase-only JTC with C=1, D=10^{-4} and m=1 in the GFAF filter. Fig. 4.4(a) and Fig. 4.4(b) shows the correlation output for the training set images after first iteration with rf set to 0.1. In less than one minute and after only 12 iterations the program converges and the correlation peaks reach within the desired error limit as shown in Fig 4.4(c), Fig 4.4(d) and Table 4.3. Fig. 4.4(e) is the final SDF, termed as r_{SDF}^{p}, which should give satisfactory performance in distortion invariant recognition.

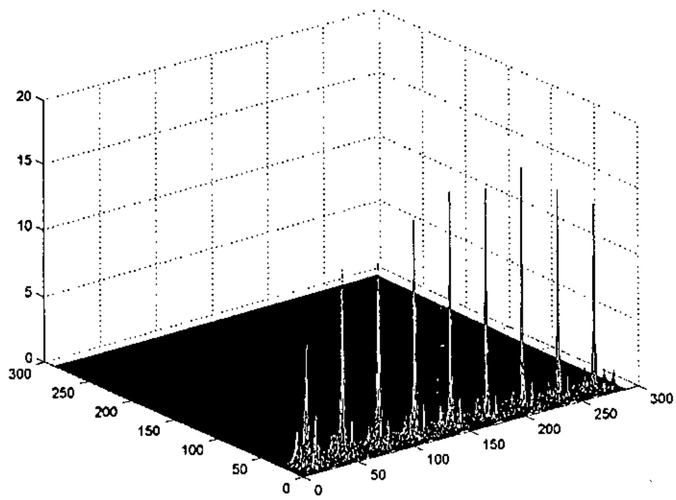

(a)

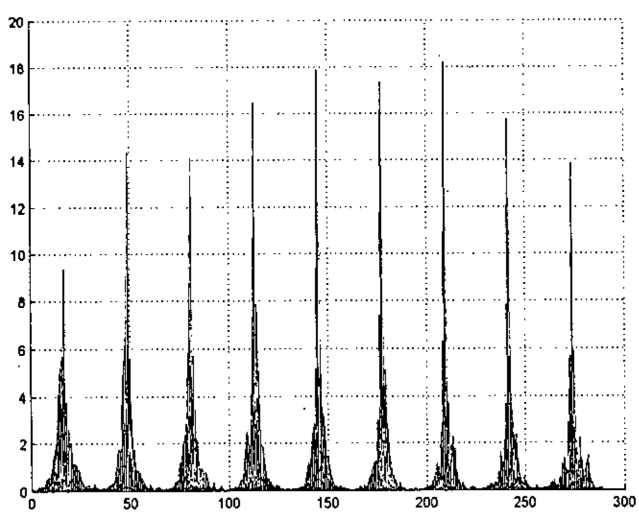

(b)

Fig. 4.4 Using phase-only JTC for SDF generation (a) Correlation output after one iteration, (b) Two dimensional view of the correlation output of (a).

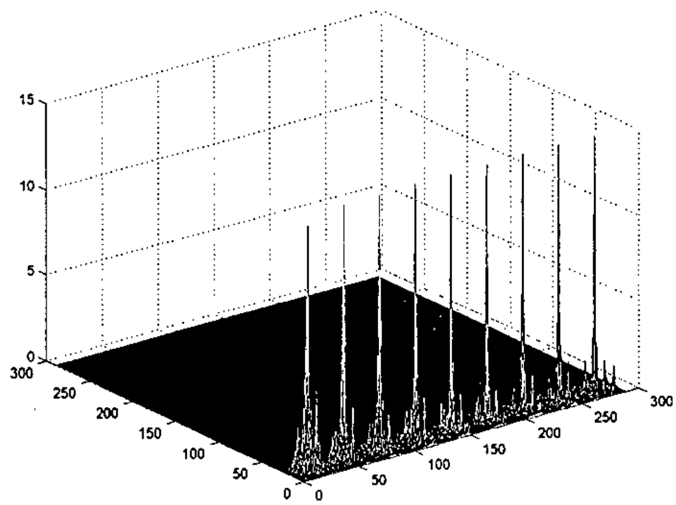

(c)

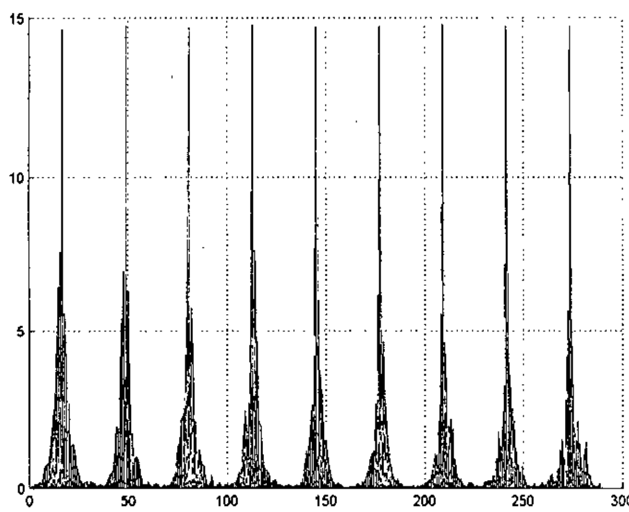

(d)

Fig. 4.4 (contd.) (c) Correlation output after 12 iterations, (d) Two dimensional view of the correlation output of (c).

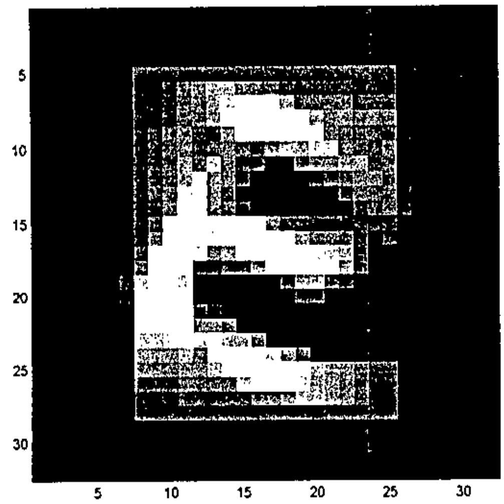

(e)

Fig. 4.4 (contd.) (e) Spatial SDF r_{SDF}^{p} after 12 iterations.

Table 4.3 Correlation peak intensities for the training images of Fig. 4.1(a) after all iterations using phase-only JTC

	Image 1	Image 2	Image 3	Image 4	Image 5
Correlation peak intensity	14.6380	14.7354	14.7082	14.7575	14.7229
	Image 6	Image 7	Image 8	Image 9	
Correlation peak intensity	14.7264	14.7709	14.7294	14.7120	

4.3.2.4 Performance Evaluation of the Generated SDFs

To evaluate the performance of the generated SDFs an input scene is taken with the four images from the training set. Fig. 4.5(a) shows the input joint image with the reference as undistorted image. Fig. 4.5(b) shows the correlation output with fringe-adjusted JTC and Fig. 4.5(c) shows the correlation output with phase-only JTC. It is seen that a pair of correlation peaks is obtained only for the undistorted image while there is no or negligible peaks for the distorted images. So without using SDF both fringe-adjusted JTC and phase-only JTC fail to detect the distorted images of the input scene.

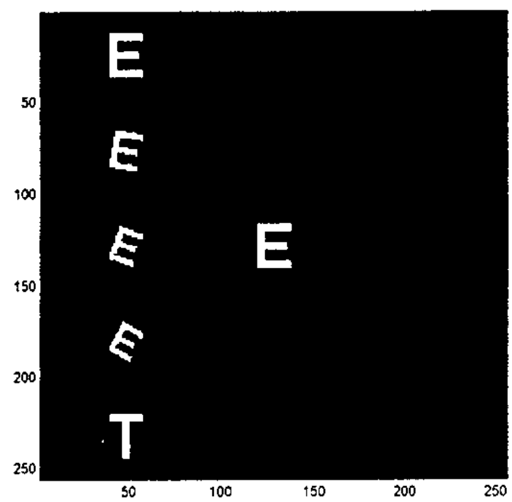

(a)

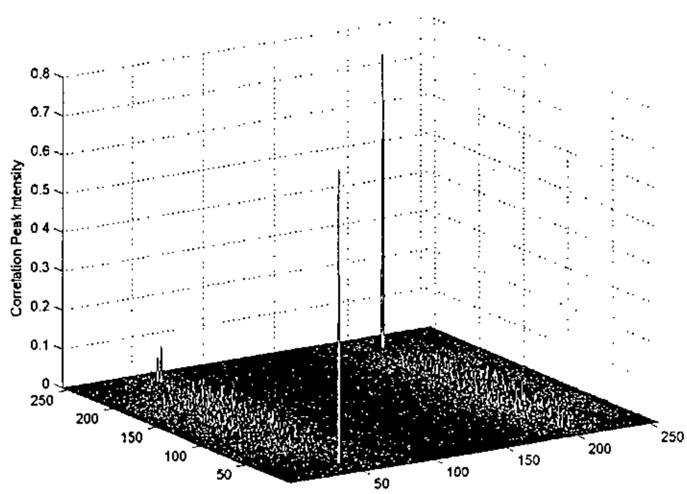

(b)

Fig. 4.5 (a) Input joint image with distorted and undistorted images along with undistorted image as reference, (b) Correlation output using fringe-adjusted JTC.

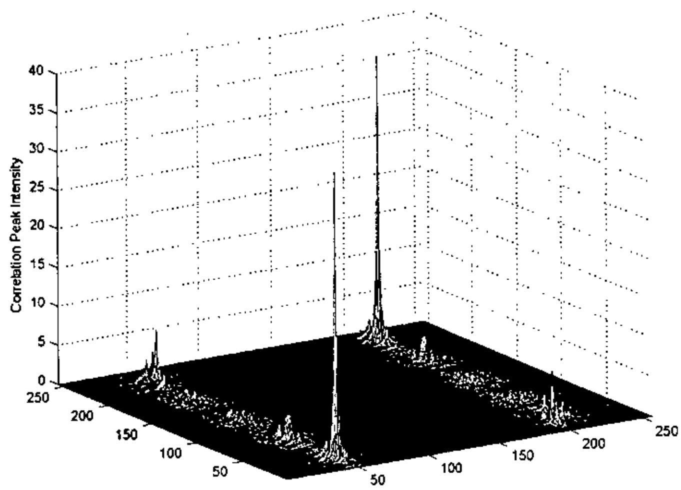

(c)

Fig 4.5 (contd.) (c) Correlation output using phase-only JTC.

Now instead of the original image as the reference, r_{SDF}^c, r_{SDF}^f and r_{SDF}^p are taken one by one to evaluate their performance by using both fringe-adjusted JTC and phase-only JTC, which are shown in the following analysis by using figures.

a) Performance of r_{SDF}^c in fringe-adjusted JTC:

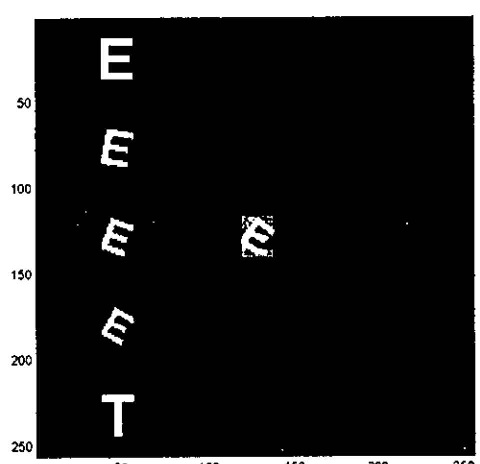

(a)

Fig. 4.6 (a) Input joint image with distorted and undistorted images along with r_{SDF}^c as reference.

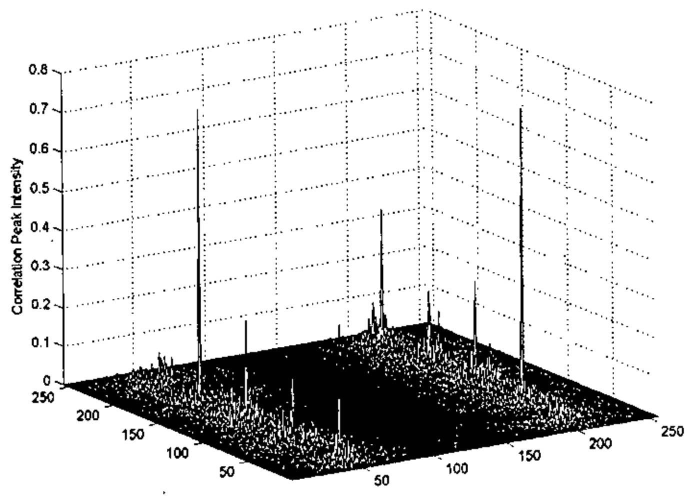

(b)

Fig. 4.6 (contd.) (b) Correlation output using fringe-adjusted JTC.

b) Performance of r_{SDF}^{f} in fringe-adjusted JTC:

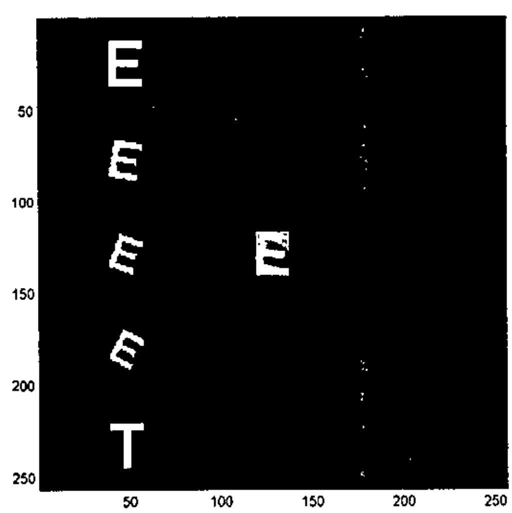

(a)

Fig. 4.7 (a) Input joint image with distorted and undistorted images along with r_{SDF}^{f} as reference.

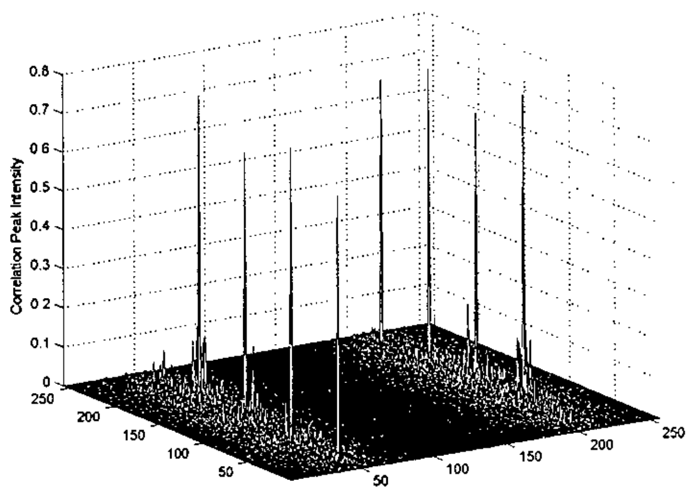

(b)

Fig. 4.7 (contd.) (b) Correlation output using fringe-adjusted JTC.

c) Performance of r_{SDF}^{P} in fringe-adjusted JTC:

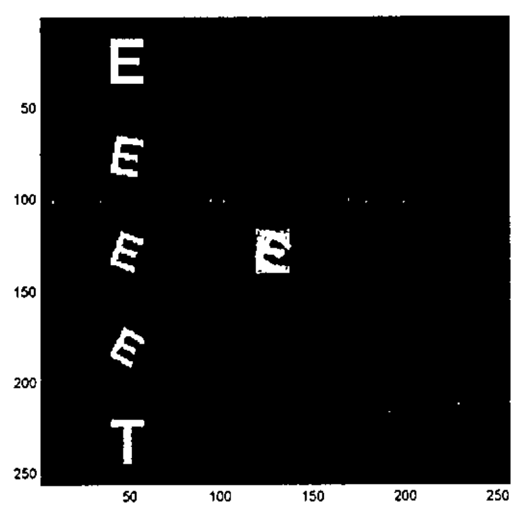

(a)

Fig. 4.8 (a) Input joint image with distorted and undistorted images along with r_{SDF}^{P} as reference.

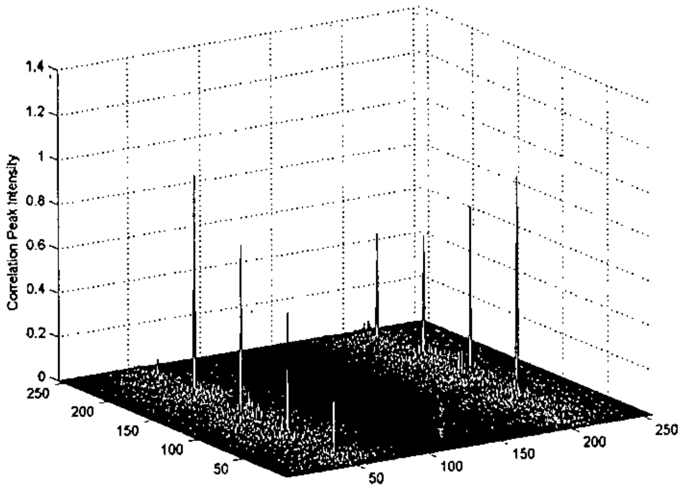

(b)

Fig. 4.8 (contd.) (b) Correlation output using fringe-adjusted JTC.

d) Performance of $r_{SDF}{}^{c}$ in phase-only JTC:

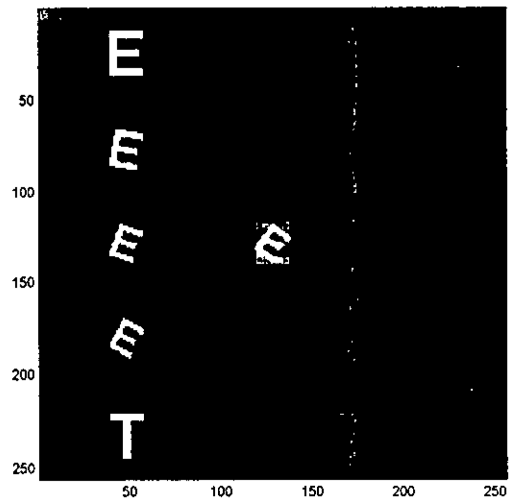

(a)

Fig. 4.9 (a) Input joint image with distorted and undistorted images along with $r_{SDF}{}^{c}$ as reference.

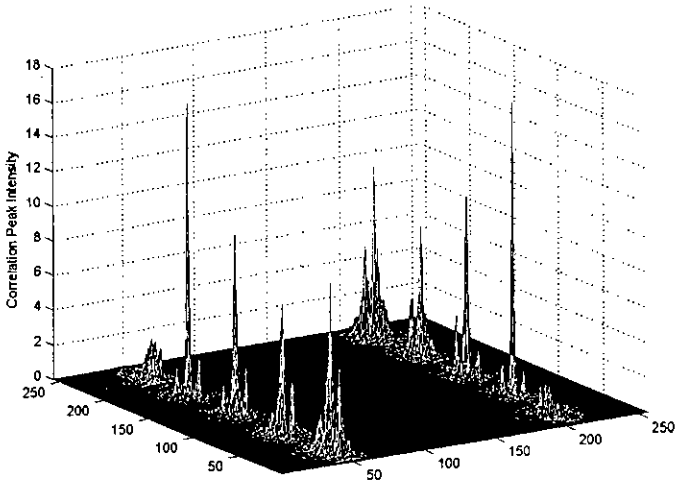

(b)

Fig. 4.9 (contd.) (b) Correlation output using phase-only JTC.

e) Performance of r_{SDF}^{f} in phase-only JTC:

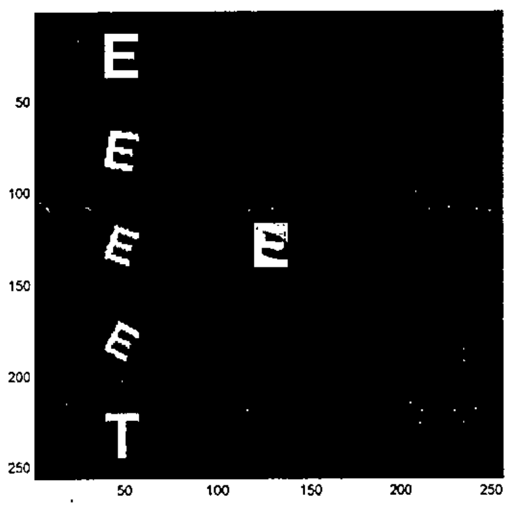

(a)

Fig. 4.10 (a) Input joint image with distorted and undistorted images along with r_{SDF}^{f} as reference.

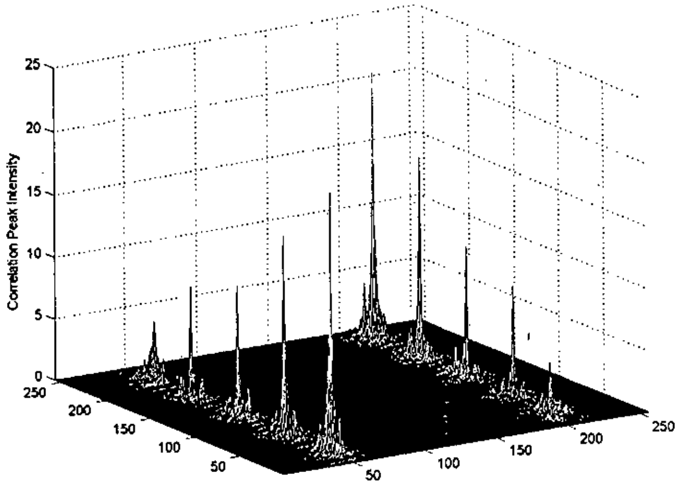

(b)

Fig. 4.10 (contd.) (b) Correlation output using phase-only JTC.

f) Performance of r_{SDF}^p in phase-only JTC:

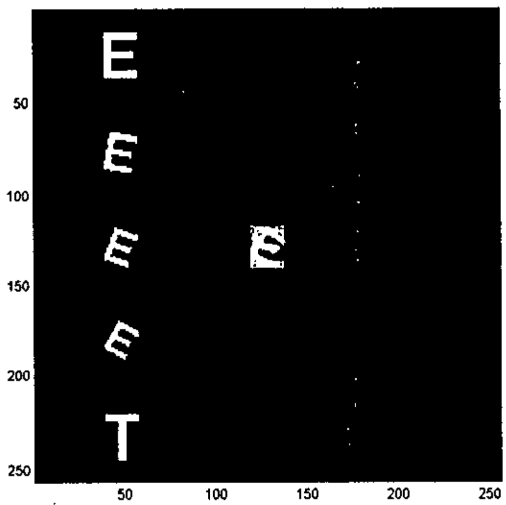

(a)

Fig. 4.11 (a) Input joint image with distorted and undistorted images along with r_{SDF}^p as reference.

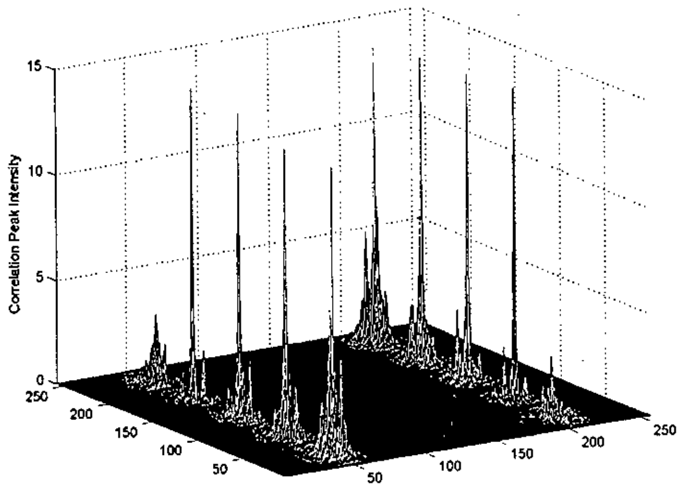

(b)

Fig. 4.11 (contd.) (b) Correlation output using phase-only JTC.

From the above analysis it is observed that for the target detection with distorted target images in the input scene fringe-adjusted JTC using SDF reference produced by fringe-adjusted JTC (r_{SDF}^{f}) and phase-only JTC using SDF reference produced by phase-only JTC (r_{SDF}^{p}) give acceptable performance. However correlation peaks obtained by using r_{SDF}^{f} for the images from the training set are not equal and the correlation output is not free from side lobes. On the other hand correlation peaks obtained by using r_{SDF}^{p} are almost equal though there are side lobes in this case too. As there may be distorted and undistorted non-target images in the input scene as well, equal peaks for all the distorted and undistorted target images are very important to clearly differentiate them from the non-targets. So SDF generated using phase-only JTC along with phase-only JTC for detection is suitable for efficient distortion invariant target recognition.

4.4 Conclusion

In this chapter a simplified iterative method of formulating SDF by using GJTC is discussed. The weights of the SDF corresponding to the training set images are determined according to the target correlation peaks of the images. These target correlation peaks, however, are set by the SDF generation algorithm, which are not fixed quantities, rather are governed by the desired error limit. The SDF is generated off-line and then implemented as reference in real time JTC. It is found that SDF program better converges when phase-only JTC is used and it gives better distortion invariant detection if phase-only JTC is used in the ultimate target detection application.

Chapter 5

DISTORTION INVARIANT CLASS-ASSOCIATIVE TARGET DETECTION

5.1 Introduction

Synthetic discriminant function (SDF) is used with the JTC techniques for obtaining distortion invariant target detection such as detection of scaled or rotated images with equal correlation peak as obtained for undistorted images. Multi-target detection algorithm based class-associative target detection technique employing JTC is used to detect a class of similar or dissimilar objects with equal correlation peak for all the images of the class. However if the images of the class are rotated or have scale variation or other types of distortion, this class associative target detection technique fails to detect the distorted images. On the other hand making SDF from the undistorted and distorted images of the class and using that SDF as the reference in usual JTC techniques does not work in detection of distorted and even undistorted images of the class. So to get distortion invariant class-associative target detection SDF based reference image can be employed for each object of the class in the class-associative target detection technique. In this chapter the processes or conditions necessary to employ SDF in class-associative target detection will be shown and the performance of the technique will be evaluated for both binary and gray level images with and without noise in the input scene.

5.2 Theoretical Analysis

In section 3.3 it is shown that if there are two objects or images of the class, then there will be two reference images $r_1(x,y)$ and $r_2(x,y)$ to be used to make two sets of input spectra and to formulate the class-associative generalized fringe-adjusted filter (CGFAF) for class detection. To get distortion invariant detection the reference image $r_1(x,y)$ should be synthesized from the training set containing the possible or expected distortions of the image along with the undistorted one. So instead of undistorted $r_1(x,y)$, the reference is now synthesized SDF given by $r_{SDF1}(x,y)$. Similarly $r_2(x,y)$ is replaced by $r_{SDF2}(x,y)$. The Fourier transform of $r_{SDF1}(x,y)$ may be given by $R_{SDF1}(u,v)$ and Fourier transform of $r_{SDF2}(x,y)$ may be given by $R_{SDF2}(u,v)$. So for SDF based distortion invariant detection of a two-object class, Eq. (3.8) to Eq. (3.16) are modified by replacing $r_1(x,y)$ with $r_{SDF1}(x,y)$, $r_2(x,y)$ with $r_{SDF2}(x,y)$, $R_1(u,v)$ with $R_{SDF1}(u,v)$ and $R_2(u,v)$ with $R_{SDF2}(u,v)$. Thus using $r_{SDF1}(x,y)$ and $r_{SDF2}(x,y)$ gives distortion invariant detection of the images of the class.

5.3 Simulation

It is observed in section 4.3.2 that SDF generated by using phase-only JTC along with phase-only JTC for target detection gives better correlation performance for distortion invariant recognition. So for class associative target detection SDF based reference images obtained by using phase-only JTC and in the class-associative detection algorithm the class-associative generalized fringe-adjusted filter (CGFAF) as a phase-only filter could be directly chosen. But as class-associative target detection employs a multi-target detection algorithm based on JTC, which is different from other JTCs, the analysis is made first to find the suitable filter for SDF generation and suitable filter for class detection. Once a decision is reached, subsequent analyses are made with the best choice for the above-mentioned two cases. First, analysis is made to show the distortion invariant class-associative target detection for binary images such as English alphabets. Then this same analysis is done for gray level images.

5.4 Detection of Binary Images

5.4.1 Distorted Images with Undistorted References

At first alphabets 'E' and 'H' are taken as the desired class of binary images. To see the effect of distortion of these images an input scene is considered with undistorted and distorted versions of these two images as shown in Fig. 5.1(a). Now if the undistorted images are used as references as shown in Fig. 5.1(b) and Fig 5.1(c), then correlation output is obtained as Fig 5.1(d) if fringe-adjusted filter is used and as Fig. 5.1(e) if phase-only filter is used. It is observed that there are correlation peaks only for the undistorted images of the class. So, class-associative detection technique fails to detect the distorted images with the undistorted images as the references.

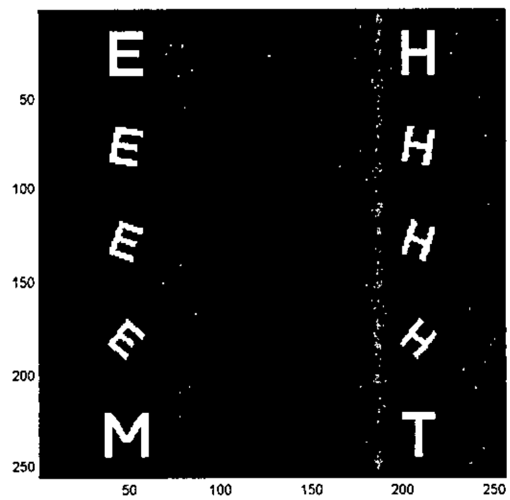

(a)

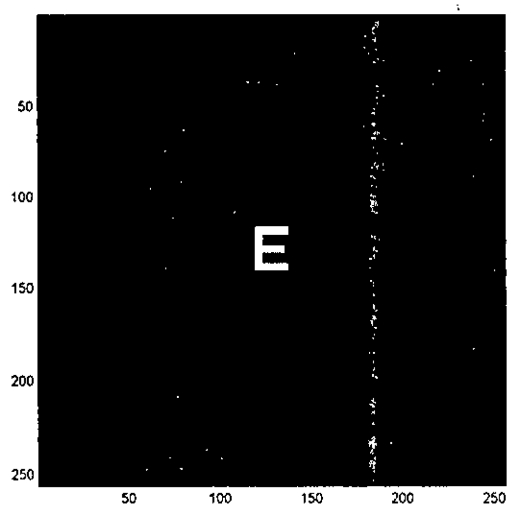

(b)

Fig. 5.1 (a) Input scene with multiple distorted and undistorted images of the class and multiple non-targets, (b) Reference image 1.

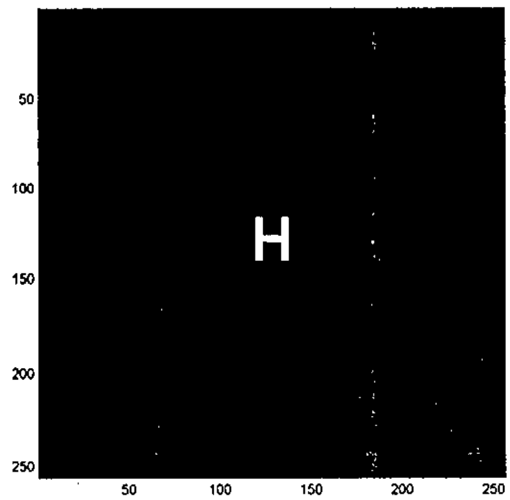

(c)

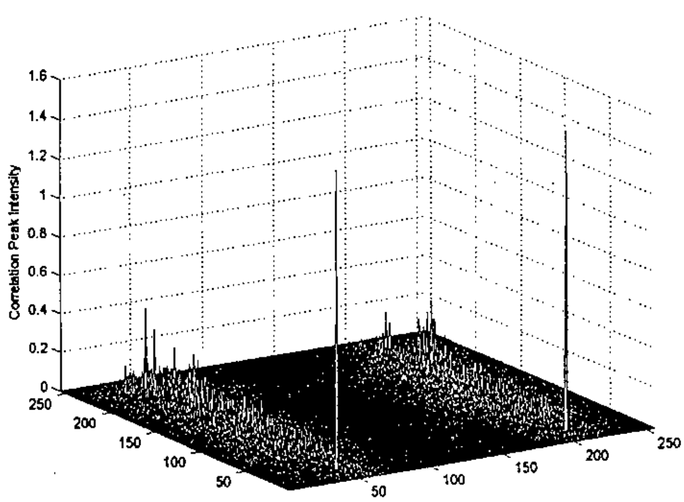

(d)

Fig. 5.1 (contd.) (c) Reference image 2, (d) Correlation output using fringe-adjusted filter

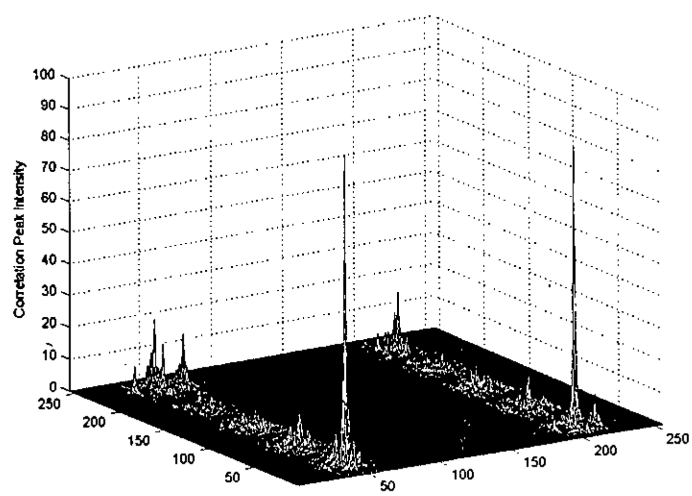

(e)

Fig. 5.1 (contd.) (e) Correlation output using phase-only filter.

5.4.2 Distorted Images with SDF References

To get SDF image of 'E' a training set has been taken by rotating the image up to an angle of 40 degrees clockwise at a step of 5 degrees. This rotation is made by MATLAB image processing toolbox using simple nearest neighbor interpolation, which is responsible for the other distortions and scaling of the images as well. So in total there are 9 images in the training set including the undistorted one as is given in Fig. 5.2(a). In the same way training set for 'H' is obtained as is given in Fig 5.2(b).

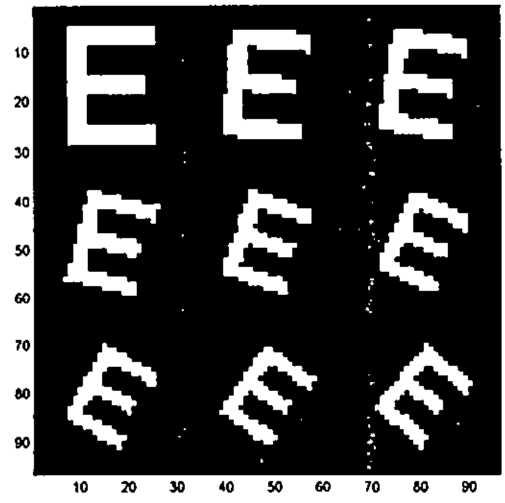

(a)

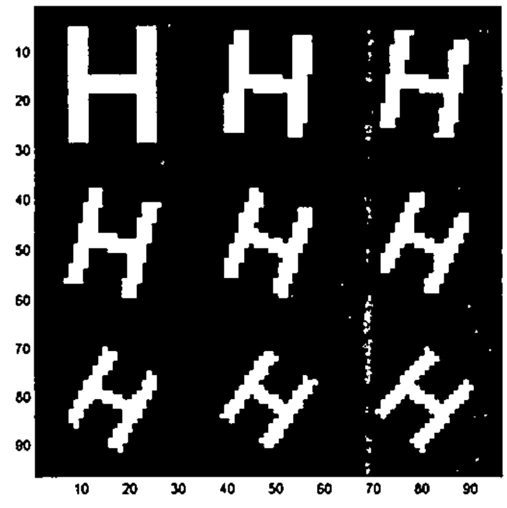

(b)

Fig. 5.2 (a) Training set of image 1 ('E'), (b) Training set of image 2 ('H').

Now SDF based reference images are created from both the training sets using both fringe-adjusted JTC and phase only JTC. These SDF references are used to get distortion invariant class-associative target detection (Appendix II). Fig. 5.3(a) and Fig. 5.3(b) shows the SDF references generated by using fringe-adjusted JTC. The input scene is same as that of Fig 5.1(a) containing the distorted images from the training set. Fig 5.4(a), Fig 5.4(b) and Fig 5.4(c) give the correlation output for the input scene images using fringe-adjusted filter in class-associative target detection technique. Here the correlation peaks for the targets of the class are very much different and the highest peaks are obtained for the non-targets.

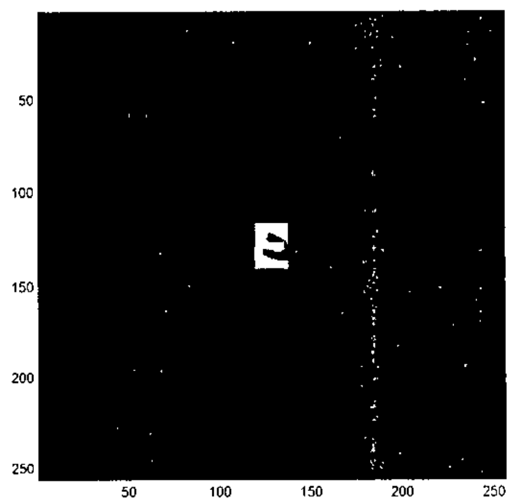

(a)

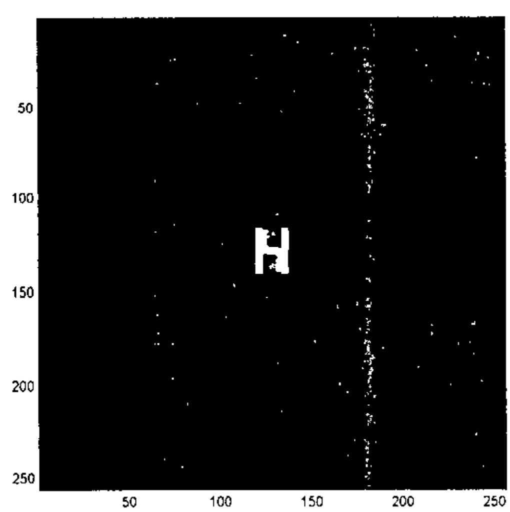

(b)

Fig. 5.3 (a) SDF reference image 1, generated by using fringe-adjusted JTC, (b) SDF reference image 2, generated by using fringe-adjusted JTC.

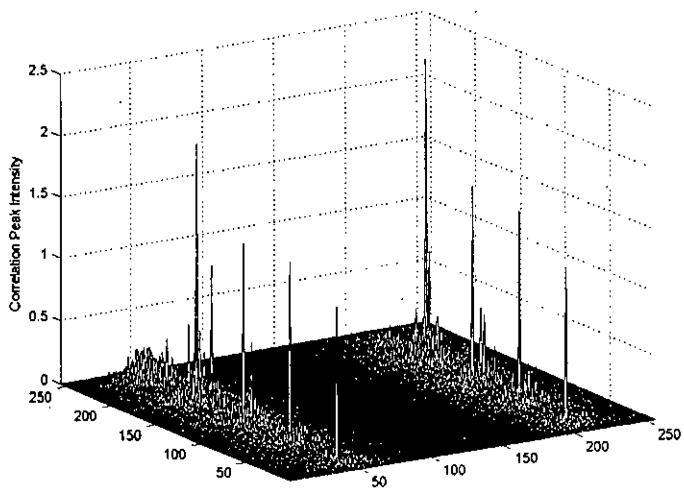

(a)

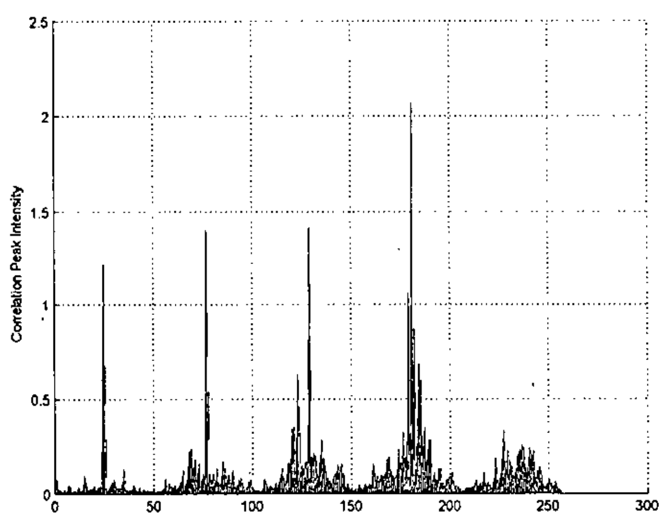

(b)

Fig. 5.4 (a) Correlation output for Fig. 5.1(a) and Fig 5.3 using fringe-adjusted filter, (b) Correlation output for left-side images.

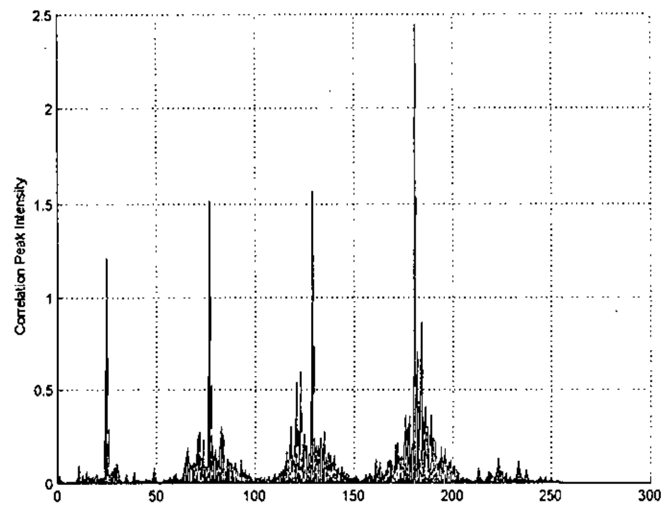

(c)

Fig. 5.4 (contd.) (c) Correlation output for right-side images.

Fig. 5.5(a), Fig. 5.5(b) and Fig 5.4(c) shows the correlation output for the same input scene images of Fig 5.1(a) using phase-only filter in class-associative target detection technique. Here also the SDF references are generated by using fringe-adjusted JTC as given in Fig. 5.3(a) and Fig 5.3(b).

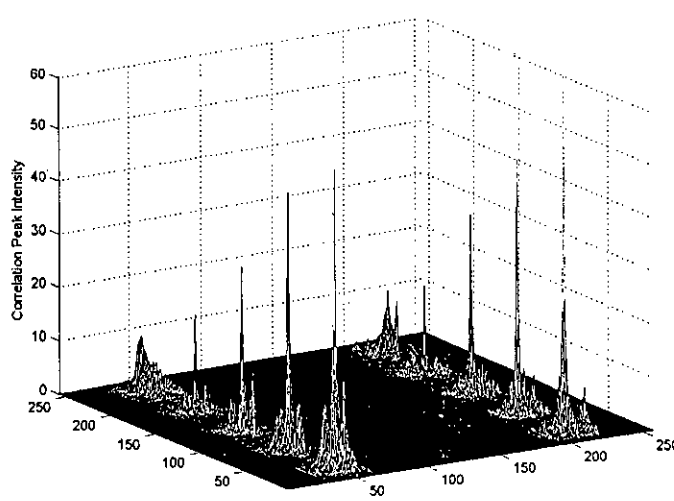

(a)

Fig. 5.5 (a) Correlation output for Fig. 5.1(a) and Fig 5.3 using phase-only filter.

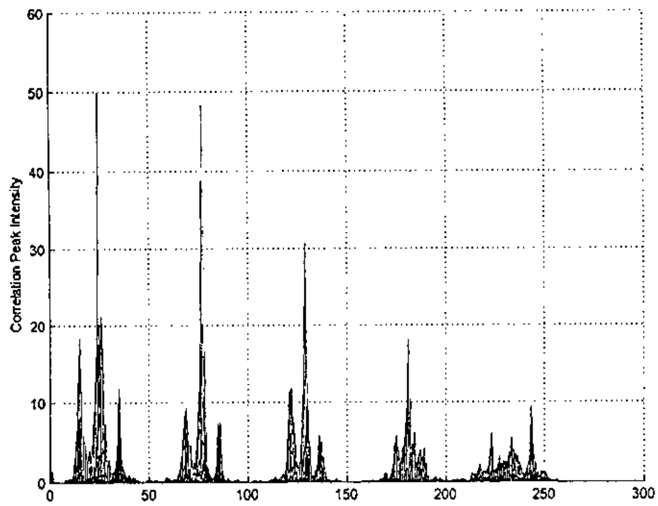

(b)

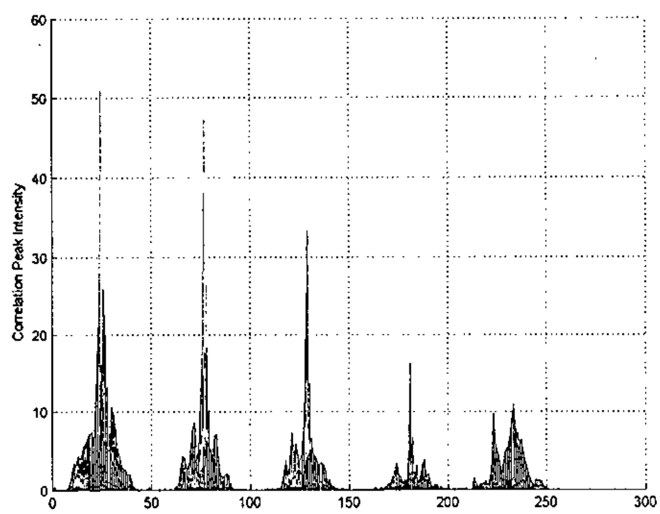

(c)

Fig. 5.5 (contd.) (b) Correlation output for left-side images, (c) Correlation output for right-side images.

In this case also correlation peaks for the targets are very much different though the non-target peaks are smaller. So from Fig. 5.4 and Fig 5.5 it can be concluded that SDF references generated by using fringe-adjusted JTC fail in distortion-invariant class detection whether fringe-adjusted filter or phase-only filter is chosen in the class-associative generalized fringe-adjusted filter (CGFAF).

Fig 5.6(a) and Fig 5.6(b) are the SDF references generated by using phase-only JTC. These are now used for the class detection for the input scene of Fig 5.1(a) using fringe-adjusted filter in class-associative recognition technique. The corresponding correlation output is given in Fig. 5.7(a), Fig 5.7(b) and Fig 5.7(c).

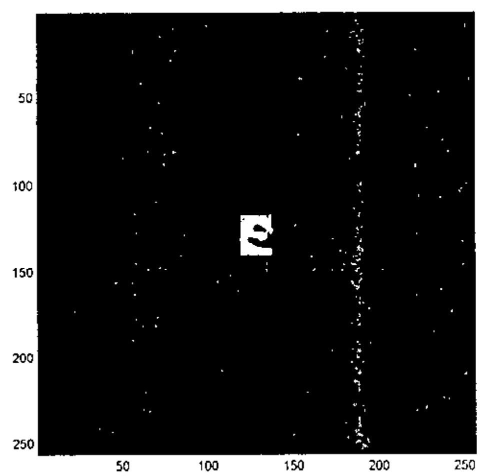

(a)

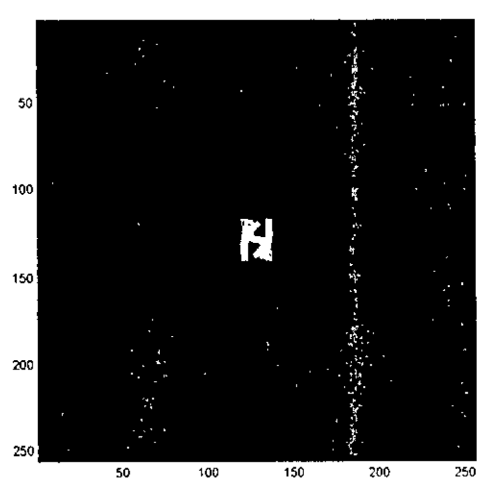

(b)

Fig. 5.6 (a) SDF reference image 1, generated by using phase-only JTC, (b) SDF reference image 2, generated by using phase-only JTC.

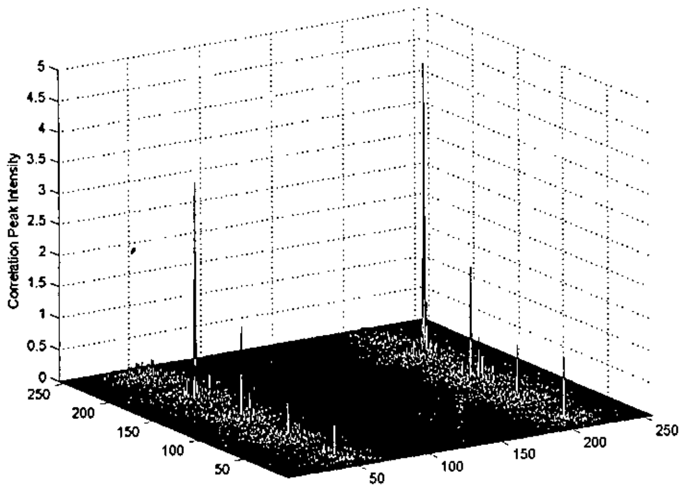

(a)

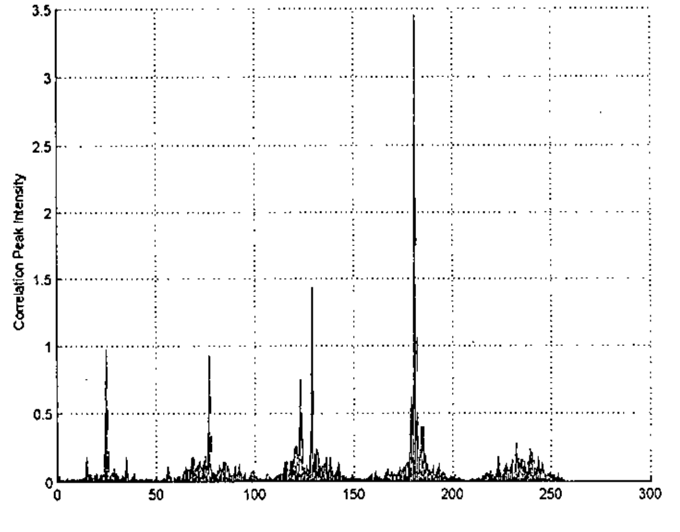

(b)

Fig. 5.7 (a) Correlation output for Fig. 5.1(a) and Fig. 5.6 using fringe-adjusted filter, (b) Correlation output for left-side images.

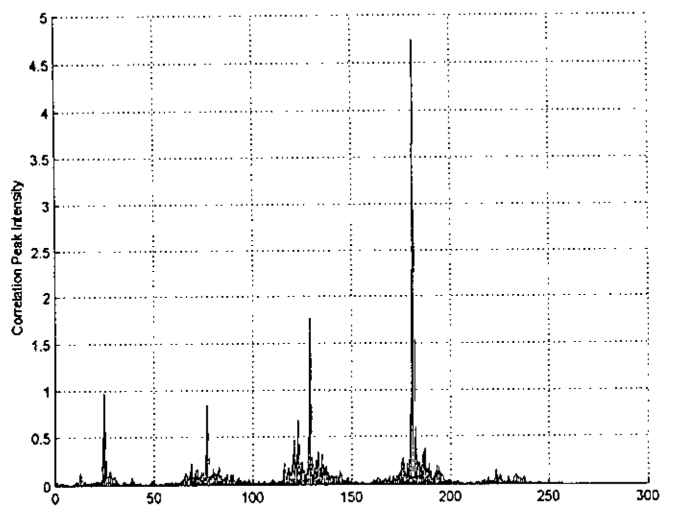

(c)

Fig. 5.7 (contd.) (c) Correlation output for right-side images.

It is seen that even if the SDF references are generated by phase-only JTC, the class-associative detection technique fails to successfully detect all the distorted and undistorted images of the class when the CGFAF is a fringe-adjusted filter.

As a final attempt the SDF references of Fig. 5.6 are used in the class-associative target detection technique using phase-only filter in CGFAF for the same input scene of Fig. 5.1(a). The correlation output is given in Fig 5.8(a), Fig 5.8(b) and Fig 5.8(c). It is evident that this is the most successful correlation performance with almost equal peaks for the distorted and undistorted images of the class and negligible peaks for the non-targets. So it is concluded here that for distortion invariant class-associative target detection the SDF reference must be generated by using phase-only JTC and in class-associative detection technique the generalized filter CGFAF should be a phase-only filter.

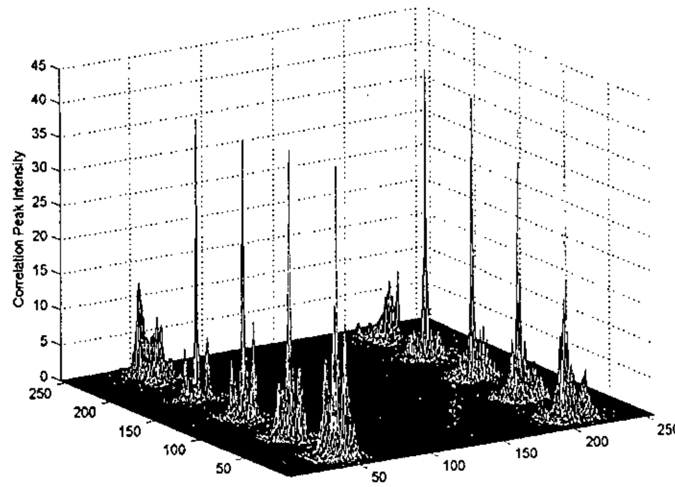

(a)

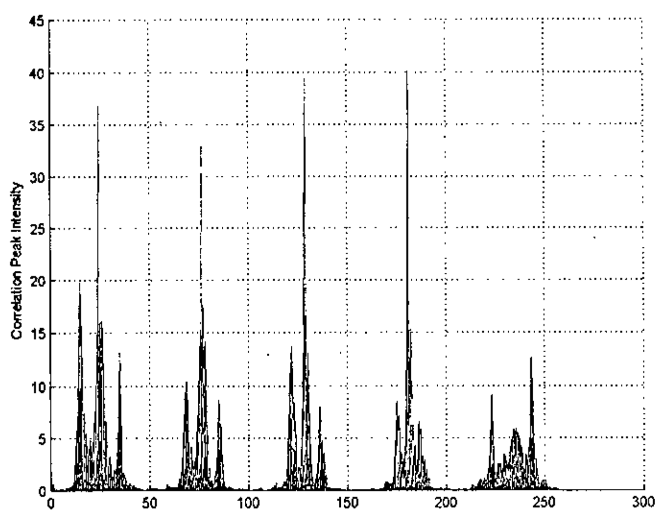

(b)

Fig. 5.8 (a) Correlation output for Fig. 5.1(a) and Fig. 5.6 using phase-only filter, (b) Correlation output for left-side images.

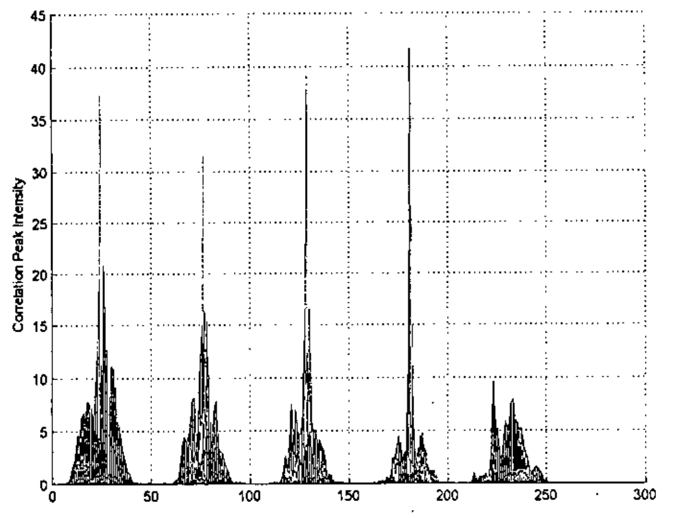

(c)

Fig. 5.8 (contd.) (c) Correlation output for right-side images.

5.4.3 Look-alike Non-target Image in the Input Scene

Let us assume that input scene contains a non-target image 'F' which is very much similar (look-alike) to the target image 'E' as shown in Fig 5.9(a). The SDF references for 'E' and 'H' generated by using phase-only JTC are shown in Fig 5.9(b) and Fig 5.9(c). The class-associative target detection technique is now employed using phase-only filter for Fig. 5.9 to obtain the correlation output of Fig 5.10. Here it is observed that the correlation peak for 'F' is very near to the target peaks and thus deteriorates the detection performance. The correlation peaks for all the images of the input scene are summarized in Table 5.1 and the performance of the correlation is summarized in Table 5.2. Here the ratio of maximum target peak to minimum target peak is 1.064 whereas the ratio of minimum target peak to maximum non-target peak is 1.204. So when there is a non-target very much similar to the target in the input scene, the class-associative target detection technique gives poor performance.

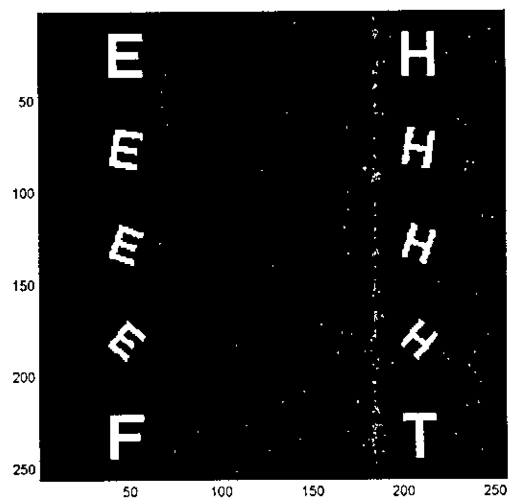

(a)

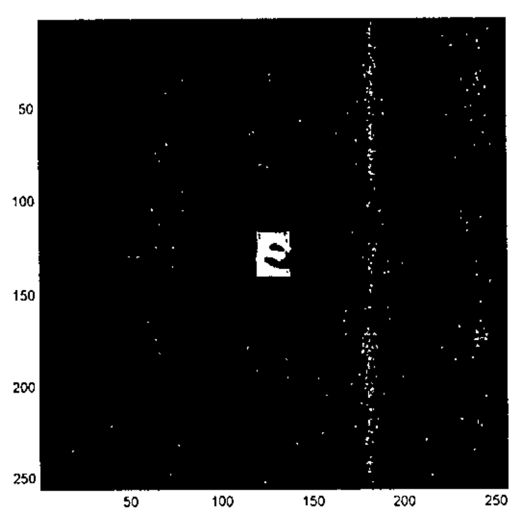

(b)

Fig. 5.9 (a) Input scene, (b) SDF Reference image 1.

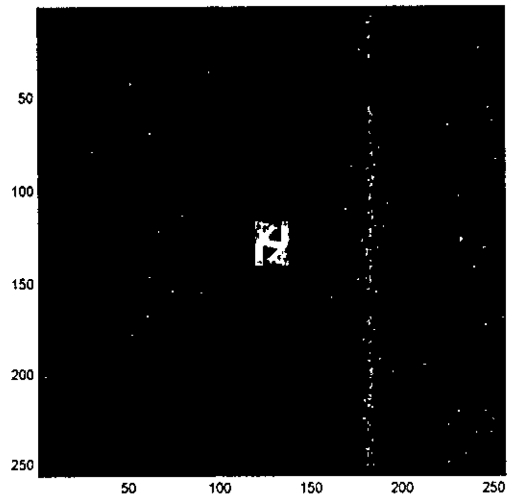

(c)

Fig. 5.9 (contd.) (c) SDF Reference image 2.

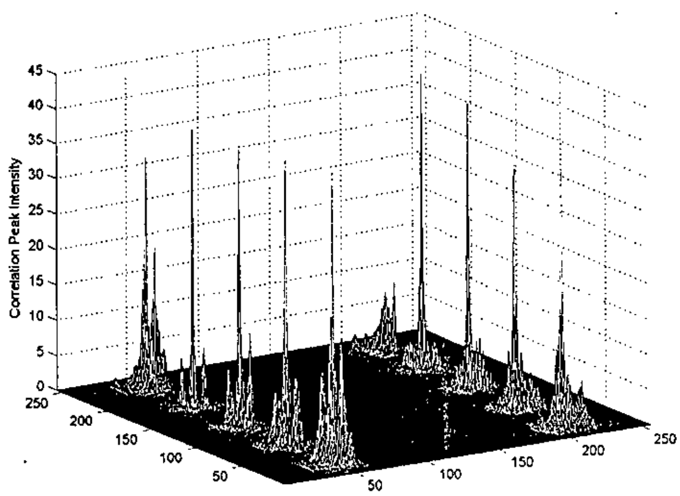

(a)

Fig. 5.10 (a) Correlation output for Fig. 5.9.

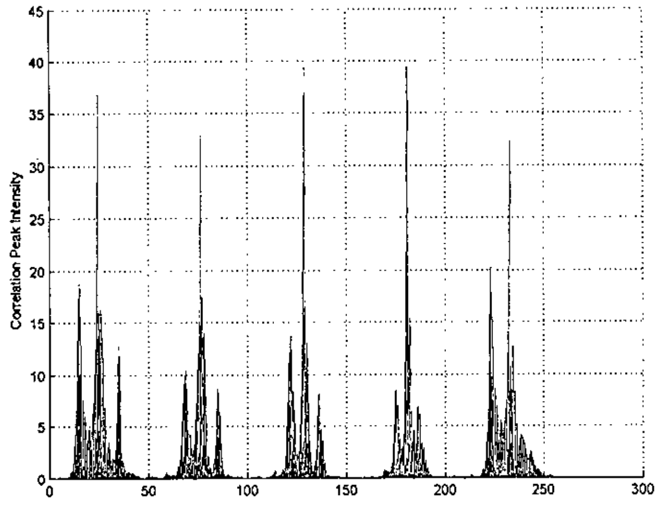

(b)

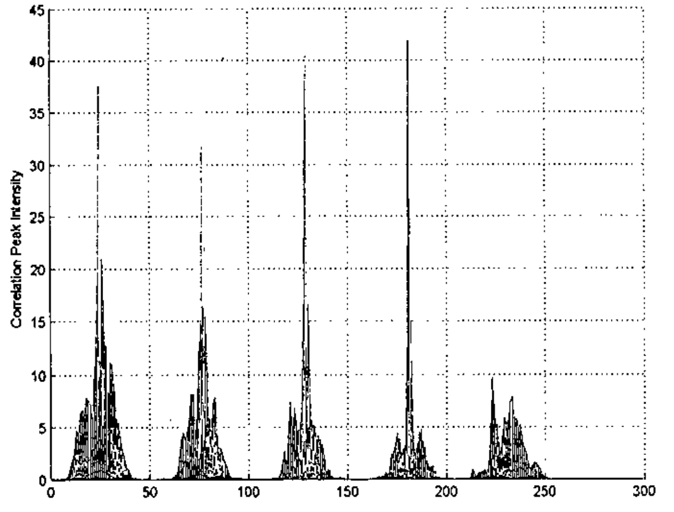

(c)

Fig. 5.10 (contd.) (b) Correlation output for left-side images, (c) Correlation output for right-side images.

Table 5.1 Correlation peak intensities for the input scene of Fig. 5.9(a)

	Correlation Peak Intensity				
	Image 1	Image 2	Image 3	Image 4	Image 5
For left-side	41.6964	40.8152	39.3258	39.4298	32.6538
For right-side	41.7362	39.3821	40.4845	41.8249	9.6857

Table 5.2 Detection performance using Table 5.1

Maximum Target Peak TG_{max}	Minimum Target Peak TG_{min}	Maximum Non-target Peak NTG_{max}	TG_{max}/TG_{min}	TG_{min}/NTG_{max}
41.8249	39.3258	32.6538	1.064	1.204

To get rid of the above problem the correlation output can be raised to a power of 4 by using two successive square law devices at the output plane to receive the output signal. Corresponding simulated correlation output is shown in Fig. 5.11.

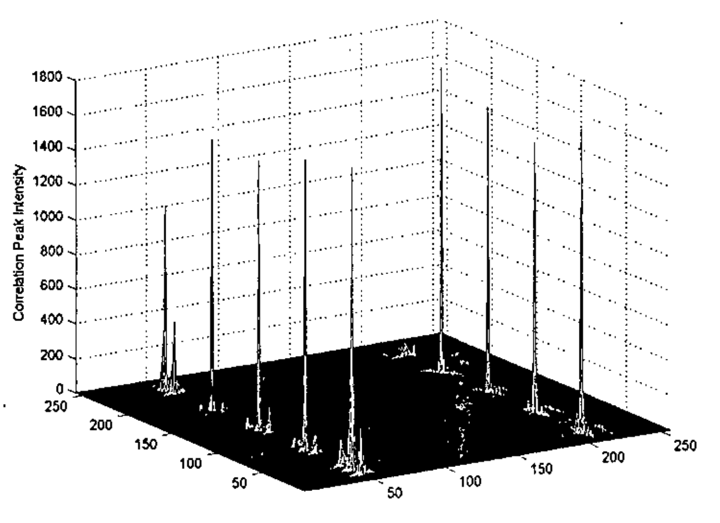

(a)

Fig. 5.11 (a) Correlation output Fig. 5.9 with correlation intensity enhancement.

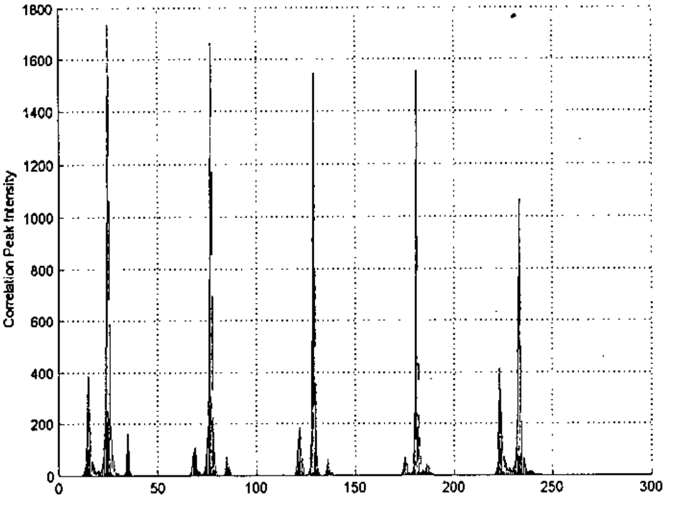

(b)

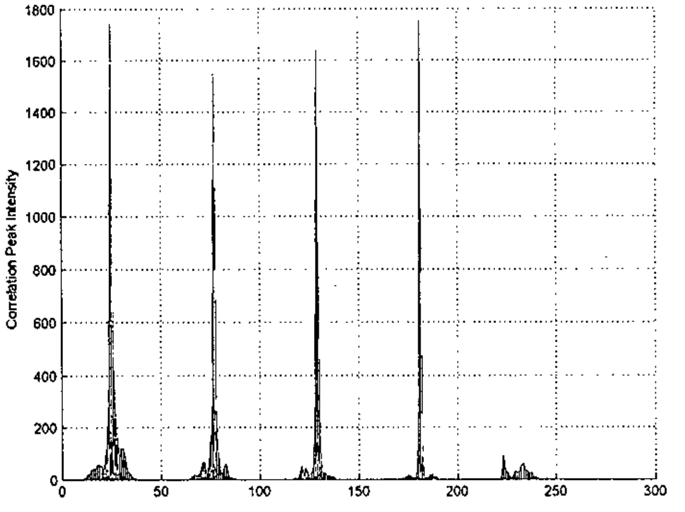

(c)

Fig. 5.11 (contd.) (b) Correlation output for left-side images, (c) Correlation output for right-side images.

Table 5.3 Correlation peak intensities for the input scene of Fig. 5.9(a)

	Correlation Peak Intensity				
	Image 1	Image 2	Image 3	Image 4	Image 5
For left-side	1739	1666	1547	1555	1066
For right-side	1742	1551	1639	1749	94

Table 5.4 Detection performance using Table 5.2

Maximum Target Peak TG_{max}	Minimum Target Peak TG_{min}	Maximum Non-target Peak NTG_{max}	TG_{max}/TG_{min}	TG_{min}/NTG_{max}
1749	1547	1066	1.131	1.451

This above technique of raising the correlation intensity may be termed as correlation intensity enhancement. The correlation peak intensities for Fig 5.11 are given in Table 5.3 while the performance is evaluated in Table 5.4. Here the correlation performance improves, as the maximum non-target peak due to look-alike non-target is significantly lower than the target peaks while the target peaks are almost equal. The ratio of maximum target peak to minimum target peak in this case is 1.131 while the ratio of minimum target peak to maximum non-target peak is 1.451. The difference between these two ratios is much higher than in the previous case. So correlation intensity enhancement may be used in this way to clearly differentiate look-alike non-targets.

5.4.4 Input Scene with Random Noise

Let us apply a random noise with signal to noise ratio (SNR) of 2 in the input scene as shown in Fig 5.12(a). For the same target images or references of Fig. 5.6 or Fig. 5.9, the correlation output is obtained without applying correlation intensity enhancement as shown in Fig 5.12(b), Fig 5.12(c) and Fig 5.12(d). It is observed that with such noise, the correlation output is good enough to detect the distorted and undistorted images of the class while rejecting the non-targets.

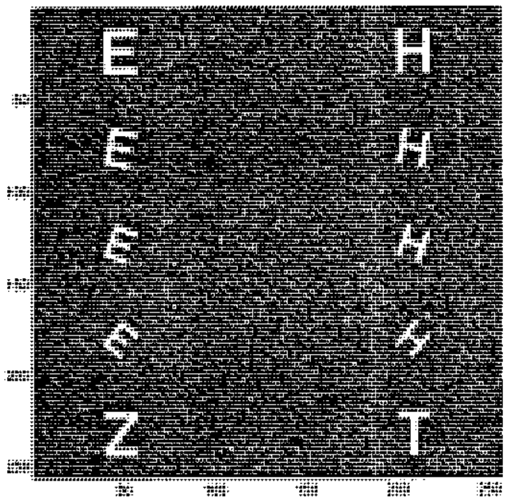

(a)

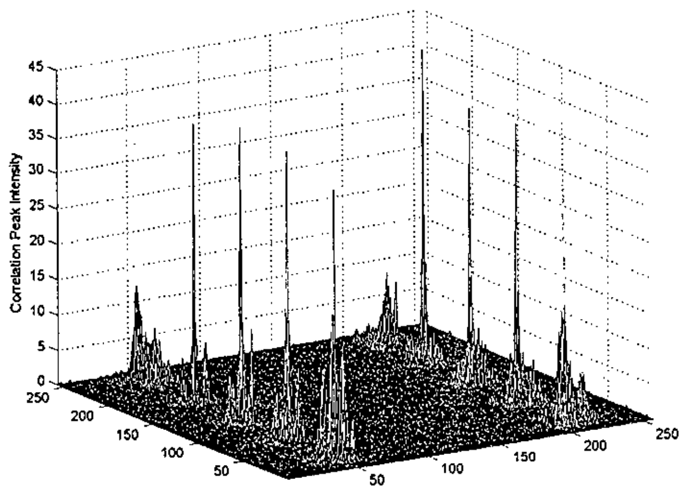

(b)

Fig. 5.12 (a) Input scene with noise, (b) Correlation output.

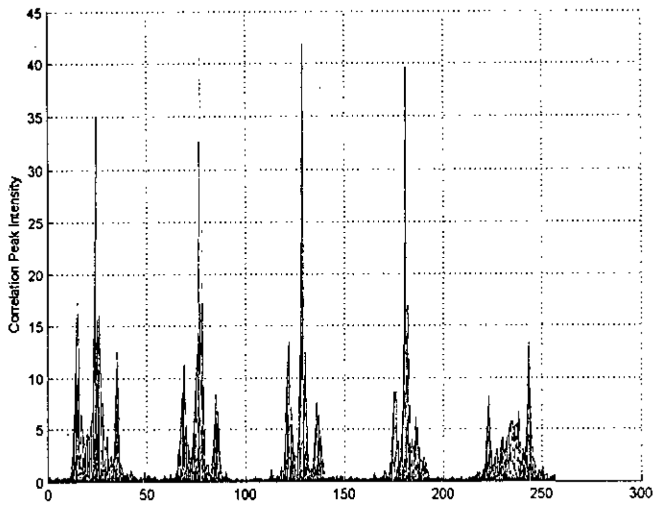

(c)

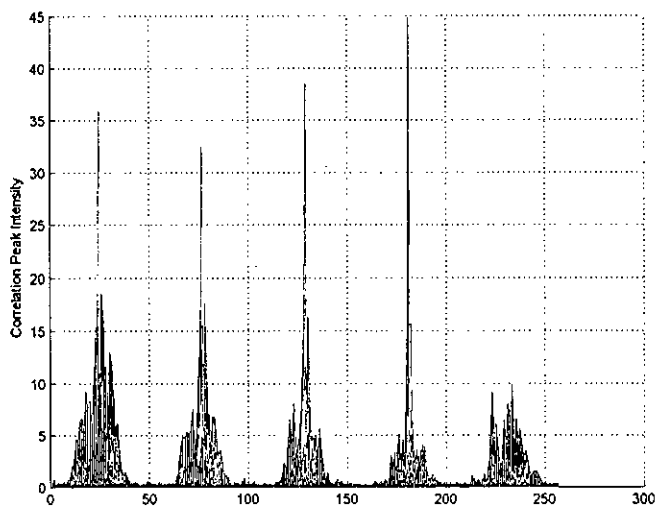

(d)

Fig. 5.12 (contd.) (c) Correlation output for left-side images, (d) Correlation output for right-side images.

5.4.5 Images Rotated up to 90 Degrees

In the previous analyses of section 5.4.1 to 5.4.4 it has been assumed that the images are rotated to an angle of 40 degrees at a step of 5 degrees from the initial or usual position. The SDF references were generated from those images or training sets. Here the original image is rotated up to 90 degrees clockwise at steps of 5 degrees using nearest neighbor interpolation of MATLAB. The training sets thus obtained for 'E' and 'H' are shown in Fig 5.13(a) and Fig 5.13(b), which contain images with scale variation and other distortions too. The set of images is then used to produce the SDF reference for a particular image such as 'E'. In the same way the SDF reference is generated for 'H'. In the input scene the images are chosen now from these training set images of the two members of the class. Fig. 5.14(a) is the input scene and Fig. 5.14(b) and Fig 5.14(c) are the reference images for this analysis. Corresponding correlation output is shown in Fig 5.15(a), Fig 5.15(b) and Fig 5.15(c) without using correlation intensity enhancement.

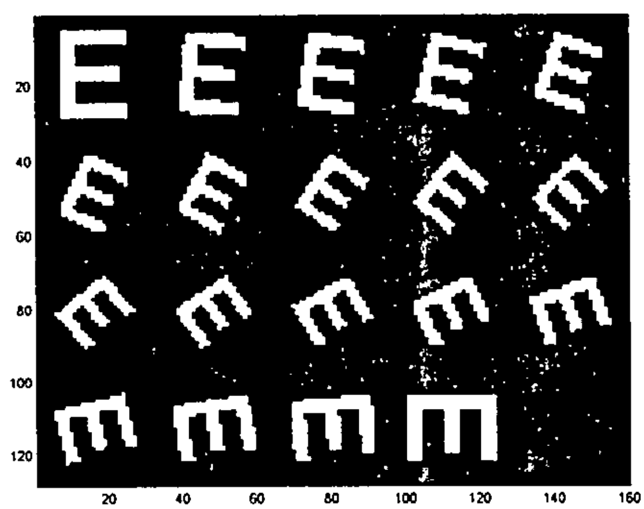

(a)

Fig. 5.13 (a) Training set for image 1 ('E').

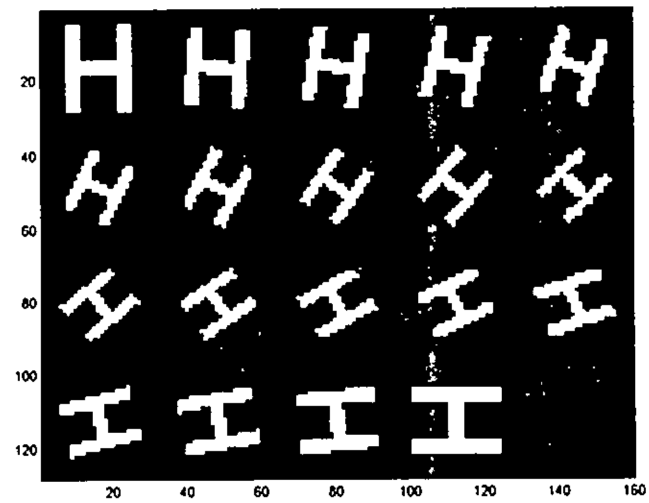

(b)

Fig. 5.13 (contd.) (b) Training set for image 2 ('H').

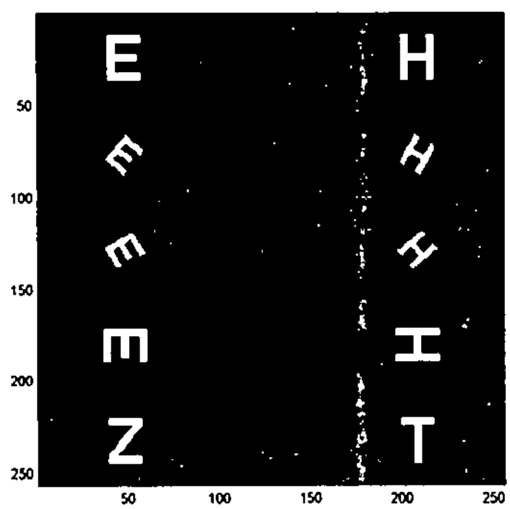

(a)

Fig 5.14 (a) Input scene.

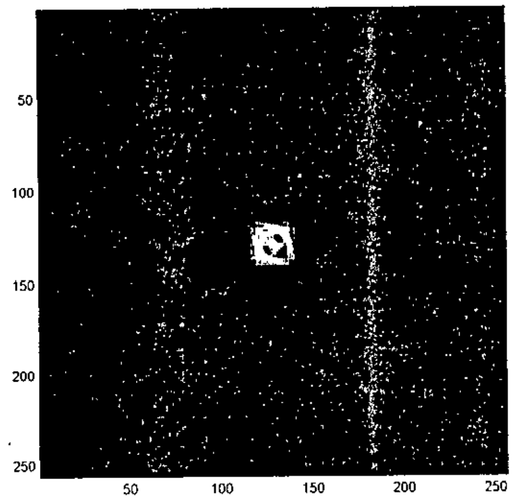

(b)

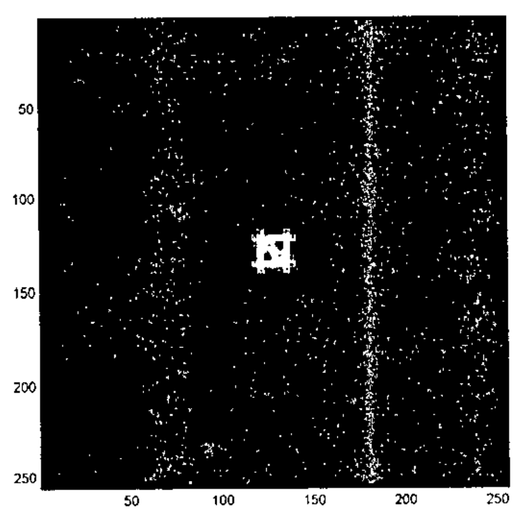

(c)

Fig. 5.14 (contd.) (b) SDF reference image 1, (c) SDF reference image 2.

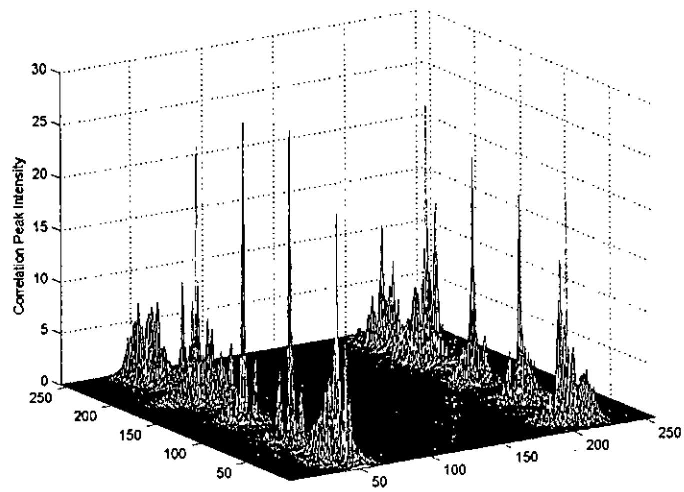

(a)

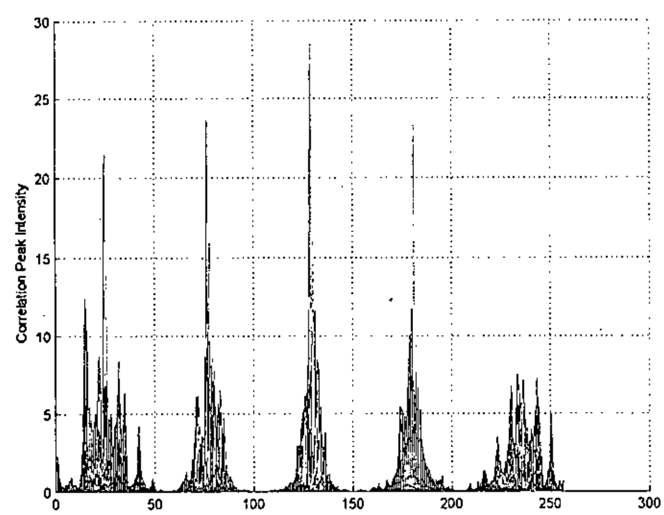

(b)

Fig. 5.15 (a) Correlation output for input and references of Fig 5.14, (b) Correlation output for left-side images.

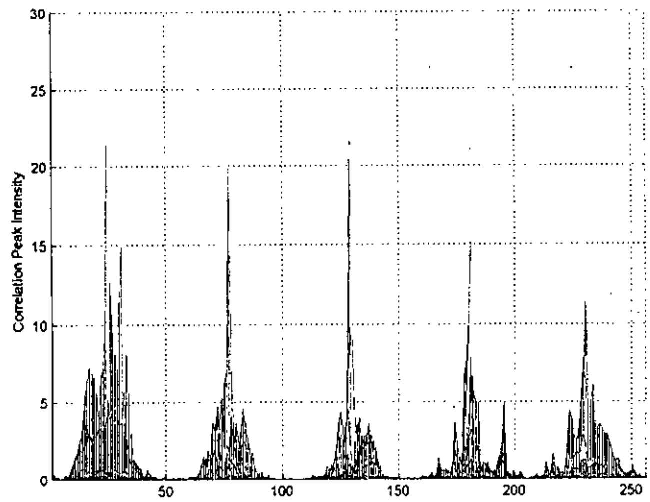

(c)

Fig. 5.15 (contd.) (c) Correlation output for right-side images.

Here identifiable correlation peaks are obtained for the targets of the class though the differences in peak heights among the targets are quite large. There are also considerable sidelobes around the correlation signals. However this SDF based distortion-invariant class-associative target detection technique is successful for detecting the images with rotation of even 90 degrees in case of binary images.

5.5 Detection of Gray Level Images

In section 5.4 we have seen successful detection of distorted and undistorted images of a class giving almost equal correlation peak for the targets. However those images were binary images. In this section the class-associative target detection will be investigated for gray level images when there are distortions in the images. As gray level images the images of different fruits are chosen. The actual color images were taken first and later converted to gray level in the computer. The gray level images were then reduced and processed for the simulation by MATLAB. As in the case of binary image, SDF reference generated by using phase-only JTC along with phase-only filter in CGFAF have been found to be the best choice for distortion invariant class-associative recognition of gray level images too in the simulation. So in the following subsections the distortion invariant recognition technique for gray level images of a class is discussed for the above mentioned filter combination.

5.5.1 Images Rotated up to 40 Degrees

Let us assume that 'banana' and 'mango' are the two targets of the desired class. So for distortion invariant detection, SDF references should be created from the training set of the distorted images for each target image of the class. Accordingly the training set for 'banana' has been produced first by rotating the image of 'banana' up to an angle of 40 degrees at a step of 5 degrees by using 'bicubic' interpolation of MATLAB. Thus there are 9 images in the training set. Similarly the training set for 'mango' has been formed. Fig. 5.16(a) and Fig. 5.16(b) shows these two training set images.

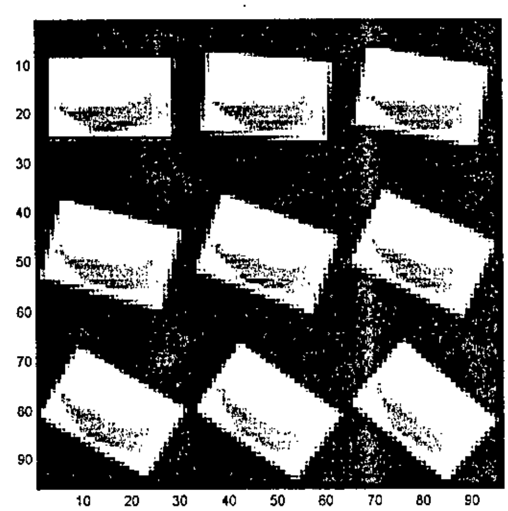

(a)

Fig. 5.16 (a) Training set images for 'banana'.

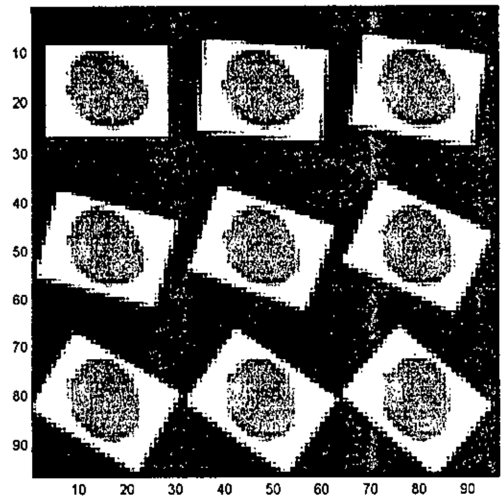

(b)

Fig. 5.16 (contd.) (b) Training set images for 'mango'.

Now let us take the input scene of Fig. 5.17(a) with multiple distorted and undistorted images of the class along with multiple non-targets. The SDF reference images are shown in Fig. 5.17(b) and Fig. 5.17(c). Corresponding correlation output is given in Fig. 5.18(a), Fig. 5.18(b) and Fig. 5.18(c). To reject any possible look-alike non-target image in the input scene, previously suggested correlation intensity enhancement is adopted for this simulation. It is obvious that the target images of the class can be clearly identified from the correlation output though the correlation peaks for all the targets are not fully equal.

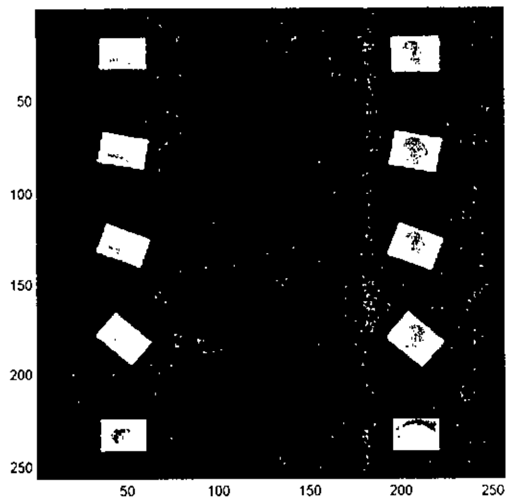

(a)

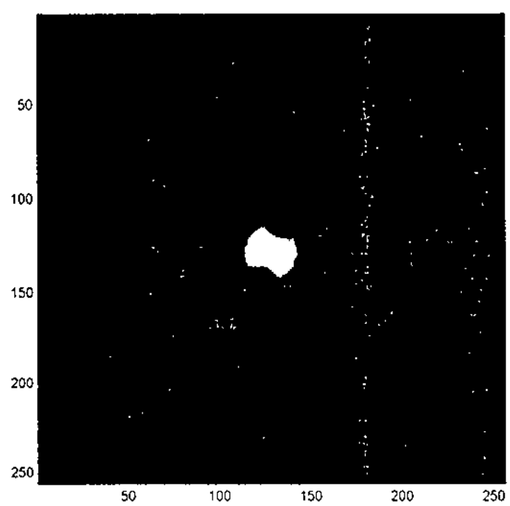

(b)

Fig. 5.17 (a) Input scene with multiple distorted and undistorted target images with multiple non-target, (b) SDF reference image 1.

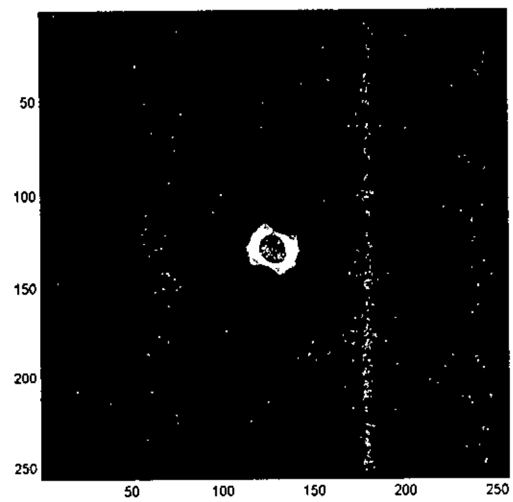

(c)

Fig. 5.17 (contd.) (c) SDF reference image 2.

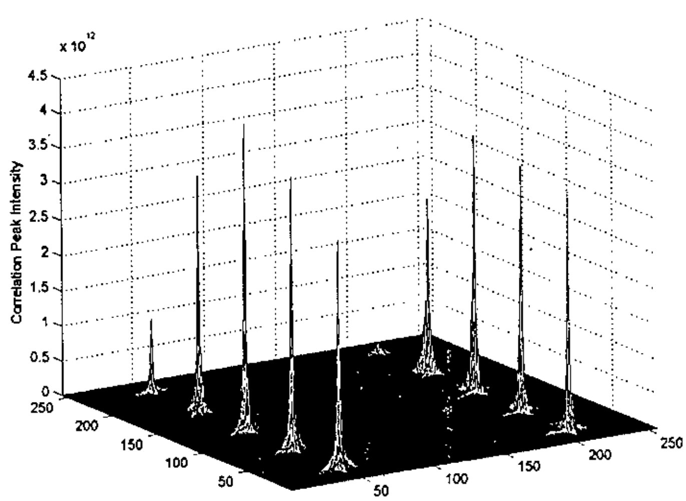

(a)

Fig. 5.18 (a) Correlation output for Fig. 5.17.

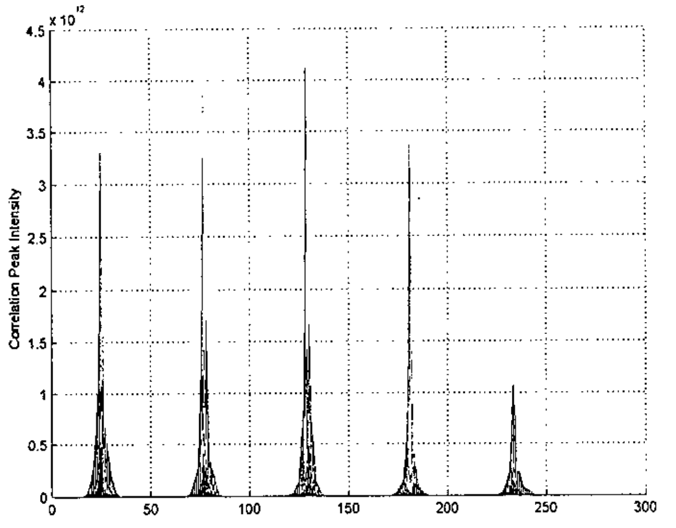

(b)

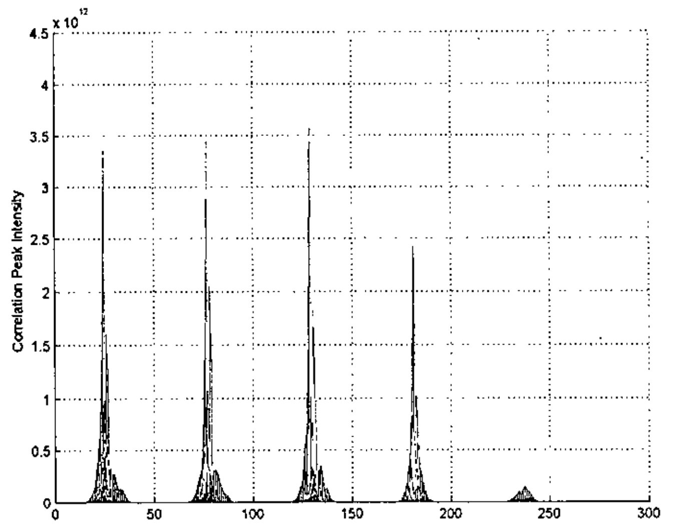

(c)

Fig. 5.18 (contd.) (b) Correlation output for left-side images, (c) Correlation output for right-side images.

5.5.2 Images Rotated up to 180 Degrees

As in section 5.5.1 let us take 'banana' and 'mango' as our target images of the class. To see the effect of rotation of the images up to 180 degrees, each original image has been rotated up to 180 degrees at a step of 10 degrees by using 'bicubic' interpolation of MATLAB. So for each image of the class there are total 19 images in the training set, which are then used to generate the corresponding SDF reference. Fig. 5.19(a) and Fig 5.19(b) are the training set of 'banana' and 'mango' respectively.

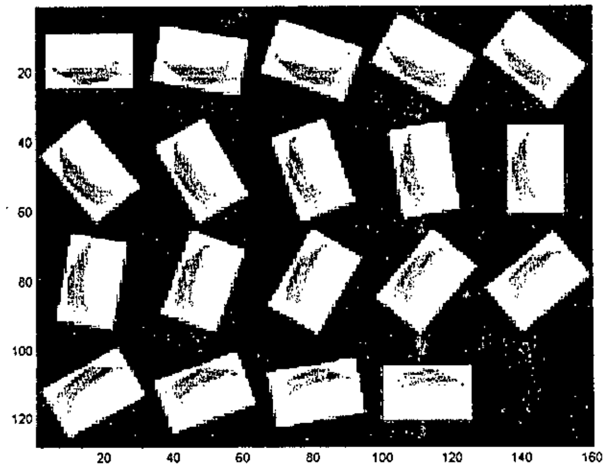

(a)

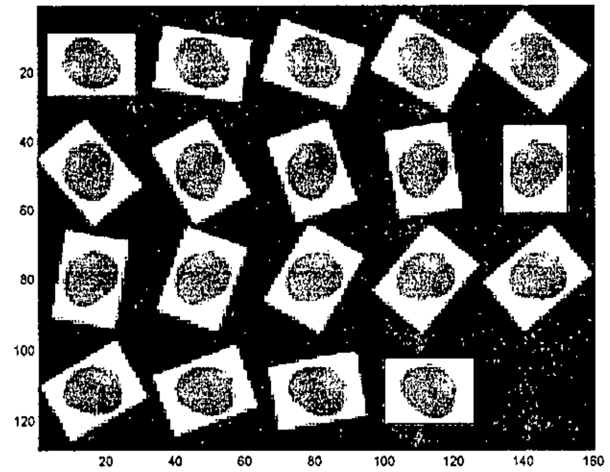

(b)

Fig. 5.19 (a) Training set images for 'banana', (b) Training set images for 'mango'.

Now let us take the input scene of Fig. 5.20(a) with multiple distorted and undistorted images of the class along with multiple non-targets. The SDF reference images are shown in Fig. 5.20(b) and Fig. 5.20(c). Corresponding correlation output by applying correlation intensity enhancement is given in Fig. 5.21. Here also it is obvious that the target images of the class can be clearly identified from the correlation output though the correlation peaks for all the targets are not fully equal and there are considerable sidelobes. However this sidelobes will not hinder in the detection, rather they will only decrease the optical efficiency of the system.

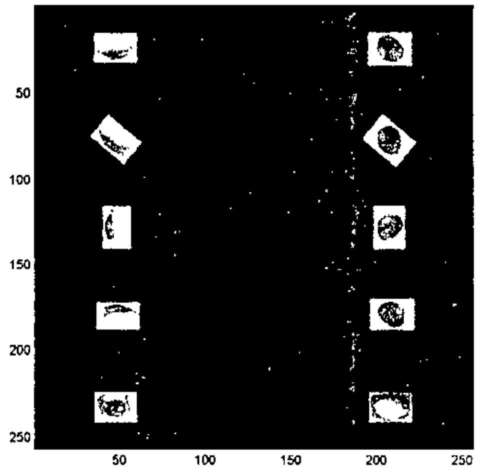

(a)

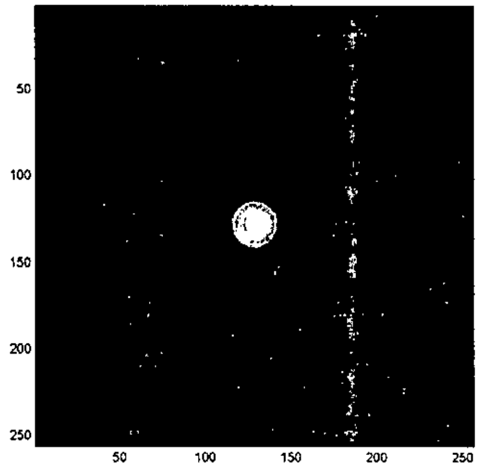

(b)

Fig. 5.20 (a) Input scene with multiple distorted and undistorted target images with multiple non-targets, (b) SDF reference image 1.

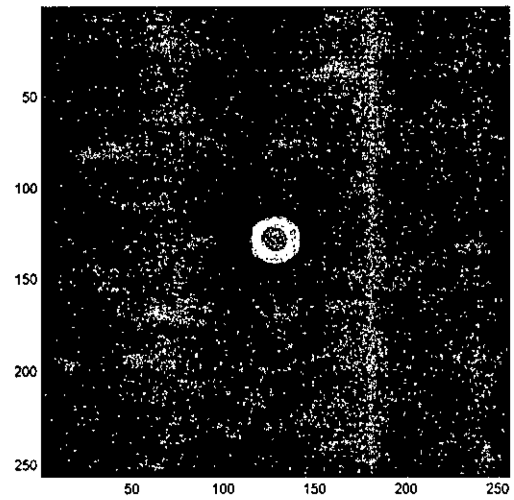

(c)

Fig. 5.20 (contd.) (c) SDF reference image 2.

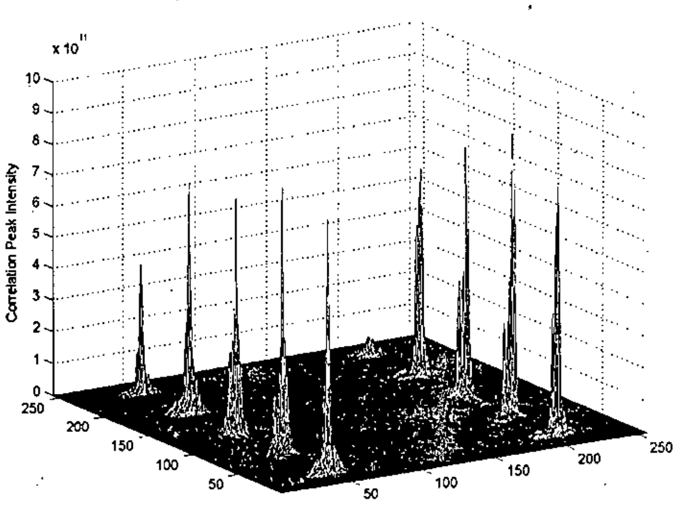

(a)

Fig. 5.21 (a) Correlation output for Fig 5.20.

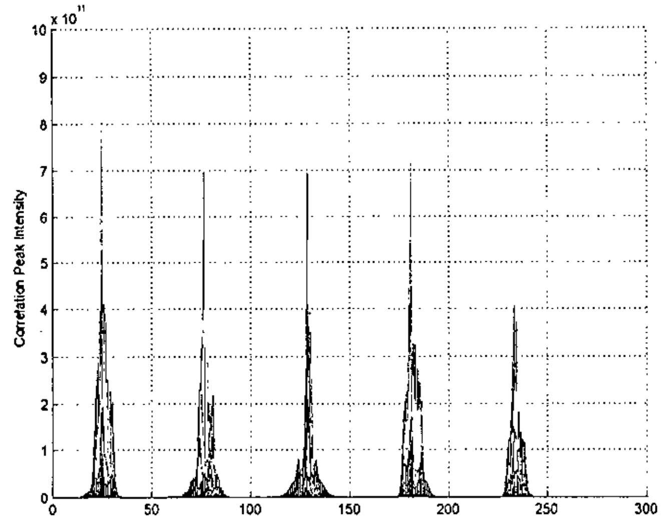

(b)

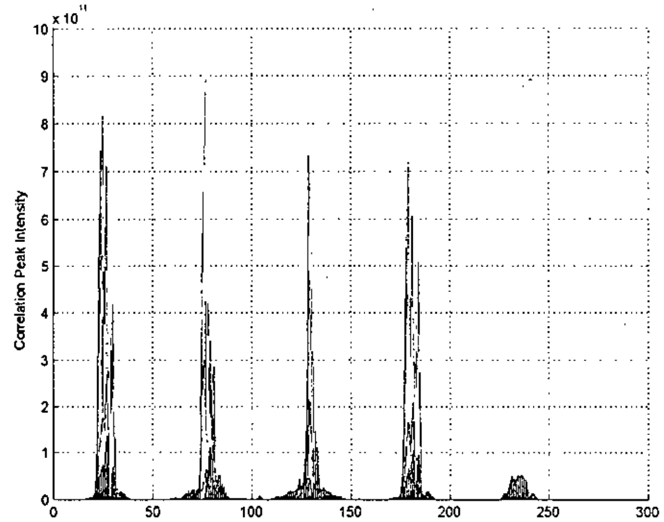

(c)

Fig. 5.21 (contd.) (b) Correlation output for left-side images, (c) Correlation output for right-side images.

5.6 Conclusion

Synthetic discriminant function (SDF) is incorporated in the class-associative target detection to get distortion invariant detection. The multiple references of the class-associative detection are replaced by the SDF based reference images. It is found that SDF generated by using phase-only JTC along with phase-only filter in CGFAF give the best distortion invariant performance. SDF can be formulated for both binary and gray level images. And this SDF based distortion invariant class-associative target detection works for both types of images.

Chapter 6

CONCLUSIONS

6.1 Conclusion

Optical correlators, especially joint transform correlators are versatile tool for pattern recognition or pattern classification. They provide real time detection of the targets with very high optical efficiency and reduced cost. Since the advent of joint transform correlators, various works have been performed on it and various modifications and/or improvements have been made. Among various forms of joint transform correlation fringe-adjusted joint transform correlation and recently devised multi-target detection algorithm are suitable for successful detection of objects or images when there are multiple targets and non-targets in the input scene. Between these two techniques, the later one facilitates class-associative target detection by using multiple references whereby two or more dissimilar objects representing a class can be detected with equal correlation peaks. But as shown in the previous chapters, both these two techniques are sensitive to target distortion such as scale variation or rotation. Synthetic discriminant function (SDF) is a tool in the areas of joint transform correlation for distortion invariant recognition.

In this work this synthetic discriminant function has been adopted with the multi-target detection algorithm based class-associative target recognition theory to get distortion invariant detection for all the objects of the class with equal correlation peaks. To achieve this goal a simplified iterative method based on generalized fringe-adjusted joint transform correlation has been used to obtain the synthetic discriminant function from a training set of distorted and undistorted images of an object. It is found that when the generalized fringe-adjusted filter is a phase-only filter, the SDF generation program better converges and the SDF generated in this way, when used as the reference, is more successful in giving equal correlation peaks for all of the multiple distorted and undistorted images present in the input scene.

To apply this SDF in class-associative target detection, each of the reference images of the class is synthesized from respective training set by using the proposed iterative method. Thus the undistorted multiple references of the class-associative detection theory are replaced by SDF references. It is found that when the class-associative generalized fringe-adjusted filter is a phase-only filter, the correlation outputs for all the images of the class are almost equal irrespective of their nature of distortion and the non-target peaks are negligible compared to the target peaks. As, a modification has been made in the combination of the set of input spectra by rearranging the phase information, the correlation peaks are obtained at the exact location of the objects providing the information of target positions easily. To get rid of the look-alike non-targets a method termed as correlation intensity enhancement technique is also suggested and applied which works by increasing the target peaks compared to the look-alike non-target peak.

In this work the proposed distortion invariant class-associative target detection is employed first for binary images such as English block-lettered alphabets. In this case though the training set was produced by rotating the original image, it automatically assumed scaling and some other types of distortions. So the tested distortion invariant property of the scheme is scale invariant as well. For binary image up to 90 degree rotation has been tested in the view that alphabet-like binary image may not appear rotated more than this amount in the input scene if it is considered as character recognition scheme. However for alphabets, rotation at more angles deteriorates the performance. On the other hand for gray level images the proposed distortion invariant class-associative target detection has been tested with the images rotated up to 180 degrees and has been found to be quite successful. This class-associative target detection technique inherently rejects noise and clutters. But for random noise as that one which is applied in the simulation, the performance degrades in the sense that it gives unequal correlation peaks for multiple distorted and undistorted target images of the class present in the input scene. Above all it can be said that the proposed distortion invariant class-associative target detection technique is a successful one though more works can be done on it for further excellence.

6.2 Future Works

In this work the rotation distortion that is considered or applied is actually in-plane rotation. But any real 3-D object may experience 3-D distortions such as out-of-plane rotation. Though SDF is sometimes successful in case of 3-D distortions, a projection-slice SDF is more suitable for such case. When a composite image is created using the regular SDF, it is generated by a weighted average of the various frequency components of the training images. According to the projection-slice theorem a 1-D Fourier transform along a projected line in an image corresponds to a slice in the 2-D Fourier transform of that image along the same line. By taking different slices from the training images, a composite image can be created such that the frequency components from different images do not interfere with each other. So work can be done to apply SDF or projection-slice SDF in the class-associative detection to get 3-D distortion invariant class-associative target detection.

On the other hand, all real objects are color objects and contain more information than a binary or gray level image does. To properly represent an object it must be represented in color image. Hence, for successful distortion invariant recognition color image should be dealt with to formulate the SDF or projection-slice SDF and the class-associative target detection technique. So this work can also be extended by analyzing or experimenting with color image. To work with color image the three primary color information from an actual color image may be separated first. Then three channels can be adopted independently for these three colors. At the end the output from those three channels may be fused to get the final or actual correlation output.

APPENDIX I

SAMPLE MATLAB PROGRAM FOR SDF FORMULATION

```
%%%--------------------------------------------------------------------------%%%
%%% file name: chap4_sdf.m
%%% sdf generation using gjtc with all the images of the training set together
%%% in the joint image
%%%--------------------------------------------------------------------------%%%


clear all;
close all;
%----------------------------------------------------------------------------
%generating the image array


load aefhmotz32; %loading the mat file containing the images


step=5; %rotation step in angle
initial_angle=0;
final_angle=40;
target_rotation=final_angle-initial_angle;
turn=-1; %-1 for clockwise rotation and 1 for anticlockwise rotation
```

```
if target_rotation==360,
  total_image=round(target_rotation/step);
else
  total_image=round(target_rotation/step+1);
end

image=E; %giving the input to be rotated
[sizer,sizec]=size(image);
initial_image=imresize(image,4);
initial_image=imrotate(initial_image,turn*initial_angle);
initial_image=imresize(initial_image,1);

%rotating the image and placing into array
for i=1:total_image,
  ref(:,:,i)=imresize((imrotate(initial_image,(turn*(i-1)*step))),[sizer sizec]);
end
%'ref' is the image array

%ploting the image array
figure(1);
im(ref(:,:));
%-----------------------------------------------------------------------------

%------------------------------------------------------------------------
%%%finding sdf reference (ref_sdf) using gfaf%%%
```

```
c=ones(1,total_image); %initialization of coefficients of sdf

ref_sdf=zeros(sizer,sizec); %initialization of sdf

%calculating the sdf (ref_sdf) with unity coefficients
for i=1:total_image,
  ref_sdf=ref_sdf+c(i)*ref(:,:,i);
end
ref_sdf=ref_sdf/max(max(ref_sdf));

%figure of SDF with unity coefficients
figure(2);
im(ref_sdf);
axis square;
title('SDF with unity coefficients');

%gjtc between sdf with unity coefficients & training set images

%initialization of input, reference and joint image plane
ref_input=zeros(sizer*total_image,sizec*total_image); %input plane
ref_ref=zeros(sizer*total_image,sizec*total_image);   %reference plane
ref_joint=zeros(sizer*total_image,sizec*total_image); %joint image

%putting training set into input plane
```

```
for i=1:total_image,
  ref_input(1:sizer,((i-1)*sizec+1):(sizec*i))=ref(:,:,i);
end

%putting sdf in reference plane
indxr1=(total_image*sizer/2-sizer/2+1);
indxr2=((total_image*sizer/2-sizer/2+1)+(sizer-1));
indxc1=(total_image*sizec/2-sizec/2+1);
indxc2=((total_image*sizec/2-sizec/2+1)+(sizec-1));

ref_ref(indxr1:indxr2,indxc1:indxc2)=ref_sdf;

%joint input (sdf & training set)
ref_joint=ref_input+ref_ref;
figure(3);
im(ref_joint);
axis square;
title('joint image (sdf & training set)');

%fourier transform
ref_input_F=fftshift(fft2(ref_input));
ref_ref_F=fftshift(fft2(ref_ref));
ref_joint_F=fftshift(fft2(ref_joint));

%finding the intensity (power spectrum)
```

```
ps_ref_input_F=(abs(ref_input_F)).^2;

ps_ref_ref_F=(abs(ref_ref_F)).^2;

ps_ref_joint_F=(abs(ref_joint_F)).^2;


%fourier plane image subtraction

sub_jps=ps_ref_joint_F-ps_ref_input_F-ps_ref_ref_F;


%generalized fringe adjusted filter (gfaf) parameters

C=1;

D=(10^(-4));

m=1; %phase only filter


%applying gfaf filter

value_ref_ref_F=abs(ref_ref_F);

FAF = (C)./(D + (value_ref_ref_F.^m));

faf_sub_jps= sub_jps.*FAF;


%correlation

corr_sdf_input = (abs(ifftshift(ifft2(faf_sub_jps)))).^2;


%zero padding the undesired lobes for clarity

corr_sdf_input(sizer+1:sizer*total_image,1:sizec*total_image)=zeros((sizer*tota
l_image-sizer),sizec*total_image);


figure(4);
```

```
mesh(corr_sdf_input);
title('Correlation of training set and sdf  using gfaf');


figure(5);
mesh(corr_sdf_input);
view(0,0);
title('2-D view of correlation between training set and sdf using gfaf');


%calculating the correlation peaks after first gjtc operation
for i=1:total_image,
  peak_corr(i)=max(max(corr_sdf_input(1:sizer,((i-1)*sizec+1):(sizec*i))));
end
%---------------------------------------------------------------


%continuing gjtc for further iterations
%---------------------------------------------------------------
iteration=500;


for iter=1:iteration,


  %update the coefficients by an empirical formula
  for i=1:total_image
    rf=0.1; %relaxation factor
    if abs(target_corr-peak_corr(i))>0.01,
       c(i)=c(i)+(target_corr-peak_corr(i))*rf;
```

```
  end
end

ref_sdf=zeros(sizer,sizec); %reinitialization of sdf

%calculating sdf with new coefficients
for i=1:total_image,
   ref_sdf=ref_sdf+c(i)*ref(:,:,i);
end
ref_sdf=ref_sdf/max(max(ref_sdf));

%gjtc between sdf with nrew coefficients & training set images

%reinitialization of reference and joint image plane
ref_ref=zeros(sizer*total_image,sizec*total_image);
ref_joint=zeros(sizer*total_image,sizec*total_image);

%putting reference and finding joint image
ref_ref(indxr1:indxr2,indxc1:indxc2)=ref_sdf;
ref_joint=ref_input+ref_ref;

figure(6);
im(ref_joint);
axis square;
```

```
title('joint image (sdf & training set)');


%fourier transform
ref_ref_F=fftshift(fft2(ref_ref));
ref_joint_F=fftshift(fft2(ref_joint));


%finding the intensity (power spectrum)
ps_ref_ref_F=(abs(ref_ref_F)).^2;
ps_ref_joint_F=(abs(ref_joint_F)).^2;


%fourier plane image subtraction
sub_jps=ps_ref_joint_F-ps_ref_input_F-ps_ref_ref_F;


%applying gfaf filter
value_ref_ref_F=abs(ref_ref_F);
gfaf = (C)./(D + (value_ref_ref_F.^m));
faf_sub_jps= sub_jps.*FAF;


%correlation
corr_sdf_input = (abs(ifftshift(ifft2(faf_sub_jps)))).^2;
%zero padding the undesired lobes
corr_sdf_input(sizer+1:sizer*total_image,1:sizec*total_image)=zeros((sizer*tota
l_image-sizer),sizec*total_image);
```

```
%finding new values of correlation peaks
for i=1:total_image,
  peak_corr(i)=max(max(corr_sdf_input(1:sizer,((i-1)*sizec+1):(sizec*i))));
end

max_peak=max(peak_corr);
min_peak=min(peak_corr);
error=(max_peak-min_peak)/max_peak;
target_corr=max_peak;

figure(7);
mesh(corr_sdf_input);
title('Correlation of training set and sdf  using gfaf');

figure(8);
mesh(corr_sdf_input);
view(0,0);
title('2-D view of correlation between training set and sdf using gfaf');

%check for convergence and exit from the program
if error<0.01 | iter==iteration
  figure(9);
  im(ref_sdf);
  axis square;
  title('Final SDF with FAF filter');
```

```
    %saving the sdf as mat file
    sdf_E=ref_sdf;
        save sdf_E.mat sdf_E;

    for i=1:total_image
            peak_corr(i) %displaying the final correlation peaks
    end
    for i=1:total_image
                c(i) %displaying the final coefficients
    end
    iter %displaying the number of iterations required
    return;
  end
end
%%%------------------------------------------------------------%%%
```

APPENDIX II

SAMPLE MATLAB PROGRAM FOR SIMULATING CLASS-ASSOCIATIVE TARGET DETECTION

```
%%%------------------------------------------------------------------------%%%
%%%  file name: chap5_ca_sdf.m
%%%  class associative target detection using sdf images as references
%%%------------------------------------------------------------------------%%%

close all;
clear all;
%------------------------------------------------------------------------------
load aefhmotz32; %loading the mat file containing the images


%generating the image array
step=5;%rotation step in angle
initial_angle=0;
final_angle=40;
target_rotation=final_angle-initial_angle;
turn=-1; %-1 for clockwise rotation and 1 for anticlockwise rotation


if target_rotation==360,
```

```
  total_image=round(target_rotation/step);
else
  total_image=round(target_rotation/step+1);
end

%giving the input (1st object of the class) to be rotated
image=E;
[sizer,sizec]=size(image);
initial_image=imresize(image,4);
initial_image=imrotate(initial_image,turn*initial_angle);
initial_image=imresize(initial_image,1);

for i=1:total_image,
  ref11(:,:,i)=imresize((imrotate(initial_image,(turn*(i-1)*step))),[sizer sizec]);
end

step=5;%rotation step in angle
initial_angle=0;
final_angle=40;
target_rotation=final_angle-initial_angle;
turn=-1; %-1 for clockwise rotation and 1 for anticlockwise rotation

if target_rotation==360,
  total_image=round(target_rotation/step);
else
```

```
  total_image=round(target_rotation/step+1);
end


%giving the input (2nd object of the class) to be rotated
image=H;
[sizer,sizec]=size(image);
initial_image=imresize(image,4);
initial_image=imrotate(initial_image,turn*initial_angle);
initial_image=imresize(initial_image,1);


for i=1:total_image,
  ref22(:,:,i)=imresize((imrotate(initial_image,(turn*(i-1)*step))),[sizer sizec]);
end


inp=zeros(256,256); %initializing input plane 'inp'
ref1=zeros(256,256); %initializing reference image 1 plane 'ref1'
ref2=zeros(256,256); %initializing reference image 2 plane 'ref2'


%placing the distorted and undistorted target images and non-targets


inp(9:40,33:64)=ref11(:,:,1);
inp(61:92,33:64)=ref11(:,:,3);
inp(113:144,33:64)=ref11(:,:,5);
inp(165:196,33:64)=ref11(:,:,9);
inp(217:248,33:64)=F;
```

```
inp(9:40,193:224)=ref22(:,:,1);
inp(61:92,193:224)=ref22(:,:,3);
inp(113:144,193:224)=ref22(:,:,5);
inp(165:196,193:224)=ref22(:,:,9);
inp(217:248,193:224)=T;

%loading the mat file containing sdf reference images
load sdfoE1;
load sdfoH1;

%placing the sdf references
ref1(113:144,113:144)=sdfoE1;
ref2(113:144,113:144)=sdfoH1;

%class detection using multi-target detection algorithm
%--------------------------------------------------------------
f11 = ref1+inp;
f21= ref1+exp(-j*pi/2)*inp;
f31 = ref1-inp;
f41 = ref1-exp(-j*pi/2)*inp;
%--------------------------------------------------------------
F11 = fftshift(fft2(f11));
F21 = fftshift(fft2(f21));
F31 = fftshift(fft2(f31));
```

```
F41 = fftshift(fft2(f41));

%--------------------------------------------------------------

jps11 = (abs(F11)).^2;

jps21 = (abs(F21)).^2;

jps31 = (abs(F31)).^2;

jps41 = (abs(F41)).^2;

%--------------------------------------------------------------

%joint power spectrum for ref1 and inp

jps1 = jps11 + (exp(j*pi/2) .* jps21) - jps31 - (exp(j*pi/2) .* jps41);

%--------------------------------------------------------------

f12 = ref2+inp;

f22= ref2+exp(-j*pi/2)*inp;

f32 = ref2-inp;

f42 = ref2-exp(-j*pi/2)*inp;

%--------------------------------------------------------------

F12 = fftshift(fft2(f12));

F22 = fftshift(fft2(f22));

F32 = fftshift(fft2(f32));

F42 = fftshift(fft2(f42));

%--------------------------------------------------------------

jps12 = (abs(F12)).^2;

jps22 = (abs(F22)).^2;

jps32 = (abs(F32)).^2;

jps42 = (abs(F42)).^2;

%--------------------------------------------------------------
```

```
%joint power spectrum for ref2 and inp
jps2 = jps12 + (exp(j*pi/2) .* jps22) - jps32 - (exp(j*pi/2) .* jps42);
%-------------------------------------------------------------
%power spectra parameters
alpha=0.436;
beta=1-alpha;

%total jps
jps = alpha.*jps1 + beta.*jps2;

% class-associative generalized fringe adjusted filter (cgfaf) parameters
C=1;
D=(10^(-4));
m=1; %phase-only filter

%applying cgfaf
R1 = fftshift(fft2(ref1));
R2 = fftshift(fft2(ref2));
value_R1 = abs(R1);
value_R2 = abs(R2);

cgfaf = (C)./(D + (value_R1.^m) + (value_R2.^m));

modified_jps = jps.*cgfaf;
```

```
n=2; %correlation output power
corr = (abs(fftshift(ifft2(modified_jps)))).^n;

figure(1);
im(ref1);
axis square;
title('sdf reference image 1');

figure(2);
im(ref2);
axis square;
title('sdf reference image 2');

figure(3);
im(inp);
axis square;
title('input scene')

figure(4);
mesh(corr);
zlabel('Correlation Peak Intensity');
view(-32,20);
title('correlation output');
```

```
%calculating the correlation peaks for the input scene objects

peak_row1col1=max(max(corr(9:40,33:64)))
peak_row2col1=max(max(corr(61:92,33:64)))
peak_row3col1=max(max(corr(113:144,33:64)))
peak_row4col1=max(max(corr(165:196,33:64)))
peak_row5col1=max(max(corr(217:248,33:64)))

peak_row1col2=max(max(corr(9:40,193:224)))
peak_row2col2=max(max(corr(61:92,193:224)))
peak_row3col2=max(max(corr(113:144,193:224)))
peak_row4col2=max(max(corr(165:196,193:224)))
peak_row5col2=max(max(corr(217:248,193:224)))
%-----------------------------------------------------------------
```

REFERENCES

[1] Robert Schalkoff, "*Pattern Recognition, Statistical, Structural and Neural Approaches*," John Wiley & Sons, New York, 1992.

[2] Richard O. Duda, Peter E. Hart, David G. Stork, "*Pattern Classification*," Second Edition, Wiley-Interscience, 2000.

[3] Rafael C. Gonzalez, Richard E. Woods, "*Digital Image Processing*," Addison-Wesley Publishing Company, Inc., 1992.

[4] J. W. Goodman, "*Introduction to Fourier Optics*," McGraw Hill, New York, 1968.

[5] Eugene Hecht and Alfred Zajac, "*Optics*," Addison-Wesley Publishing Company, Phillipines, 1979.

[6] A. VanderLugt, "Signal detection by complex spatial filtering," *IEEE Trans. Inf. Theory* IT-10, pp. 139-146, 1964.

[7] H. J. Caulfield and R. Haimes, "Generalized matched filtering," *Appl. Opt.*, Vol. 18, No. 2, pp. 181-183, 1980.

[8] D. A. Gregory, "Real-time pattern recognition using a modified LCTV in a coherent optical correlator," *Appl. Opt.*, Vol. 25, pp. 467-469, 1986.

[9] A. D. Gara, "Real-time tracking of moving objects by optical correlation," *Appl. Opt.*, Vol. 18, pp. 172-172, 1989.

[10] A. Mahalanobis and D. Casasent, "Performance evaluation of minimum average correlation filters," *Appl. Opt.*, Vol. 30, pp. 561-572, 1991.

[11] R. R. Kallman and D. H. Goldstein, "Phase-encoding input image for optical pattern recognition," *Opt. Eng.*, Vol. 33, pp. 1806-1813, 1994.

[12] D. Casasent and A. Furman, "Sources of correlation degradation," *Appl. Opt.*, Vol. 16, pp. 1652-1661, 1977.

[13] X. J. Lu, F. T. S. Yu and D. A. Gregory, "Comparison of VanderLugt and joint transform correlator," *Appl. Phys. B. Photophys. Laser Chem.*, Vol. 51, pp. 153-164, 1990.

[14] Purwadi Purwosumarto and Francis T. S. Yu, "Robustness of joint transform correlator versus VanderLugt correlator," *Opt. Eng.*, Vol. 36, No. 10, pp. 2775-2780, 1997.

[15] P. D. Gianino and J. L. Horner, "Phase-only Matched Filtering," *Appl. Opt.*, Vol. 23, No. 6, pp. 812-816, 1984.

[16] G. G. Mu, X. M. Wang, and Z. Q. Wang, "Amplitude-compensated matched filtering," *Appl. Opt.*, Vol. 27, No. 16, pp. 3461-3463, 1988.

[17] C. S. Weaver and J. W. Goodman, "A technique for optically convolving two functions." *Appl. Opt*, Vol. 5, No. 7, pp. 1248-1249, 1966.

[18] F. T. S. Yu and X. J. Lu, "A real-time programmable joint transform correlator," *Opt. Commun.* Vol. 52, No. 10, pp. 10-16, 1984.

[19] F. T. S. Yu, S. Jutamulia, T. W. Lin and D. A. Gregory, "Adaptive real-time pattern recognition using a liquid crystal TV based joint transform correlator," *Appl. Opt.*, Vol 26, pp. 1370-1372, 1988.

[20] B. Javidi and C. Kuo, "Joint transform image correlation using a binary spatial light modulator at the Fourier plane," *Appl. Opt.*, Vol 27, pp. 663-665, 1988.

[21] S. K. Rogers, J. D. Cline and M. Kabrisky, "New binarization techniques for joint transform correlation," *Opt. Eng.*, Vol. 29, No. 9, pp. 1018-1023, 1990.

[22] B. Javidi, J. Wang, and Q. Tang, "Multiple-object binary joint transform correlation using multiple-level threshold crossing," *Appl. Opt.*, Vol. 31, No. 29, pp. 4816-4822, 1992.

[23] M. S. Alam and M. A. Karim, "Improved correlation discrimination in a multiobject bipolar joint transform correlator," *Opt. & Laser Tech*, Vol. 24, pp. 45-50, 1992.

[24] W. B. Hahn and D. L. Flannery, "Design elements of a binary joint transform correlator and selected optimization techniques," *Opt. Eng.*, Vol. 31, No. 5, pp. 896-905, 1992.

[25] F. T. S. Yu, F. Cheng, T. Nagata and D. A. Gregory, "Effects of fringe binarization of multi-object joint transform correlation," *Opt. Eng.*, Vol. 28, No. 5, pp. 2988-2990, 1989.

[26] Q. Tang and B. Javidi, "Multiple-object detection with a chirp-encoded joint transform correlator," *Appl. Opt.*, Vol. 32, pp. 4344-4350, 1993.

[27] S. Jutamulia, G. M. Storti, D. A. Gregory and J. C. Kirsch, "Illumination-independent high-efficiency joint transform correlator," *Appl. Opt.*, Vol 30, No. 29, pp. 4173-4175, 1991.

[28] S. Jutamulia and D. A. Gregory, "Soft blocking of the dc term in Fourier optical systems," *Opt. Eng.*, Vol. 37, No. 1, pp. 49-51, 1998.

[29] C. Li, S. Yin and F. T. S. Yu, "Nonzero-order joint transform correlator," *Opt. Eng.*, Vol. 37, No. 1, pp. 58-65, 1998.

[30] F. T. S. Yu, C. Li and S. Yin, "Comparison of detection efficiency for nonzero-order and conventional joint transform correlation," *Opt. Eng.*, Vol. 37, No. 1, pp. 52-57, 1998.

[31] G. Lu, Z. Zhang, S. Wu and F. T. S. Yu, "Implementation of a non-zero order joint transform correlator by use of phase shifting techniques," *Appl. Opt.*, Vol. 36, No. 2, pp. 470-483, 1997.

[32] D. Feng, H. Zhao and S. Xia, "Amplitude-Modulated JTC for Improving Correlation Discrimination," *Opt. Commun.*, Vol. 86, pp. 260-264, 1991.

[33] M. S. Alam and M. A. Karim, "Fringe-adjusted joint transform correlator," *Appl. Opt.* Vol. 32, No. 23, pp. 4344-4350, 1993.

[34] M. S. Alam and M. A. Karim, "Joint transform correlation under varying illumination," *Appl. Opt.*, Vol. 32, pp. 4344-4350, 1993.

[35] M. S. Alam, "Fractional power fringe-adjusted joint transform correlator," *Opt. Eng.* Vol. 34, pp. 3208-3216, 1995.

[36] J. Khoury, G. Asimellis and C. woods, "Incoherent-erasure nonlinear joint transform correlator," *Opt. Lett.*, Vol. 20, pp. 2321-2323, 1995.

[37] M. S. Alam and J. Khoury, "Fringe-adjusted Incoherent Erasure Joint Transform Correlator," *Journal of Optical Engineering*, Vol. 37, pp. 75-82, 1998.

[38] M. S. Alam and M. A. Karim, "Multiple target detection using a modified fringe-adjusted joint transform correlator," *Opt. Eng.* Vol. 33, pp. 1610-1617, 1994.

[39] M. S. Alam, "Multi-target Photorefractive Fringe-adjusted Joint Transform Correlation," *Journal of Optical Memory and Neural Networks*, Vol. 6, pp. 287-296, 1998.

[40] A. A. S. Awwal, M. A. Karim and S. R. Jahan, "Improved Correlation Discrimination Using an Amplitude Modulated Phase-only Filter," *Appl. Opt.* Vol. 29, p. 233-236, 1990.

[41] T. Nomura, "Phase-encoded joint transform correlator to reduce the influence of extraneous signals," *Appl. Opt.*, Vol. 37, pp. 3651, 1998.

[42] G. Lu and F. T. S. Yu, "Performance of a phase transformed input joint transform correlator," *Appl. Opt.*, Vol. 35, pp 304, 1996.

[43] Mohammad S. Alam, "Phase-encoded fringe-adjusted joint transform correlation," *Opt. Eng.*, Vol. 39, No. 5, pp. 1169-1176, 2000.

[44] M. K. Hu, "Visual pattern recognition by moment invariance," *IRE Trans. Inf. Theory,* IT-8, pp. 179-187, 1962.

[45] D. Cassasent and D. Psaltis, "Optical pattern recognition using normalized invariant moments," *Proc. SPIE,* Vol. 201, pp. 107-114, 1979.

[46] Y. Li, "Reforming the theory of invariant moments of pattern recognition," *Pattern Recog.*, Vol. 25, No. 7, pp. 723-730, 1992.

[47] A. Goshtasby, "Template matching in rotated images," *IEEE Trans. Pattern Anal. Mach. Intel.*, PAMI, Vol. 7, No. 3, pp. 338-344, 1985.

[48] Y. Sheng and H. H. Arsenault, "Object detection from a real scene using the correlation peak coordinates of multiple circular harmonic filters," *Appl. Opt.*, Vol. 28, No. 2, pp. 245-249, 1989.

[49] M. T. Manry, "Compound filter using the circular harmonic expansion," *Appl. Opt.*, Vol. 26, No. 17, pp. 3622-3627, 1987.

[50] D. Mendlovic, E. Maron and N. Konforti, "Shift and scale invariant pattern recognition using Mellin radial harmonics," *Opt. Commun.,* vol. 67, No. 3, pp. 172-176, 1988.

[51] Y. Sheng, C. Lejeune and H. H. Arsenault, "Frequency-domain Fourier-Mellin descriptors for invariant pattern recognition," *Opt. Eng.,* Vol. 27, No. 5, pp. 354-357, 1988.

[52] M. Fang and G. Hausler, "Class of transforms invariant under shift, rotation and scaling," *Appl. Opt.,* Vol. 29, No. 5, pp. 704-708, 1990.

[53] W. S. Shao and Y. S. Chen, "Pattern analysis on shift, rotation and scaling," *Electron. Lett.,* Vol. 28, No. 25, pp. 2271-2272, 1992.

[54] D. Casasent, "Unified synthetic discriminant function computational formulation," *Appl. Opt.*, Vol. 23, pp. 1620-1627, 1984.

[55] B. V. K. V. Kumar, "Minimum variance synthetic discriminant function," *J. Opt. Soc. Am. A*, 3, pp. 1579-1584, 1986.

[56] A. Mahalanobis, B. V. K. V. Kumar and D. Cassasent, "Minimum average correlation energy filters," *Appl. Opt.*, Vol. 26, pp. 3633-3640, 1987.

[57] D. Cassasent and W. T. Chang, "Correlation synthetic discriminant functions," *Appl. Opt.*, Vol. 25, pp. 2343-2350, 1986.

[58] Z. Bahri and B. V. K. V. Kumar, "Generalized synthetic discriminant functions," *J. Opt. Soc. Am. A*, 5, pp. 562-571, 1988.

[59] B. Javidi, "Synthetic discriminant function based binary nonlinear optical correlator," *Appl. Opt.*, Vol. 28, pp. 2490-2493, 1989.

[60] R. Wang, C. R. Chatwin and L. Shang, "Synthetic discriminant function fringe-adjusted joint transform correlator," *Opt, Eng.*, Vol. 34, No. 10, pp. 2935-2944, 1995.

[61] X. W. Chen, M. A. Karim and M. S. Alam, "Distortion-invariant fractional power fringe-adjusted joint transform correlation," *Opt. Eng.*, Vol. 37, No. 1, pp. 138-143, 1998.

[62] V. R. Riasati and M. Abushagur, "Projection-slice synthetic discriminant functions for optical pattern recognition," *Appl. Opt.*, Vol. 36, pp. 3022-3034, 1997.

[63] D. Casasent, J. Smokelin and A. Ye, "Wavelet and Gabor transforms for detection," *Opt. Eng*, Vol. 31, pp. 1893-1898, 1992.

[64] F. Ahmed, M. S. Alam and M. A. Karim, "Wavelet transform based correlator for the recognition of rotationally distorted images," *Opt. Eng.*, Vol. 34, pp. 3187-3192, 1995.

[65] B. Javidi, J. Li and Q. Tang, "Optical implementation of neural networks for face recognition by use of nonlinear joint transform correlator," *Appl. Opt.*, Vol. 34, pp. 3950-3962, 1995.

[66] A. R. Alsamman and M. S. Alam, "Invariant face recognition using fringe-adjusted joint transform correlator based neural network," in *Optical Pattern*

Recognition XII, D. P. Casasent and T. H. Chao, Eds., *Proc. SPIE,* Vol. 4387, pp. 164-175, 2001.

[67] D. Casasent and B. Telfer, "Key and recollection vector effect on heteroassociative memory performance," *Appl. Opt.*, Vol. 28, pp. 272-283, 1989.

[68] J. Khoury, P. D. Gianino and Charles L. Woods, "Class associative correlation filter using cross correlation enhancement," *Optical Pattern Recognition XI*, D. P. Casascent and T. H. Chao, ods., *Proc. SPIE,* Vol. 4043, pp. 7456-7463, 2000.

[69] M. S. Alam and M. M. Rahman, "Class-associative multiple target detection by use of fringe-adjusted joint transform correlation," *Appl. Opt.*, Vol. 41, No. 35, pp. 1-8, 2002.